1-1-2008

Analytical modeling of the contact pressure at the steel-concrete interface

Sini Bhaskar
Ryerson University

ANALYTICAL MODELING OF THE CONTACT PRESSURE AT THE STEEL-CONCRETE INTERFACE

By

Sini Bhaskar

Master of Technology in Civil Engineering
Cochin University of Science and Technology, India, July, 2005

A thesis presented to Ryerson University

In the partial fulfillment of the
requirements for the degree of

Master of Applied Science
in the program of
Civil Engineering

Toronto, Ontario, Canada, 2008

AUTHOR'S DECLARATION

I hereby declare that I am the sole author of this thesis.

I authorize Ryerson University to lend this thesis to other institutions or individuals for the purpose of scholarly research.

Author's signature ____ _____ Date__ ___

I further authorize Ryerson University to reproduce this thesis by photocopying or by other means, in total or in part, at the request of other institutions or individuals for the purpose of scholarly research.

Author's signature____ _____Date____

ANALYTICAL MODELING OF THE CONTACT PRESSURE AT THE STEEL-CONCRETE INTERFACE

Master of Applied Science 2008

By

Sini Bhaskar
Department of Civil Engineering
Ryerson University, Toronto

ABSTRACT

This research studies the effect of corrosion on bond strength at the steel-concrete interface in a reinforced concrete member. Bond stress, which can be defined as the shear stress which develops along the lateral surface of the bar, is expressed as a function of contact pressure at the steel-concrete interface. An analytical model of bond which describes the contact pressure between the reinforcing bar and concrete in a reinforced concrete member is developed. The expression for the reduction in contact pressure due to the accumulation of corrosion products is then developed using the model developed for the uncorroded reinforcing steel bar. The developed analytical model was implemented in a finite element analysis, which was conducted using ABAQUS, of pull-out specimens conducted by Amleh (2000). A reasonable good agreement between the experimental and finite element analysis results was obtained.

ACKNOWLEDGEMENTS

I consider this as the most important section of the report because; this is where I get an opportunity to express my sincere gratitude to all the people who have extended their support to successfully complete the thesis. First and foremost, my heartfelt thanks to Dr. Lamya Amleh, my advisor without whom I couldn't get an opportunity to do this research. Whatever I have achieved has been possible, only due to the help, unconditional support and continuous encouragement extended by her. Dr.Amleh's guidance to systematically approach a masters level thesis made my job easy.

Let me take this opportunity to thank two very important people Dr. Mohamed Lachemi and Dr. Anwar Hossain for their invaluable inputs during the course of my masters at Ryerson. Their inspiration played a great role in my successful completion of the entire program. My extended thanks to Dr. Reza Kianoush and Dr. Khaled Sennah for their help to successfully complete the courses during the program.

My special thanks to my colleagues Kavitha, Assim, Shahriar for being so supportive during my masters program at Ryerson.

Last but not the least, it is my family whom I should thank especially my beloved husband Cirosh who had been a motivating force and unconditional support throughout my tenure. Also I am very thankful to my parents for showing the light to liberation through higher education.

TABLE OF CONTENTS

ABSTRACT..... iii
ACKNOWLEDGEMENTS..... iv
TABLE OF CONTENTS..... v
LIST OF TABLES..... ix
LIST OF FIGURES..... x
LIST OF SYMBOLS..... xiv
Chapter 1 Introduction..... 1
1.1 Introduction..... 1
1.2 Scope and objective of the study..... 2
1.3 Thesis organization..... 2
Chapter 2 Fundamental aspects of bond between steel and concrete..... 4
2.1 Introduction..... 4
2.2 Bond stress..... 5
2.3 Components of bond resistance..... 5
2.4 Types of bond strength tests..... 7
2.4.1 Theoretical analysis of pullout tests..... 8
2.5 Bond mechanisms..... 14
2.6 Modes of bond failure..... 18
2.7 Factors affecting bond strength..... 20
2.7.1 Concrete Compressive strength..... 20
2.7.2 Concrete Cover Thickness..... 21
2.7.3 Size of the bar..... 21
2.7.4 Geometry of the rib..... 21
2.7.5 Steel yield strength..... 22
2.7.6 Amount and distribution of transverse steel..... 22
2.7.7 Load history..... 22
2.7.8 Temperature..... 22
2.7.9 Effects of corrosion..... 23
2.8 Bond behavior under cyclic loads..... 24

2.9 Analytical bond models of uncorroded bar in reinforced concrete..... 25
2.9.1 L. Vandewalle and F. Mortelmans (1988)..... 25
2.9.2 Cairns-Abdullah model (1996)..... 28
2.9.3 Lundgren – Gyltoft model (2000)..... 30
2.9.4 Choi - Lee model (2002)..... 33
2.10 Analytical bond models of corroded bar in reinforced concrete..... 37
2.10.1 Lundgren's model (2001)..... 37
2.10.2 Coronelli's model (2002)..... 39
2.10.3 Amleh-Ghosh model (2006)..... 43
2.10.4 Bhargava-Ghosh-Mori-Ramanujam model (2007)..... 46
Chapter 3 General aspects of corrosion in reinforced concrete..... 48
3.1 Introduction..... 48
3.1.1 General definition of corrosion..... 48
3.1.2 Corrosion – An electro chemical process..... 49
3.2 Effects of corrosion on structural performance of reinforced concrete..... 51
3.3 Factors influencing the corrosion of reinforced concrete..... 53
3.3.1 General factors influencing breakdown of passive layer..... 57
3.4 Previous experimental investigation regarding reinforced concrete corrosion..... 58
Chapter 4 Analytical Modeling of Contact pressure at the Interface between Concrete and Reinforcing steel with Uncorroded and Corroded Condition..... 61
4.1. Proposed analytical model for contact pressure..... 61
4.1.1 Assumption for the study..... 63
4.1.2 Derivation of the expression for contact pressure..... 63
4.2 Proposed Analytical Model for Contact pressure in a corroded reinforced Concrete..... 70
4.2.1 Assumptions..... 70
4.2.2 Mechanical behavior of corrosion products..... 70
4.2.3 Terms associated with reinforced bar corrosion..... 71
4.2.4. Reduction in contact pressure..... 72

4.3 Modeling bond-stress at steel-concrete interface..... 75
4.3.1 Friction coefficient at uncorroded steel rebar–concrete interface..... 76
4.3.2 Friction coefficient at corroded steel rebar–concrete interface..... 78
4.4 Numerical Example for reduction in contact pressure due to corrosion..... 79
Chapter 5 General aspects of corrosion in reinforced concrete..... 88
5.1 Specimen Details..... 88
5.2 Material properties of steel..... 89
5.3 Material properties of concrete..... 89
5.3.1 Elastic properties..... 90
5.3.2 Plastic properties..... 90
5.3.2.1 Compressive behaviour..... 90
5.3.2.2 Smeared cracking..... 95
5.4 Finite element modeling..... 99
5.5 Modeling the contact between steel and concrete..... 100
5.5.1 Modeling the contact pressure and friction at the uncorroded steel-concrete interface..... 101
5.5.2. Modeling the contact pressure and friction at the corroded steel-concrete interface..... 101
5.6 Mesh generation..... 102
Chapter 6 Results and discussion of finite element analysis..... 105
6.1 Bond stress-slip relation for the specimen with uncorroded condition..... 105
6.2 Effect of concrete cover thickness on bond strength..... 109
6.3 Comparison with Ghosh (2004) FEA results..... 112
6.4 Bond stress-slip relation for the specimen with corroded condition..... 113
6.4.1 Comparison between FEA and experimental results of corroded Specimen..... 124
6.5 Validation of the model with the results of Al-Sulaimani et al. (1990)..... 125
6.5.1 Pullout tests of Al-Sulaimani et al. (1990)..... 125
Chapter 7 Conclusions and Recommendations..... 127
7.1. Summary and Conclusions..... 127
7.2. Future recommendations..... 128

REFERENCES..... 129
APPENDIX..... 137

LIST OF TABLES

Table 4.1 : Volume of corrosion products..... 71

Table 4.2 : Reduction in contact pressure with increase in depth of corrosion attack... 84

Table 4.3 : Reduction in Bond stress with the reduction in contact pressure due to corrosion..... 86

Table 5.1 : Input data for tension stiffening..... 97

Table 5.2 : Input data for stress ratios and strain ratio..... 99

Table 6.1 : Comparison of bond strength for 50MPa concrete mixtures..... 112

Table 6.2 : Comparison of bond strength for 60MPa concrete mixtures..... 113

Table 6.3 : Percentage loss of average bond strength at different levels of corrosion for 50MPa concrete mixture..... 124

Table 6.4 : Percentage loss of average bond strength at different levels of corrosion For 60MPa concrete mixture..... 125

LIST OF FIGURES

Figure 2.1 : Definitions of bond stress..... 5
Figure 2.2 : Idealized force transfer mechanism..... 6
Figure 2.3 : Stresses in an element..... 9
Figure 2.4 : Tension test..... 16
Figure 2.5 : Typical bond stress-slip relationship..... 17
Figure 2.6 : Splitting failure..... 19
Figure 2.7 : Pullout failure..... 20
Figure 2.8 : Crushing of concrete in front of the lugs..... 24
Figure 2.9 : Steel bar embedded in a concrete cylinder..... 26
Figure 2.10 : Model of a thick-walled cylinder subjected to an internal compression..... 27
Figure 2.11 : Variation of tangential stress with radius of the bar..... 28
Figure 2.12 : Forces acting below bearing face of bar rib..... 29
Figure 2.13 : Resolution of radial bursting forces..... 29
Figure 2.14 : The stress in the inclined compressive struts determines the upper limit..... 31
Figure 2.15 : Physical interpretation of variables t_n, t_t, u_n and u_t 32
Figure 2.16 : The yield lines..... 33
Figure 2.17 : Stresses acting on rib of bar..... 35
Figure 2.18 : Stresses along interface with angle..... 36
Figure 2.19 : Physical interpretation of the variables in the corrosion model..... 37
Figure 2.20 : Corrosion depth (X) and bar expansion (t)..... 39
Figure 2.21 : Corrosion crack patterns: (a) corrosion cracks smaller cover; and
(b) corrosion cracks both sides..... 41
Figure 2.22 : Forces acting at the steel concrete interface..... 45
Figure 3.1 : Basic form of an electrochemical cell..... 50
Figure 3.2 : Mixed electrode in reinforced concrete..... 51
Figure 3.3 : Corrosion induced damage of RC structures..... 52
Figure 3.4 : Stages in Corrosion-induced damage..... 55
Figure 3.5 : Pitting corrosion..... 56
Figure 4.1 : Tensile stress in concrete ring due to the force transfer between steel and

Concrete..... 62
Figure 4.2 : Forces exerted by the concrete on a ribbed bar in a reinforced concrete..... 62
Figure 4.3 : Concrete ring with internal radial pressure..... 63
Figure 4.4 : Concrete pressure acting at the bar lug..... 66
Figure 4.5 : Resolution of radial bursting forces..... 67
Figure 4.6 : Orientation of the rib..... 67
Figure 4.7 : Corrosion depth (X) and bar expansion (t)..... 72
Figure 4.8 : Frictional model for bond..... 75
Figure 4.9 : Friction coefficient as a function of the slip evaluated from tests of Tepfers and Olsson (1992), together with a selected function from Lundgren and Gylltoft..... 76
Figure 4.10 : Friction model for different values of decay coefficients..... 78
Figure 4.11 : Variation of reduction in contact pressure 'V' with the increase in depth of corrosion attack 'x'..... 85
Figure 4.12 : Variation of reduction in bond stress with reduction in contact pressure..... 87
Figure 5.1 : Details of pullout specimen..... 89
Figure 5.2 : Variation of compressive stress with strain for 60MPa concrete..... 92
Figure 5.3 : Variation of compressive stress with strain for 50MPa concrete..... 93
Figure 5.4 : Variation of compressive stress with plastic strain for 60MPa concrete.... 94
Figure 5.5 : Variation of compressive stress with plastic strain for 50MPa concrete.... 94
Figure 5.6 : Tension stiffening model..... 96
Figure 5.7 : Yield and failure surfaces in plane stress..... 98
Figure 5.8 : Finite element model for the pull-out specimen..... 100
Figure 5.9 : Finite element mesh with eight noded solid elements..... 103
Figure 5.10 : Applied boundary condition..... 104
Figure 5.11 : Applied load at the top of the reinforcing bar..... 104
Figure 6.1 : Variation of the average bond stress with slip for 25mm concrete cover for 50MPa concrete mixtures..... 106
Figure 6.2 : Variation of the average bond stress with slip for 25mm concrete cover for 60MPa concrete mixtures..... 106
Figure 6.3 : Variation of the average bond stress with slip for 50mm concrete cover

for 50MPa concrete mixtures..... 107
Figure 6.4 : Variation of the average bond stress with slip for 50mm concrete cover for 60MP concrete mixtures..... 107
Figure 6.5 : Variation of the average bond stress with slip for 75mm concrete cover for 50MPa concrete mixtures..... 108
Figure 6.6 : Variation of the average bond stress with slip for 75mm concrete cover for 60MPa concrete mixtures..... 108
Figure 6.7 : Bond strength ratio versus level of corrosion (different cover thickness and bar diameter (c/d_b) ratio..... 110
Figure 6.8 : Variation of the average bond stress with slip for three different cover thicknesses for 50MPa concrete mixtures..... 111
Figure 6.9 : Variation of the average bond stress with slip for three different cover thicknesses for 60MPa concrete mixtures..... 111
Figure 6.10 : FEM results of the variation of average bond stress with slip at different corrosion levels for 25 mm concrete cover in 50MPa concrete mixture... 114
Figure 6.11 : Comparison of the 'variation of average bond stress with slip' at 2.5% massloss (FEM) Vs 2.53% mass loss (EXP) for 25 mm concrete cover for 50MPa concrete mixture..... 115
Figure 6.12 : FEM results of the variation of average bond stress with slip at different corrosion levels for 50 mm concrete cover in 50MPa concrete mixture... 115
Figure 6.13 : Comparison of the 'variation of average bond stress with slip' at 2.5% massloss (FEM) Vs 2.53% mass loss (EXP) for 50 mm concrete cover for 50MPa concrete mixture..... 116
Figure 6.14 : Comparison of the 'variation of average bond stress with slip' at 5% massloss (FEM) Vs 5.1% mass loss (EXP) for 50 mm concrete cover for 50MPa concrete mixture..... 116
Figure 6.15 : FEM results of the variation of average bond stress with slip at different Corrosion levels for 75 mm concrete cover for 50MPa concrete mixture.. 117
Figure 6.16 : Comparison of the 'variation of average bond stress with slip' at 2.5% massloss (FEM) Vs 2.25% mass loss (EXP)for 75 mm concrete cover for 50MPa concrete mixture..... 118

Figure 6.17 : Comparison of the 'variation of average bond stress with slip' at 5% massloss (FEM) Vs 4.95% mass loss (EXP)for 75 mm concrete cover for 50MPa concrete mixture..... 119
Figure 6.18 : Variation of average bond stress with slip at different corrosion levels for 25 mm concrete cover for 60MPa concrete mixture..... 120
Figure 6.19 : Comparison of the 'variation of average bond stress with slip' at 2.5% massloss (FEM) Vs 2.2% mass loss (EXP) for 25 mm concrete cover for 60MPa concrete mixture..... 120
Figure 6.20 : Comparison of the 'variation of average bond stress with slip' at 5% Massloss (FEM) Vs 3.78% mass loss (EXP)for 25 mm concrete cover for 60MPa concrete mixture..... 121
Figure 6.21 : Variation of average bond stress with slip at different corrosion levels for 50 mm concrete cover for 60MPa concrete mixture..... 121
Figure 6.22 : Comparison of the 'variation of average bond stress with slip' at 2.5% massloss (FEM) Vs 2.85% mass loss (EXP)for 50 mm concrete cover for 60MPa concrete mixture..... 122
Figure 6.23 : Comparison of the 'variation of average bond stress with slip' at 5% massloss (FEM) Vs 7.26% mass loss (EXP)for 50 mm concrete cover for 60MPa concrete mixture..... 122
Figure 6.24 : Variation of average bond stress with slip at different corrosion levels for 75 mm concrete cover for 60MPa concrete mixture..... 123
Figure 6.25 : Comparison of the 'variation of average bond stress with slip' at 2.5% massloss (FEM) Vs 2.65% mass loss (EXP)for 75 mm concrete cover for 60MPa concrete mixture..... 123
Figure 6.26 : Validation of average bond stress with slip at different levels of corrosion..... 126

LIST OF SYMBOLS

φ	= Friction angle between steel and concrete
φ_a	= Maximum size of aggregate
μ	= Coefficient of friction
μ_k	= Coefficient of kinetic friction
μ_s	= Coefficient of static friction
υ_{rs}	= Ratio between the volumes of the corroded and virgin steel
δ	= Angle between face of the rib and the bar axis
γ_{eq}	= Slip
σ_θ	= Tangential stress
σ_c	= Stress in concrete
σ_{crack}	= Residual tensile strength of concrete after cracking
σ_n	= Normal stress
σ_r	= Radial bond stress
σ_s	= Stress in steel
τ	= Bond stress
ε_c	= Concrete strain
ε_{el}	= Elastic strain
ε_{pl}	= Plastic strain
ε_s	= Bar strain
A_c	= Area of concrete
A_r	= Rib area in the plane at right angles to the bar axis
A_s	= Area of steel
c	= Cover thickness
d_c	= Decay coefficient
d_b	= Diameter of the bar
E_c	= Elastic modulus of concrete
E_s	= Elastic modulus of steel
E_{st}	= Modulus of elasticity of stirrups
f_{coh}	= Adhesion strength

f_{ct0} = Concrete tensile strength when crack begins to open

f'_c = Compressive strength of concrete

h_r = Rib height

κ = Experimentally determined coefficient related to fracture energy

L = Percentage loss of contact pressure

M = Percentage massloss of steel bar

n = Number of transverse ribs at a section

P = Contact pressure

P_1 = Contact pressure after corrosion

$P_{corr}(X)$ = Pressure developed by corrosion product expansion

$P^{max}(X)$ = Maximum pressure at anchorage bond failure

P_R = Reduction in contact pressure

r_b = Radius of the bar

R_b = Pure tensile strength

R_{bf} = Bending tensile strength

s_c = Extension of concrete

s_s = Extention of the bar

s_x = Local slip

S_r = Rib spacing

t = Thickness of corrosion products

w = Crack width

X_{cr} = Corrosion depth at the onset of primary cracking

Chapter 1

Introduction

1.1. Introduction

Repair and rehabilitation of existing structures has become a crucial part of civil engineering activities all over the world. Corrosion of the reinforcement is one of the principal reasons for deterioration of reinforced concrete structures from both the safety and economical point of view. The major effects of corrosion in reinforced concrete are the loss of the rebar cross section; increase in bar diameter due to the volumetric expansion of the corrosion products, and variation in the mechanical characteristics of the bar-concrete interface due to the formation of corrosion products and concrete-cover cracking (Coronelli, 2002). Hence, the damage due to the corrosion of reinforcement eventually leads to the structural failure of the whole structure. Therefore, it is necessary to prevent the premature failure of reinforced concrete structures by appropriate controlling and monitoring of reinforcement corrosion.

The forecast of the variations in the mechanical behavior of reinforced concrete structures in the course of their ageing is an important factor in structural design. This may help in the decision to plan the repair of the structure, establish a maintenance program or, to visualize the demolition and reconstruction of the structure. The major electrochemical processes involved in the mechanism of corrosion of the steel are well understood. In spite of various researches carried out to study the effects of corrosion on bond capacity, corrosion induced bond deterioration and its effects on the strength and serviceability of

the structural elements are not perfectly known. By mathematical modeling of the effect of reinforcement corrosion in concrete, it is possible to find out solution for various problems such as the determination of corrosion rate and the actual amount of corrosion, measurement of the reduction in contact pressure at the steel concrete interface and the loss of bond strength due to corrosion etc. A model is a simplified representation of reality, based on hypothesis and equations used to rationalize observations. By providing a rational environment, models can lead to deeper and more general understanding and hence by the use of these models, it is possible to make more accurate predictions.

1.2. Scope and objective of the study

The primary aim of this study is to give a clear picture of the behavior of bond between the reinforcing bar and the surrounding concrete. The main objectives of the research are:

i. to develop a bond model with the influence of contact pressure on the uncorroded reinforcing bar,
ii. to implement the effects of corrosion on the previously developed bond model,
iii. to verify the model with the finite element analysis using ABAQUS, and
iv. to compare the results with the previous experimental results.

1.3. Thesis organization

This report is organized from chapter 1 to chapter 7. Chapter 1 gives a brief introduction and scope and objective of the present study. Some fundamental aspects of bond between steel and concrete is presented in chapter 2. Chapter 3 describes some general aspects of corrosion of concrete. Chapter 4 presents an analytical modeling of contact pressure at

the interface between concrete and reinforcing steel with uncorroded and corroded condition. Finite element modeling of the bond between steel and concrete using the software ABAQUS is described in chapter 5. Results and discussion of the finite element analysis is depicted in chapter 6. Finally, a summary with conclusion and future work are described in Chapter 7.

Chapter 2

Fundamental aspects of bond between reinforcing steel and concrete

A review of the current literature was carried out in order to gain insight into aspects of the bond behavior of a reinforcing steel bar embedded in concrete. In this chapter, possible bond mechanisms are discussed and the results of bond studies carried out by others are presented. It describes the fundamental aspects of bond behavior such as the bond stress, components of bond resistance, failure modes, bond mechanisms and the factors affecting the bond at the steel concrete interface. The stress redistribution and deformations in concrete associated with the bond are also presented.

2.1. Introduction

Bond is defined as the adhesion of concrete or mortar to the reinforcement or to the surface against which it is placed. Bond strength is the resistance to separation of concrete or mortar from the reinforcing steel and other materials to which it is in contact. Bond has also been defined as "that property which causes hardened concrete to grip an embedded steel bar in such a manner as to resist forces tending to slide the bar longitudinally through the concrete" (Raymond and Henry, 1965). In reinforced concrete structures, bond can be considered as an interaction between steel and the surrounding concrete which transfers the stresses that makes it possible to combine the compressive strength of concrete and tensile strength of reinforcement. That is, if the bar gets stressed by a tensile force the bar will try to transfer the stress into the concrete by the bond.

2.2. Bond stress

Bond stress may be considered as a shear stress over the surface of a bar, while this corresponds to some generalization of the actual behavior. More specifically, "Bond stress" is the name assigned to shear stress at the steel interface which, by transferring load between the structural steel and the surrounding concrete, (Lu and Dong, 2006). Normally bond stress can be defined as the stress per nominal unit area of the bar surface (ignores the extra area created by the ribs and lugs of the deformed bar). Bond stress can also be measured by the rate of change of steel stress in the bar. That means there will not be any change in bar stress without bond stress or vice versa. Figure 2.1 below depicts the definition of bond stress where T_i, C_i, M_i and d_i are the tensile force, compressive force, moment and effective depth at section i and ΔL is the length of bar over which bond stress is computed.

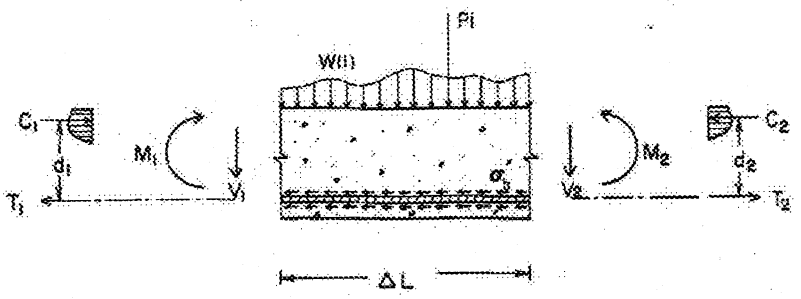

Fig 2.1-Definitions of bond stress (ACI Committee 408, 2005)

2.3. Components of bond resistance

Three bond mechanisms that have been identified as mechanisms in which force is transferred from the reinforcement to the concrete: adhesion, friction and bearing of the lugs against the concrete.

Adhesion is related to the shear strength of steel concrete interface and is mainly due to the chemical bonding between mortar paste and the bar surface. The increase in the applied load causes the loss of adhesion, and eventually the friction and the bearing of the lugs come in to play. For low slip values, adhesion contributes to the bond strength. However, when the slip increases the role of friction and bearing of the lugs to the bond strength also increases. In the case of plain bars mainly chemical adhesion and friction contributes to bond even though there is some mechanical interlocking caused by the roughness of the bar surface. However, the deformed bars have better bond than plain bars, since most of the steel force is transferred through the lugs of the bar to concrete with the increase of slip (Kwak and Filippou, 1990). Figure 2.2 shows the Idealized force transfer mechanism where V_a is the adhesion, V_b is the mechanical anchorage due to bearing of the lug and V_f is the frictional resistance.

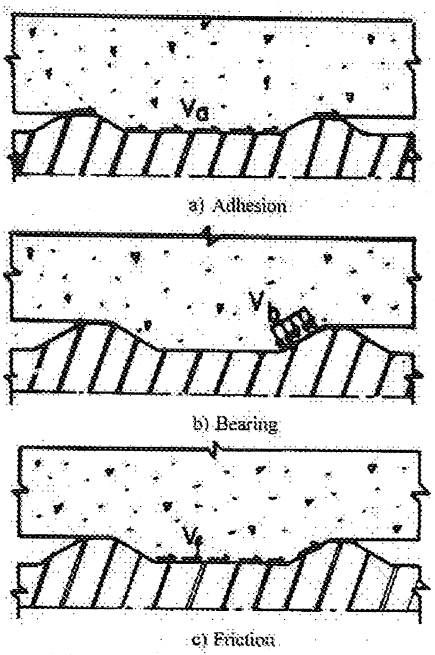

Fig 2.2-Idealized force transfer mechanism (ACI Committee 408, 2005)

Friction is the resistance to a parallel displacement between two surfaces kept in contact by a compressive force perpendicular to the contact plane. However, the bearing of the lugs become significant for the bond between steel and concrete. Concentrated bearing forces in front of the lugs radiate out into the surrounding concrete with a certain inclination. These forces can be split into the direction parallel and perpendicular bar axis. Parallel components induce the bond force and the radial (perpendicular) components induce the circumferential tensile stresses (normal stress or splitting stress) into the surrounding concrete. When these tensile stresses become larger than the tensile strength of the concrete, the bond failure due to splitting occurs if sufficient confinement is not provided (Lundgren, 2005). With sufficient confinement, pull out failure will occur instead of splitting failure.

2.4. Types of bond strength tests

A good overview of the current methods used to determine the bond characteristics of reinforcing bar can be found in ACI Committee 408 (2005) and CEB Task group VI (1981). Bond tests can be classified into three groups: pull-out tests, embedded bar tests and beam tests (Nawy, 1996). Each type of test has its strengths and weaknesses. The main purpose of the bond test is to find out how well the steel transfers the load to the concrete and vice versa under service conditions.

Pullout tests are relatively simple to perform. The steel is cast into a concrete sample to a known length. The steel is pulled upon while the concrete is restrained. This is continued until the steel either yields or is pulled out of the concrete. This test has the advantage of

simplicity and ease of determination of the bond strength. Moreover, it allows the simultaneous measurement of slip between the concrete and the steel. The concrete behaves differently in compression and tension and has little tensile strength and it exhibits cracking at low tensile loads. These aspects are not represented in this type of test.

An embedded bar test consists of a bar extended through a section of concrete. The bar is then pulled at both ends. The concrete will then crack and, based upon the crack spacing and widths, the bond stresses can be determined. This test accurately models the stress field and is relatively simple to prepare. It is difficult to accurately monitor the crack spacing and widths. Moreover, it is rather difficult to interpret the data to give a direct stress.

The aim of the third test known as beam test is to model a section of a beam with a known length of reinforcing steel embedded inside. This is then caused to bend so that the steel and the surrounding concrete are in tension. It is simple to understand and interpret.

2.4.1. Theoretical analysis of pull-out tests

Regardless of the assumed bond stress-slip distribution, equilibrium and compatibility conditions must be satisfied. Consider a reinforced concrete element of length dx (Fig. 2.3) which is located a distance x from the end of the specimen. From equilibrium, the forces on the left hand side of the element, $A_c \bullet \sigma_c + A_s \bullet \sigma_s$, must equal the forces on the

right hand side of the element, $A_c \bullet (\sigma_c + d\sigma_c) + A_s \bullet (\sigma_s + d\sigma_s)$, where A is the area of the material under consideration and σ is the stress. The parameters associated with either the concrete or the steel are denoted by the subscript c and s respectively.

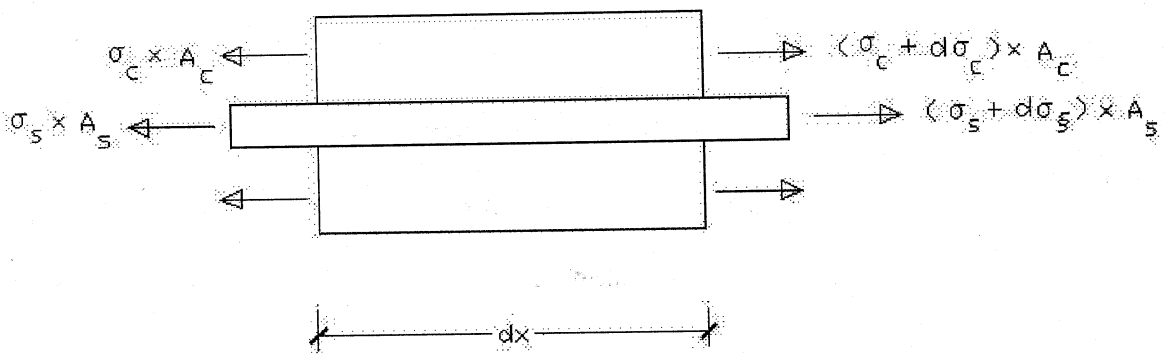

(a) Element length dx with steel and concrete stresses

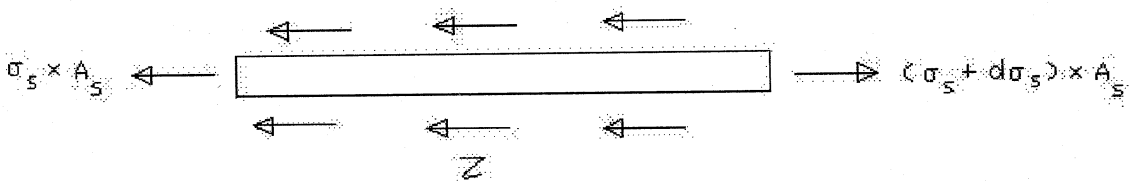

(b) Free body diagram of steel bar of length dx

Fig 2.3-Stresses in an element

$$d\sigma_c.A_c + d\sigma_s.A_s = 0 \qquad (2.1)$$

Equilibrium equations can also be established to describe the relationship between the force in the reinforcing bar and the shear stress, τ, acting at the steel bar/concrete interface as shown in Fig. 2.3.

$$d\sigma_s = \frac{-A_c.d\sigma_c}{A_s} \tag{2.2}$$

Or $$d\sigma_c = \frac{-d\sigma_s.A_s}{A_c} \tag{2.3}$$

Since the shear stress acts over the embedded perimeter of the steel bar, $\pi \bullet d_b \bullet dx$, then:

$$\tau = \frac{A_s.d\sigma_s}{d_b.\pi.dx} \tag{2.4}$$

Hence $$\frac{d\sigma_s}{dx} = \frac{4\tau}{d_b} \tag{2.5}$$

where, d_b is the diameter of the bar,

A_c and A_s area of concrete and steel bar respectively,

σ_c and σ_s are the stresses in the concrete and steel respectively,

$d\sigma_c$ and $d\sigma_s$ are the change in the concrete and steel stresses respectively.

The increment of the local slip, s_x, within an infinitesimal bar length dx at the location x can be defined as the difference between the extension of the bar, s_s, and the concrete extension, s_c, at x.

$$s_x = s_s - s_c \tag{2.6}$$

In addition, since the change in length with respect of the original length is equal to strain, it follows that the difference between the bar strain, ε_s, and the concrete strain, ε_c, is:

$$\frac{d\sigma_s}{dx} = \frac{4\tau}{d_b} \tag{2.7}$$

The value of strain can be related to stress by assuming that concrete and the steel behave elastically. Therefore, Hook's law can be used and the stress is a linear function of the strain.

$$\sigma_s = E_s.\varepsilon_s \quad \text{and} \quad \sigma_c = E_c\varepsilon_c \tag{2.8}$$

where E_s and E_c are the elastic modulus of the steel and concrete respectively.

Submitting Equation (2.8) in Equation (2.7), we have,

$$\frac{dS_x}{dx} = \frac{\sigma_s}{E_s} - \frac{\sigma_c}{E_c} \tag{2.9}$$

The differentiation of the equation (2.9) with respect to x gives:

$$\frac{d^2S_x}{dx^2} = \frac{d\sigma_s}{E_s.dx} - \frac{d\sigma_c}{E_c.dx} = \frac{d\sigma_s}{E_s.dx}\left[1 + \frac{A_s.E_s}{A_c.E_c}\right] \tag{2.10}$$

Substituting for $\frac{d\sigma_s}{dx} = \frac{4\tau}{d_b}$, results in

$$\frac{d^2 S_x}{dx^2} = \frac{1}{E_s} \cdot \frac{4\tau}{d_b}\left[1 + \frac{A_s.E_s}{A_c.E_c}\right] \tag{2.11}$$

Let $k = \frac{4}{E_s.\phi}\left[1 + \frac{A_s.E_s}{A_c.E_c}\right]$, then

$$\frac{d^2 S_x}{dx^2} = k\tau \tag{2.13}$$

As the bond stress is calculated by $\tau = \frac{A_s.d\sigma_s}{d_b.\pi.dx}$, which means that it varies with the change of axial stress resulting from the steel strain. In this case the bond stress includes two zones, one in the elastic zone and the other in the non-elastic zone.

If we consider a constant stress along the total bar length, $\tau = b_1$, where b_1 is constant, resulting in:

$$\frac{d^2 S_x}{dx^2} = kb_1 \tag{2.14}$$

Alternatively, τ can also be directly proportioned to the slip S_x, i.e., $\tau = b_2.S_x$, now the equation is

$$\frac{d^2S_x}{dx^2} = k.b_2.S_x \tag{2.15}$$

and in general

$$\frac{d^2S_x}{dx^2} = k.b_2.S_x^{\,N} \tag{2.16}$$

$\tau = b_3.S_x^{\,N}$, which means that τ is found to be as a non-linear function.

$\frac{d^2S_x}{dx^2} = kb_1$, and by integrating it, we have,

$$\frac{dS_x}{dx} - A_1x + A_2 = 0 \tag{2.17}$$

$$S_x = \frac{A_1x^2}{2} + A_2x + A_3 \tag{2.18}$$

A_1, A_2 and A_3 can be found out by defining the boundary conditions.

The above formulation is a trial for a combination between the slip and the bond stress at any distance x.

Many other studies have been made in order to get a best-fit curve for bond-slip phenomena. However, all these studies were based in one way or another on initial assumptions between the bond stress and the slip.

2.5. Bond mechanisms

The bond effect is more prominent at end anchorages of reinforcing bars and in the vicinity of cracks (Kwak and Filippou, 1990). The reason behind is that the bond stresses in reinforced concrete members occur due to the change in the steel force along the length of the reinforcing steel bar.

In the simplified analysis of reinforced concrete structures, perfect bond means assurance of complete compatibility of strains between concrete and steel. However, in reality, this happens only in regions where negligible stress transfer between two components occurs. In high stress transfer regions along the steel concrete interface, such as near cracks, the bond stress is related to the relative displacement between reinforcing steel and the surrounding concrete. In actual case, no strain compatibility exists between reinforcing steel and surrounding concrete near cracks. This incompatibility and the crack propagation cause a relative displacement, known as bond-slip, between reinforcing bar and concrete. The area under the curve of the bond stress-slip curve can be defined as bond energy (Alavi-Fard and Marzouk, 2004). The bond energy is recommended to be

used to evaluate the bond behavior rather than the maximum bond stress. Bond strength could be improved by selecting a proper lateral bar spacing and adequate concrete cover.

The longitudinal reinforcement of a reinforced concrete element is subjected to axial stress which gets gradually transferred to the surrounding concrete. As a result of this stress transfer a bond stress field is produced around the reinforcing bar, because of its relative slip to the surrounding concrete. When these stresses in the concrete exceed its tensile strength primary cracks are initiated and starts propagating to the reinforced element surface. The bond transfer falls down rapidly with the development of these cracks. Figure 2.4 shown explains this phenomenon in which the results associated to a tensile member test are presented.

Figure 2.5 shows the bond stress-slip behavior due to the evolution of concrete micro cracking around the deformed bar. In the ascending portion of the curve, the crushing of concrete in front of the lugs causes the slip. Up to the point A, the bond resistance occurs due to adhesion, followed by mechanical interlocking between the lugs and concrete. Transverse inclined cracks are created as a result of the generation of tensile stresses around the bar due to the high pressure on concrete in front of the lugs. Therefore, at point B, it modifies the response of concrete to loading as its stiffness is reduced. Splitting longitudinal cracks are caused by the inclined compressive forces spreading from the lugs into concrete. At point C, the cracks reach the concrete surface and the bond resistance will drop to zero, with the absence of sufficient confining reinforcement. However, with the presence of sufficient confinement, the load can be increased further.

Shear cracks are initiated in the concrete keys between ribs at point D which corresponds to the point of maximum bond resistance. Since the shear failure is spreading through the concrete, the bond resistance is decreased with the increasing slip. Hence the frictional resistance of concrete along the failure surface remains the only mechanism that exists at point E.

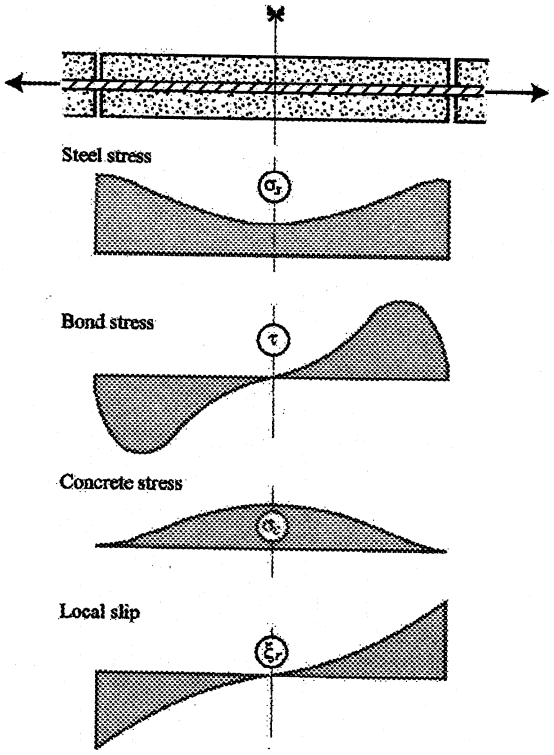

Fig 2.4-Tension test (Tassios and Yannapoulos, 1981)

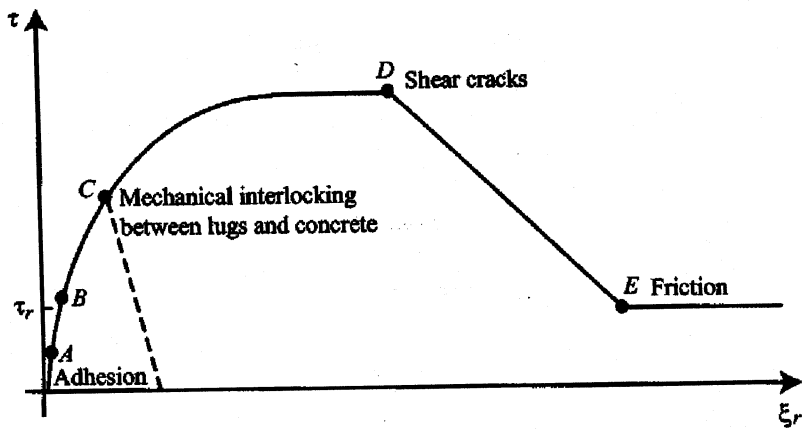

Fig 2.5-Typical bond stress-slip relationship (Girard and Bastien, 2002)

There exist different relationships between the bond stress and slip at different stages of loading. However, for simplicity, all of the bond stress-slip relationships were referred to the moment at which the bond stress reached the peak value. Under any type of loading like static or dynamic, shear mechanism is the most important one for the bond resistance of deformed bars.

For pull out tests, when the bond stress has reached the critical value, a longitudinal tensile stress and a radial tensile stress combined to produce the first internal crack from the tops of the ribs, due to the high stress concentrations in these areas. When the external loading increases, the Poisson effect in the steel causes a decrease in the bar diameter and the contact area between the ribs and the bar reduces. This would increase the bearing stress between the rib and the concrete and boost the crack development around the tip of each rib.

In the case of reinforced concrete structures it is imperative that the bond between the reinforcement and the concrete should exhibit some ductility during dynamic loading so that the dynamic energy can be transferred, absorbed and dissipated to the whole member. This bond ductility can be represented by the fracture energy that can be taken as the work done by the bond stress. The more the ductile bond, more will be the fracture energy.

Experimental studies on reinforced concrete beam–column sub assemblies have shown that perfect bond approximates the actual behavior between steel and concrete only before yielding of steel reinforcement (Elmorsi et al, 2000). Once yielding takes place, the bond resistance deteriorates along the bar portion that has yielded. This deterioration, which is due to cracking at the interface between the reinforcing bars and the concrete, results in a relative slip between them.

2.6. Modes of bond failure

Commonly, the bond failure between steel and concrete is described by two modes, that is, pull-out and splitting failures. If the ratio of concrete cover-to-bar diameter is large or the concrete is well confined, pull out bond failure occurs due to the shearing off of the concrete keys between the bar ribs. Conversely, if the concrete cover is small or the steel bars are closely spaced, tensile splitting cracks tend to develop under the radial component of the rib bearing forces parallel to the steel bars causing premature splitting bond failure as shown in Figure 2.6. The splitting failure occurs when concrete cover is less than approximately three times the bar diameter (Cairns and Abdullah, 1996). For

most structural applications, bond failures are governed by splitting of the concrete rather than by pull-out.

Bond splitting can be divided in to two types. In one type of splitting failure, bearing of the rib shears of a wedge of concrete once the concrete splits. In the other type of splitting failure, the inclined failure surface runs along the interface between the rib and the concrete and not through the concrete. The various factors such as the rib face angle and the surface conditions of the bar etc. will determine which type of splitting mode of failure occur under specific circumstances (Cairns and Abdullah, 1996). The main parameters that influence the average bond strength of developed or spliced bars when the mode of bond failure by splitting include the following: ratio of concrete cover to bar diameter, the development or splice length, the concrete compressive strength, the geometry of the bar ribs, and concrete confinement. Figure 2.7 shows typical pull out failure.

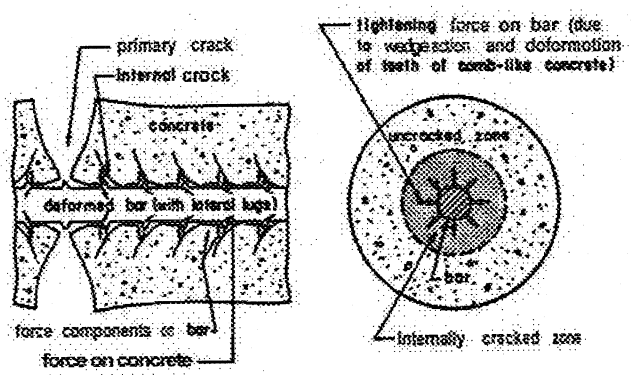

Fig 2.6-Splitting failure (ACI Committee 408, 2005)

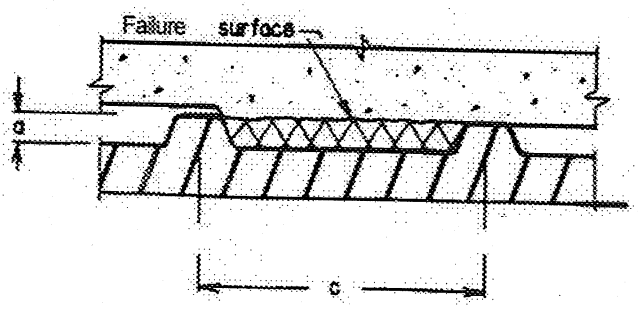

Fig 2.7-Pullout failure (ACI Committee 408, 2005)

2.7. Factors affecting bond strength

There are several factors that influence the bond strength between the reinforcing steel and the concrete. Concrete and steel strengths, bar size and profile, concrete cover thickness, embedment length, spacing of bars, stirrups, temperature, and corrosion are but a few of these factors. A useful review of the factors affecting bond strength is presented in the State-of-the-Art Report by ACI Committee 408 (1992).

2.7.1. Concrete compressive strength

There is general agreement that the concrete strength will have an influence on the bond behavior. Since the force in reinforced concrete is transferred by bearing and bond, and failure can occur by tensile splitting and shearing of the concrete, the compressive strength is considered to be a very important parameter in bond behavior (ACI Committee 408, 2005). It has been found that the bond of high strength concrete is proportional to the compressive strength of concrete (Alavi-Fard and Marzouk, 2002). However, the limited test result indicates that the square root is not the ideal representation for high strength concrete and may be a cubic root expression can be considered for the code equation.

2.7.2. Concrete cover thickness

It was found that the bond failure observed under monotonic loading in laboratory tests dependent on the concrete cover thickness and spacing of the reinforcement. Tepfers (1973), Orangun *et al.*, (1977), and Eligehausen (1979) observed that the concrete cover and the reinforcement spacing significantly influence the type of bond failure. If the concrete cover thickness is small, a splitting tensile failure will occur.

2.7.3 Size of the bar

The area of the reinforcement bar plays an important role in the amount of bond force that needs to be transferred over a certain length. Therefore, the larger the bar size is, the larger the bond forces required. Apart from this, when the bar sizes increases, the apparent ultimate bond stress decreases. Hence, it is better to use several of small bars instead of using a few large bars and maintain a reasonable clear distances between the bars.

2.7.4. Geometry of the rib

Because mechanical interlock between the steel bar ribs and the concrete is the most important bond mechanism, the geometry of the bar rib is of a great importance to the wedging action of these ribs. If the ratio of the bearing area to shearing area, known as 'related rib area' is larger, the bond strength and stiffness will be higher.

2.7.5. Steel yield strength

Since bond stress is directly related to the force in the steel, using lower strength steel will reduce the bond stress demand. According to the ACI Committee 408 (2005) report, it is possible to reduce the bond problems by using bars with 275.8MPa yield strength.

2.7.6. Amount and distribution of transverse steel

The splitting tensile failures are dependent on the amount and distribution of transverse steel (Tepfers, 1973; Orangun *et al.*, 1977; Eligehausen, 1979). After cracking, the properly provided transverse steel confines the concrete. Hence the transverse steel reinforcement effects considerably increase the resistance to a splitting failure, particularly in the case of cyclic loads.

2.7.7. Load history

The load repetitions, rate, frequency and long-term action etc have a significant influence on concrete strength and deformability. Hence they can affect the bond performance considerably. Therefore, the bond stress relationship and the mode of failure are influenced by the load history (Rehm and Eligehausen, 1977; Shah and Chung, 1986).

2.7.8 Temperature

It was shown that the bond strength can be significantly increased at low temperatures (Chang et al., 1986 and 1988). Conversely, at elevated temperatures or after exposing the concrete member to fire, a loss of bond strength can be observed.

2.7.9. Effects of corrosion

In an overview of the published literature, a general consensus about that when the steel bar corrodes, the increased volume of the corrosion products resulted in a "bursting" pressure which causes longitudinal splitting cracks in the specimens, with the crack width increasing with the corrosion level. This results in the breakdown of cohesion, adhesion and friction at the steel-concrete interface, excepting at low corrosion levels, when there is no longitudinal cracking, and the corrosion products have a beneficial effect of improving the bond characteristics at the steel-concrete interface. At higher corrosion levels, the steel bars display localized pitting and loss of some of the ribs over the bar length, thereby weakening the rib-concrete mechanical interlocking force transfer mechanism.

Yoon et al. (2000) expressed that the corrosion reduces the cross sectional area of the reinforcing steel which may cause some stress concentrations in the reinforcing steel, in turn decreasing the ductility of the structures particularly when pitting corrosion occurs.

An examination of the number and spacing of the transverse cracks shows that as the level of corrosion increases, the transverse crack spacing also increases, reflecting the deterioration of bond characteristics at the steel-concrete interface (Amleh and Mirza, 1999).

2.8. Bond behavior under cyclic loads

The repeated loads accelerate the rate of bond deterioration with the stress range or with the increment of the number of cycles as well as reduce the bond strength at failure (ACI Committee 408, 2005). It has been shown that significant deterioration in bond capacity takes place during cyclic loading in high strength concrete (Alavi-Fard and Marzouk, 2002).

In high cycle fatigue where the stress range is within the static elastic range, the failures occur at service loads. However, in low cycle fatigue which is characterized by inelastic stress range, failures occur at loads exceeding the unfactored design capacity of the structure. The main purpose of the low cycle loading situations is not to prevent but to limit the amount of slip and damage to the concrete surrounding the bar. The main mechanism of deterioration in the case of high cycle fatigue appears to be progressive crushing of concrete in front of the lugs as shown in Figure 2.8.

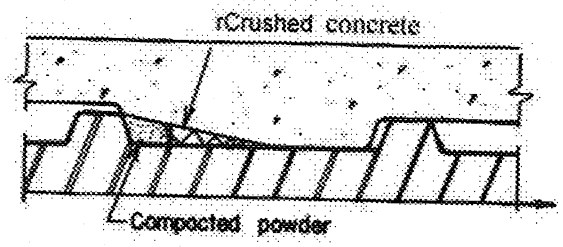

Fig 2.8-Crushing of concrete in front of the lugs (ACI Committee 408, 2005)

In most of the bond fatigue tests, mainly four separate stages are noticeable. The first one is a rapid increase in slip due to initial crushing of concrete; second one is a rapid reduction in the slip rate due to the stabilization of the process; third one is a long portion

with a constant slip rate; and the fourth one is a rapid increase in the slip rate when it approaches the failure.

In the case of steel reinforcing bars, fatigue bond failure takes place by failure of the concrete either by shearing of the concrete between the lugs or by longitudinal splitting of the concrete cover. Bond resistance before failure is basically provided by the bearing of the lugs.

The effect of cyclic loading on the reinforcement in concrete structures is to gradually reduce the bond and to extend the yielding of the bar within the development length region (Mitchell and Marzouk, 2007).

2.9. Analytical bond models of uncorroded bar in reinforced concrete

Review of some bond models, which describes the bond behavior for uncorroded steel bar at the steel-concrete interface, is depicted in this section. The following does not attempt a total review of all of the available models, but rather the results of some models that have an impact on the current research.

2.9.1. Vandewalle and Mortelmans (1988)

When the roughness of the bar is high, the bond stress, which bonds the reinforcement bar to the surrounding concrete, is more. Bond stress (τ)-slip (δ) diagram forms the basis for the calculation of the crack width and crack opening. Bond stress depends on the quality of concrete, the way it is poured (that is, parallel or perpendicular to the axis of

the reinforcement), position of the bar in the concrete (that is, upper or under reinforcement), cover and the diameter of the bar.

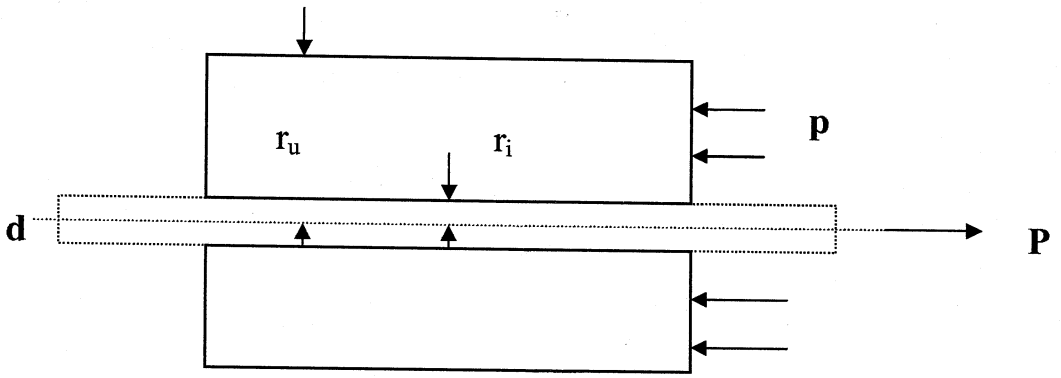

Fig 2.9-Steel bar embedded in a concrete cylinder (Vandewalle and Mortelmans, 1988)

As shown in Figure 2.9, when a pull P is applied on the bar, a pressure p is developed on the front face of the cylinder. With the increment of the force P, at certain moment the bar would be pulled out of the concrete. Then the ultimate bond stress is achieved. For greater value of the length l_d of the concrete cylinder starts yielding before the bond breaks. Therefore for practical reasons, l_d is taken as 3d (3 times the diameter of the bar). When slip happens, either the concrete around the bar crushes more or less or some plastic sliding threshold attains in the concrete. In both cases, it acts as if a radial compression stress σ' acts between the bar surface and the concrete.

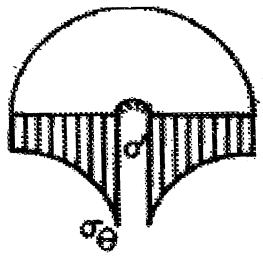

Fig 2.10- Model of a thick-walled cylinder subjected to an internal compression (Vandewalle and Mortelmans, 1988)

According to the theory of elasticity, tangential stress, σ_θ

$$\sigma_\theta = \sigma' \frac{r_i^2}{r_u^2 - r_i^2}\left(1 + \frac{r_u^2}{r^2}\right) \tag{2.19}$$

when σ_θ or σ' reaches its maximum value, failure will occur.

When $r = r_i$, σ_θ is maximum. Failure occurs when σ_θ reaches its ultimate value R_b(pure tensile strength).[that is, σ_θ is always tensile and has a maximum at the inner surface of the cylinder]

$$R_b = \sigma' \frac{r_u^2 + r_i^2}{r_u^2 - r_i^2} \tag{2.20}$$

The maximum bond stress τ_{du} and the radial pressure σ'can be related by Coulomb failure condition as,

$$\tau_{du} = A + B\sigma \tag{2.21}$$

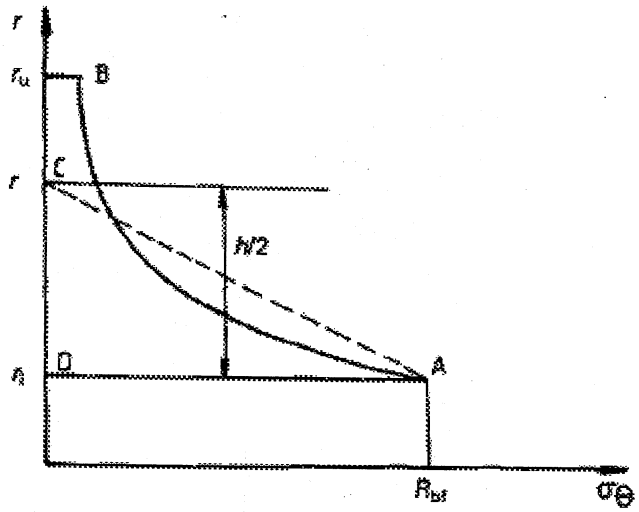

Fig 2.11-Variation of tangential stress with radius of the bar (Vandewalle and Mortelmans, 1988)

where h is the beam height and R_{bf} is the bending tensile strength

2.9.2. Cairns-Abdullah model (1996)

In the proposed model, for non-corroded reinforcing bars, failure was assumed to occur when the shear stress on the interface overcomes friction and adhesion between the rib face and the concrete. Fig 2.12 shows the forces acting below the bearing face of the rib and Fig 2.13 shows the resolution of the radial splitting force. The ultimate bond strength 'τ_{bu}' for non-corroded reinforcing bars is evaluated by the following relationships.

It was assumed that the rib is perpendicular to the bar axis and the face of rib makes an angle δ with the bar axis.

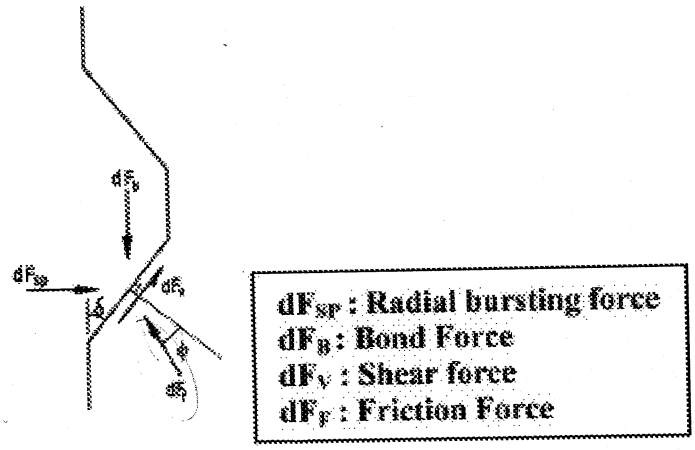

Fig 2.12-Forces acting below bearing face of bar rib (Cairns-Abdullah model, 1996)

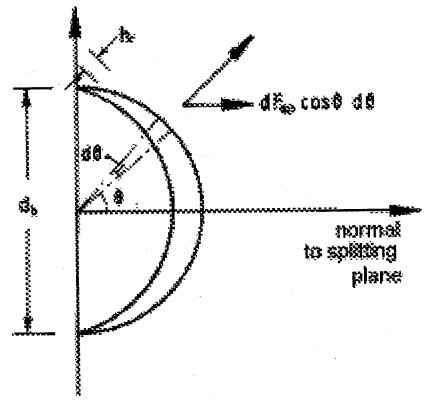

Fig 2.13-Resolution of radial bursting forces (Cairns-Abdullah model, 1996)

$$\tau_{bu} = KP_b^{\max} + \tau_b \tag{2.22}$$

$$\tau_b = \frac{nA_r f_{coh}[\cot\delta + \tan(\delta + \varphi)]}{\pi d_b s_r} \tag{2.23}$$

$$K = nA_r \tan(\varphi + \delta) / \pi n I_r \tag{2.24}$$

where $P_{\max}$ = maximum pressure at bond failure; n = number of transverse ribs at a section; A_r = rib area in the plane at right angles to the bar axis; d_b = initial diameter of

the reinforcing bar; h_r = rib height; f_{coh} = adhesion strength; δ = angle between face of the rib and the bar axis; φ = friction angle between steel and concrete; S_r = rib spacing. Also

$$A_r = \int_{-\frac{\pi}{2}}^{+\frac{\pi}{2}} h_r r_b d\theta$$
$$I_r = \int_{-\frac{\pi}{2}}^{+\frac{\pi}{2}} h_r r_b \cos\theta d\theta \qquad (2.25)$$

2.9.3. Lundgren – Gyltoft model (2000)

Lundgren and Gyltoft (2000) developed a new model to describe the bond between steel and the concrete apt for detailed three dimensional analyses. In this model the splitting stresses and the effect of cyclic loading with varying slip direction are taken in to account and the bond stress depends on the slip as well as radial deformation between the bar and the concrete.

The model is a frictional model which uses the elasto-plastic theory to describe the relations between the stresses and the deformations. The relation between the traction't' and the relative displacements 'u' is expressed in the equation below as

$$\begin{bmatrix} t_n \\ t_t \\ t_r \end{bmatrix} = \begin{bmatrix} D_{11} & \frac{u_t}{|u_t|} D_{12} & 0 \\ 0 & D_{22} & 0 \\ 0 & 0 & D_{33} \end{bmatrix} \begin{bmatrix} u_n \\ u_t \\ u_r \end{bmatrix} \qquad (2.26)$$

where D_{12} normally is negative which implies that the slip in either direction will cause negative t_n, that is, the compressive forces directed outwards in the concrete. The stiffness D_{33} prevents the bar from rotating in the concrete and the traction t_r has no influence on the yield lines.

The yield surface is defined by two yield functions in which one describes the friction F_1 by assuming that the adhesion is negligible and the other one is the yield function F_2 which describes the upper limit at a pullout failure. It is determined from the stress in the inclined compressive struts that results from the bond action as shown in the Figure 2.14.

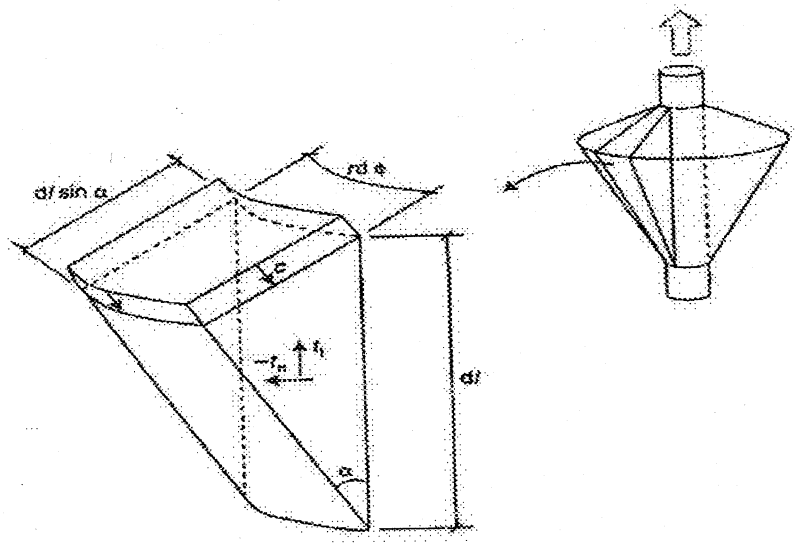

Fig 2.14-The stress in the inclined compressive struts determines the upper limit (Lundgren and Gylltoft, 2000)

$$F_1 = |t_t| + \mu t_n = 0$$
$$F_2 = t_t^2 + t_n^2 + c.t_n = 0 \qquad (2.27)$$

The yield surface is shown in Figure 2.15. For plastic loading an associated flow rule is assumed along the yield function describing the upper limit F_2. A non-associated flow rule is assumed for the yield function describing the friction F_1 for which the plastic part of the deformations is

$$du^p = d\lambda \frac{\partial G}{\partial t},$$
$$G = \frac{|u_t|}{u_t} t_t + \eta t_n = 0 \qquad (2.28)$$

where $d\lambda$ is the incremental plastic multiplier. The yield lines together with the direction of the plastic part of the deformations are shown in Figure 2.16.

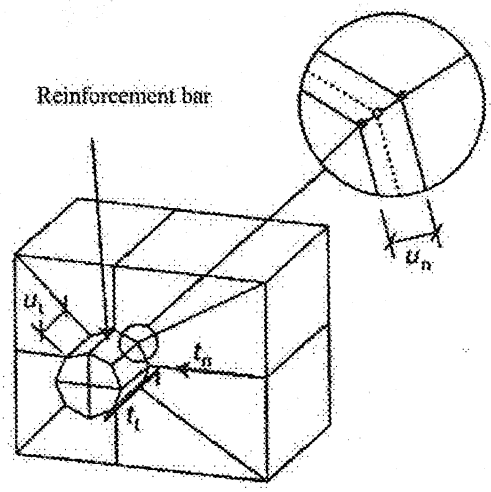

Fig 2.15-Physical interpretation of variables t_n, t_t, u_n and u_t (Lundgren and Gylltoft, 2000)

For the hardening rule of the model, a hardening parameter κ is established as

$$dk = \sqrt{du_n^{p^2} + du_t^{p^2}} \tag{2.29}$$

The variables μ and c in the yield functions are assumed to be functions of k.

According to this model, the bond stress will increase if the pressure around the bar is lost. This model can also be used for cyclic loading.

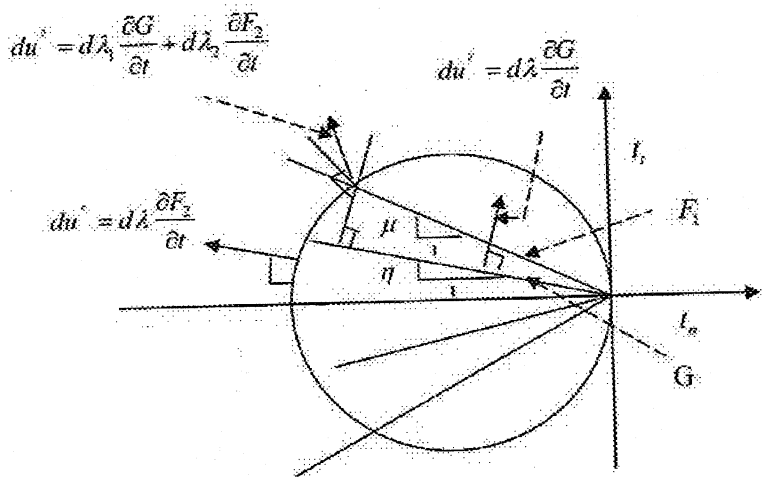

Fig 2.16-The yield lines (Lundgren and Gylltoft, 2000)

2.9.4. Choi - Lee model (2002)

Choi and Lee (2002) presented that when the cover or spacing of bar is inadequate to withstand the lateral concrete tension caused by the wedging action imparted by the bar deformations, the splitting failure in the concrete along the bar occurs. As shown in the

Figure 2.17 below, due to this wedging action bond forces can be resolved into normal stress σ_n and tangential shear stress τ.

Concrete under the bearing side of a rib is known to be in a state of triaxial compression with a major principal stress, the bearing stress σ_q, on the rib acting parallel to the bar axis. Normal to the bearing stress, the minor principal stress s_r acting radially occurs around the bar. The wedging force is applied to the concrete cover and confining bars. Splitting occurs when the wedging force exceeds the ultimate confinement strength of the concrete cover.

Bond force equal to the sum of the bearing stress on the rib area along the bonded length T_1 is given by

$$T_1 = A\frac{l_b}{s_r}\sigma_q \qquad (2.30)$$

where A_r is the projected area of rib parallel to the bar axis and is approximated as equal to $\pi d_b h_r$ where hr is the rib height; l_b / s_r is the number of ribs along the bonded length l_b; and σ_q is the bearing stress on the bar rib acting parallel to the bar axis.

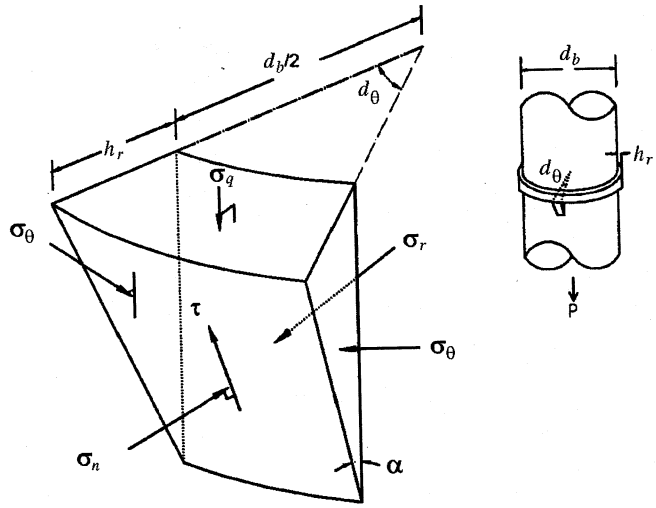

Fig 2.17-Stresses acting on rib of bar (Cairns, 1979)

The frictional force between the concrete and the steel on the inclined surface of the rib may be represented according to Figure 2.18 using the Mohr-Coulomb relation

$$\tau = c + \mu\sigma_n \tag{2.31}$$

where c is the cohesion, μ is the coefficient of friction; and σ_n is the normal stress

A simple expression to predict bond strength is derived to analyze interfacial geometry between ribbed bars and concrete.

$$T = F_x \pi \tan\alpha \frac{(1+\mu\cot\alpha)}{(1-\mu\tan\alpha)} + A_r \frac{l_b}{s_r} \frac{c}{\sin\alpha(\cos\alpha - \mu\sin\alpha)} + \pi d_b l_b c \tag{2.32}$$

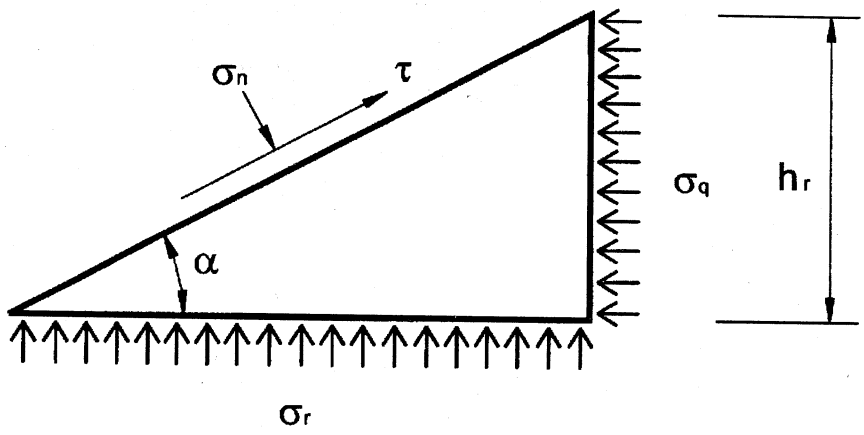

Fig 2.18-Stresses along interface with angle (Choi – Lee, 2002)

The second and third terms of the right side of Eq.2.32 are due to cohesion between the reinforcing bar and the concrete. Those terms show that the bond resistance from cohesion is a function of the projected rib area and the surface area of the embedded bar. Thus, the rib height or rib area affects the bond resistance until adhesion may be lost. Also the coefficient of friction and effective rib face angle are the key variables in determining the bond strength using the above Equation.

The first term of the right part in Eq. 2.32 shows that the mechanical friction component is independent of the relative rib area after the loss of cohesion. Thus, it implies that the relative rib areas have little effect on the bond strength of deformed bars when the bar is only governed by splitting bond failure. Variable F_x in the above Equation is the confining force which is obtained from the finite element study to simulate surface fracture of concrete cover.

2.10. Analytical bond models of corroded bar in reinforced concrete

Review of some bond models which describes the bond behavior of corroded steel bar at the steel-concrete interface is depicted in this section.

2.10.1. Lundgren's model (2001)

Figure 2.19 below (Lundgren 2001), shows the volume increase of the corrosive products compared with the virgin steel. The thickness 'x' is the depth of corrosion attack, which is considered as a function of the time.

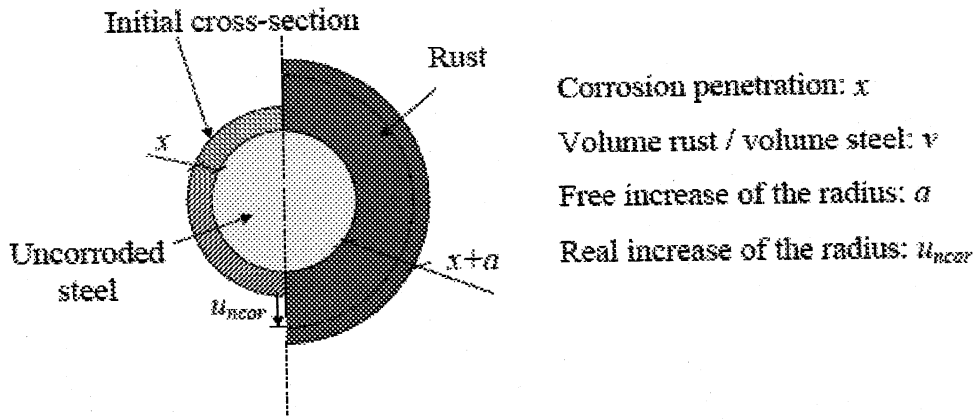

Fig 2.19- Physical interpretation of the variables in the corrosion model (Lundgren's model, 2001)

The volume of the rust is assumed to be 'υ' times the volume of the steel that has corroded (corresponding to the striped area in Fig.2.19). In Figure 2.19 'a' is considered as the free increase of radius if the normal stresses are zero. By equating the volumes in Fig. 2.19, the thickness of 'a' can be determined.

$$\pi(r+a)^2 - \pi(r-x)^2 = \upsilon(\pi r^2 - \pi(r-x)^2 = 0 \tag{2.33}$$

$$a^2 + 2ar + 2xr - x^2 - 2\upsilon xr + \upsilon x^2 = 0 \tag{2.34}$$

$$a^2 + 2ar + (1-\upsilon)(2xr - x^2) = 0 \tag{2.35}$$

Therefore,

$$a = -r + \sqrt{r^2 + (\upsilon - 1)(2xr - x^2)} \tag{2.36}$$

However, the real increase of the radius is u_{ncor} because of the concrete, corresponding to a strain in the rust:

$$\varepsilon_{cor} = \frac{u_{ncor} - a}{x + a} \tag{2.37}$$

From the strain in the rust, the normal stresses in the layer are determined.

The already developed bond model described in section 2.9.3 was combined with the corrosion layer and the deformations are related as:

$$u_n = u_{ncor} + u_{nbond} \tag{2.38}$$

$$u_t = u_{tcor},\ u_{tcor} = 0 \tag{2.39}$$

The corrosion of reinforcement was assumed to influence the coefficient of friction. The coefficient of friction is calculated by introducing a function k(x/r) as described in the equation given below.

$$\mu(k) = k(x/r).\mu_0(k), \text{ but } \mu(k) \geq 0.4 \tag{2.40}$$

2.10.2. Coronelli's model (2002)

Figure 2.20 shown below shows Coronelli's corrosion model

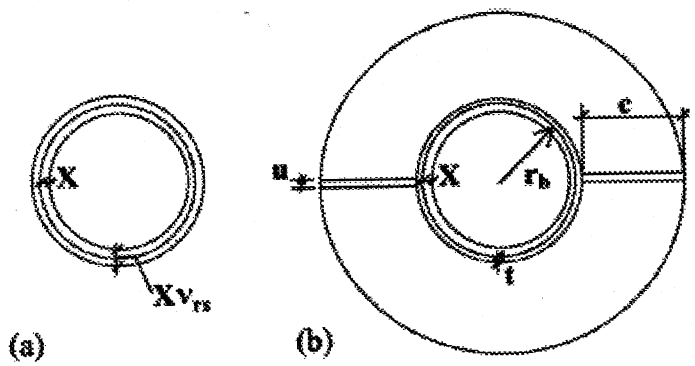

Fig 2.20-Corrosion depth (X) and bar expansion (t) (Coronelli's model, 2002)

A relation between the depth X of the corrosion attack and the total crack width W_{cr} was established by modifying the relationship proposed by Molina et al. (1993)

$$W_{cr} = \sum_i w_i^{cor} = 2\pi(\upsilon_{rs} - 1)X \tag{2.41}$$

$$w = 2\pi(\upsilon_{rs} - 1)\frac{r}{r_b + c}X \tag{2.42}$$

$$w = 2\pi(\upsilon_{rs} - 1)t \tag{2.43}$$

where

$$t = X\frac{r_b}{r_b + c} \tag{2.44}$$

υ_{rs} = ratio between the volumes of the corroded and virgin steel (υ_{rs} = 2 in this paper)

Xcr = corrosion depth at the onset of primary cracking,

w_{icorr} = opening of each single radial crack,

r_b = bar radius,

c = cover thickness,

t = actual thickness of the corrosion-products

Eq. 2.41 was derived by assuming that all corrosion products accumulate around the corroded bar. A modified version of Eq. 2.41 was proposed by Corelli because the corrosion products tend to penetrate into the cracks and reach to the external surface of the cover. The relation between the corrosion attack X and the thickness t was calculated by equating the total volume of the oxides formed per unit length of the bar to that of the layer around the bar (thickness $X + t$) plus that within the cracks (Fig. 2.20(b)).

$$2\pi r_b \vartheta_{rs}(x+t) + 2\pi tc$$
$$t = \frac{r_b(\vartheta_{rs} - 1)}{r_b + c} X \tag{2.45}$$

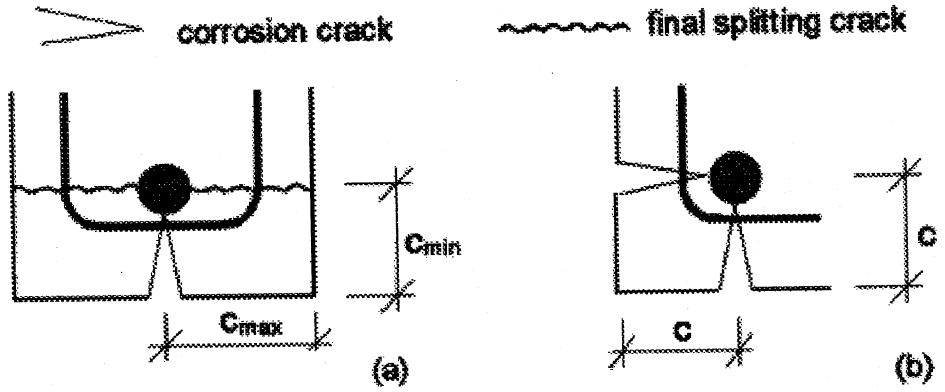

Fig 2.21-Corrosion crack patterns: (a) corrosion cracks smaller cover; and (b) corrosion cracks both sides (Coronelli's model, 2002)

Fig 2.21 shows the crack patterns for different bar positions. Corrosion cracks the smaller cover first. These primary splitting cracks are shown together with the final splitting cracks in Fig. 2.21(a); the latter propagate on loading the bar to bond failure, and correspond to the cracking of the thickest cover. Figure 2.21(b) shows a bar confined by equal cover on both sides; this occurs for corner bars or when the bar is placed in a central position in the cross section. In such cases, the primary crack pattern coincides with that of the final cracks. The final stage is attained when these cracks reach their full propagation. Once the crack width corresponding to a given corrosion level is evaluated by Eq. (2.43) and (2.44), this quantity is used to calculate the corresponding pressure at the bar concrete interface.

The proposed model of Cairns and Abdullah model (1996) for non-corroded reinforcing bars were modified by Coronelli (2002) to include the effects of corrosion of reinforcement. Corrosion-induced modifications include changes in rib angle, rib area and rib shape. Also, the accumulation of expansive corrosion products at the steel-concrete interface affects friction and adhesion stresses acting on the inclined rib face. The ultimate bond strength for corroded reinforcing bars is as follows:

$$\tau_b^{\max} = K(X)P^{\max}(X) + \tau_b^o(X) + \varphi(X)P_{cor}(X) \tag{2.46}$$

Where $P^{max}(X)$ = maximum pressure at anchorage bond failure, $t_b^{\circ}(X)$ = cohesive bond strength contribution, $P_{corr}(X)$ = pressure developed by corrosion product expansion.

The 'μ' and 'f_{coh}' between the corroded reinforcing bar and cracked concrete are proposed by Coronelli (2002) to consider the influence of accumulated rust products on the bar surface.

$$\mu = \tan\varphi = 0.3 - 0.2(X - X_{cr}) \tag{2.47}$$

$$f_{coh} = 2 - 10(X - X_{cr}) \tag{2.48}$$

where 'X' is the corrosion penetration depth ; 'X_{cr}' is the corrosion penetration depth associated with through-cracking of cover concrete.

Furthermore a 5% reduction is adopted for the tangent of the angle $\delta + \varphi$ in Eq.2.47 for a corrosion depth equal to 100 mm: This follows

$$\tan(\delta + \varphi) = 1.57 - 0.785X \tag{2.49}$$

2.10.3. Amleh-Ghosh model (2006)

Amleh and Ghosh (2006) developed a nonlinear finite element model to account for the effect of deterioration of the bond. The non linear finite element program ABAQUS was used to model the deterioration of the mechanical interaction between the corroding reinforcing steel and the concrete. The reduction of the contact pressure and friction at different levels of corrosion was modeled, which helped the computation of the bond stress at the steel–concrete interface for different levels of corrosion with different concrete strengths and cover thicknesses.

The developed equation which shows the relationship between the contact pressure and the concrete cover thickness is given by:

$$p^0 = 0.128c + 1.5 \tag{2.50}$$

where p^0 is the contact pressure and c is the cover thickness.

General equation developed to calculate the loss of contact pressure at different levels of corrosion for different types of concrete mixtures and cover thickness is established as:

$$L = [(-0.00024 f_c^{'} - 0.0028)c + 4.3]M \tag{2.51}$$

where

L= percentage loss of contact pressure,

f'_c = compressive strength of concrete,

c = concrete cover thickness, and

M = percentage massloss of steel rebar

Equation used to calculate the friction coefficient at the uncorroded steel rebar-concrete interface is given by:

$$\mu = \mu_k + (\mu_s - \mu_k)e^{-d_c \gamma_{eq}} \tag{2.52}$$

Equation used to calculate the friction coefficient at the corroded steel rebar-concrete interface is given by:

$$\mu = \mu_k + [(\exp - 0.035M) - \mu_k]\exp - [(0.0261M + 0.45)]\gamma_{eq} \tag{2.53}$$

As shown in Fig. 2.22, the radial force and the vertical component of reaction at the rebar lug cause the contact pressure at the rebar–concrete interface, which was modeled. The bond stress was computed by modeling the normal contact pressure and the friction at the steel–concrete interface and was modeled for both the uncorroded and the corroded states of the bar. Both elastic and plastic properties were assigned to express the non-linear behaviour of the steel and concrete. Eight noded solid elements were used for both the concrete and steel bar and the interface between the steel bar and the concrete was

simulated by using a surface-based interaction with an exponential decay friction factor. A monotonic load was applied on the top surface of the reinforcement, and the top concrete surface of the cylinder was prevented from translating. For each load increment, the slip was computed at the loaded end of the reinforcing steel.

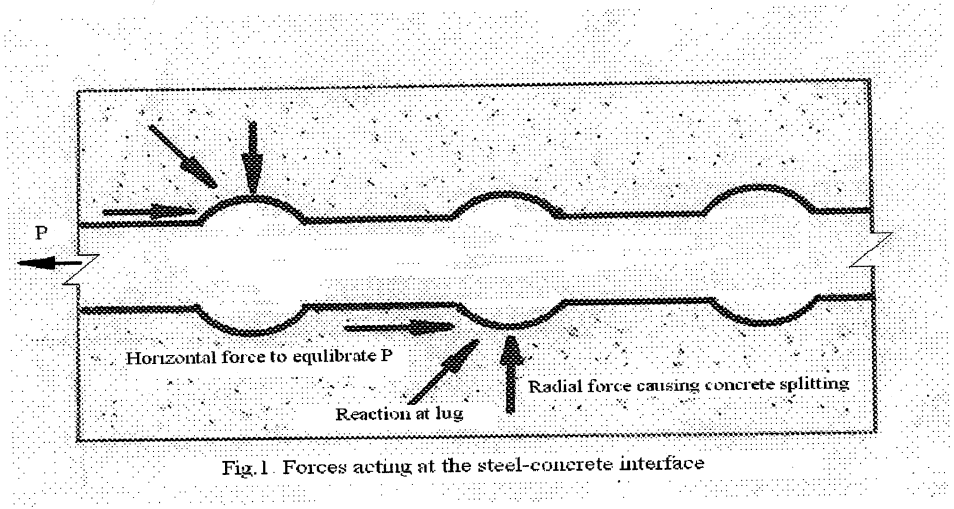

Fig.1 Forces acting at the steel-concrete interface

Fig 2.22-Forces acting at the steel concrete interface (Amleh-Ghosh model, 2006)

From the results, it was found that the contact pressure at the steel–concrete interface decreases rapidly with an increase in the corrosion level, especially in the case of any severe localized corrosion. When the reinforcing steel is corroded, the expanded volume of the corrosion products increases the hoop and radial stresses, which cause longitudinal cracks in the concrete when the tensile strength of concrete is exceeded. With the increase in the level of corrosion, these cracks propagate and their width increases, decreasing the holding capacity of the concrete, which reduces the contact pressure at the steel rebar–concrete interface. Also, the deterioration of the ribs and the reduction of the effective cross-sectional area of the steel bar cause a significant decrease in the contact

pressure because of the flakiness of the corroded layer, the friction at the steel concrete interface reduces.

2.10.4. Bhargava-Ghosh-Mori-Ramanujam model (2007)

The original relationship (Eq. 2.46) for bond strength 'τ_b' given by Coronelli (2002) is slightly modified by Bhargava et al (2007) to account for the corrosion products. The '$\mu(X\text{p})$' and '$f_{coh}(X\text{p})$' between the corroded reinforcing bar and cracked concrete are also proposed as follows to consider the influence of accumulated rust products on the bar surface. These relationships are proposed based on the range of values suggested by Coronelli (2002) for the parameters associated with '$\mu(X\text{p})$' and '$f_{coh}(X\text{p})$'.

$$\tau_b(X_p) = \frac{nA_r(X_p)f_{coh}(X_p)[\cot\delta(X_p) + \tan(\delta+\varphi)(X_p)]}{\pi d_b(X_p)s_r} \tag{2.54}$$

$$\mu(X_p) = \tan\varphi(X_p) = 0.37 - 0.26(X - X_{cr}) \tag{2.55}$$

$$f_{coh}(X_p) = 3.68 - 22.08(X - X_{cr}) \tag{2.56}$$

where 'X' is the corrosion penetration depth corresponding to corrosion level 'Xp'; 'Xcr' is the corrosion penetration depth associated with through-cracking of cover concrete. In addition , the following relationship has been proposed for '$\tan(\delta + \varphi)(X\text{p})$' after considering initial values for 'δ' and '$\tan\varphi$' as 45° and 0.3, respectively for noncorroded reinforcing bar and a 5% reduction in '$\tan(\delta + \varphi)(X\text{p})$' for a corrosion penetration depth of about 100 μm.

$$\tan(\delta+\varphi)(X_p)=1.857-0.9285X \tag{2.57}$$

The maximum pressure at bond failure at any corrosion level '*X*p' is proposed to be evaluated as follows by considering the confining actions due to the residual tensile strength of the cracked concrete and the stirrup legs. The original relationship of Giuriani et al. (1991) has been modified Bhargava et al (2007) to incorporate the effect of corrosion products.

$$P_{\max c}(X_p)=\left[\frac{b}{n_b\{D_r(X_p)+2d_c(X_p)\}}-1\right]f_t(X_p) \tag{2.58}$$

$$P_{\max s}(X_p)=\left[\frac{n_s A_s}{n_b\{D_r(X_p)+2d_c(X_p)\}s_v}\right]\times E_{st}\sqrt{\frac{a_2 w(X_p)^2}{D_s^2\alpha^2}+\frac{a_2 w(X_p)}{D_s\alpha}+a_0} \tag{2.59}$$

$$P_{\max}(X_p)=P_{\max c}(X_p)+P_{\max s}(X_p) \tag{2.60}$$

where b = width of member; n_b = number of reinforcing bars; d_c = thickness of the corrosion products; f_t = residual tensile strength of the racked concrete; w = fictitious splitting crack opening; n_s = number of legs of the stirrups in the cross section width 'b' ; A_s = cross sectional area of the stirrup leg; S_v = spacing of the stirrups; E_{st} = modulus of elasticity of the stirrup steel; a_0, a_1, a_2 = coefficients taken from the reference (Giuriani et al., 1991); α = shape factor characterizing stirrup bar = 2.

Chapter 3

General aspects of corrosion in reinforced concrete

This chapter discusses the fundamental aspects of corrosion in reinforced concrete. Major causes of corrosion, factors influencing corrosion and the effects of corrosion on the structural performance of reinforced concrete are depicted in this chapter. In addition a review of some past experimental findings of reinforced concrete corrosion is also described in this chapter.

3.1 Introduction

In Canada, the cost of monitoring, rehabilitating and replacing our civil infrastructure due to corrosion in reinforced concrete is estimated to be three billion dollars per year (www.infrastructure.gc.ca). Apart from the cost, corrosion is a danger to the structural safety and adversely affects the serviceability of the structure, thereby weakening the system durability. In order to solve these problems of corrosion in reinforced concrete structures, it is better to understand the basics of corrosion.

3.1.1 General definition of corrosion

Corrosion is defined as the deterioration of a substance (usually metal) due to its reaction with the environment (Bosich, 1970). Main principle of corrosion states that all metals are thermo-dynamically and unstable undergoes a reaction with chemical species in the environment, producing stable compounds such as oxides or carbonates. The chemical species are principally oxygen and water.

There are three distinct chemical reactions occur during the corrosion of steel in normal conditions (Joseph, F. Bosich, 1970).

$$Fe \rightarrow Fe^{2+} + 2e^{-} \quad (3.1)$$

$$O_2 + 4e^{-} + 2H_2O \rightarrow 4OH^{-} \quad (3.2)$$

$$2Fe^{2+} + \tfrac{1}{2}O_2 + 4OH^{-} \rightarrow 2FeO.OH + H_2O \quad (3.3)$$

Each of these reactions occurs at different locations in the chemical system.

Reaction [3.1] - The ion dissociates at anode.

Reaction [3.2] - Oxygen and water reacts in the electrolyte producing hydroxide ions.

Reaction [3.3] – Hydroxide ion reacts at the cathode to form corrosion products.

The rate of corrosion of metals in the atmosphere varies greatly with seasonal changes in natural atmospheric conditions, type and extends of pollution, length of time the object remains wet.

3.1.2 Corrosion – An Electrochemical process

The classic approach for understanding of corrosion is an understanding of electrolytic cell. The electrolytic cell can be of two electrodes of dissimilar metals immersed in ionic solutions. An electrical conductor connects electrodes externally and there is a means of the transfer of ions between the solutions. The anode corrodes and the reaction ions are deposited on the cathode. Therefore, the driving force of the corrosion reaction between

metal and environment is electrochemical. Basic form of an electrochemical cell is shown in Fig 3.1. The cell may be easily constructed in a laboratory and is familiar as a form of battery.

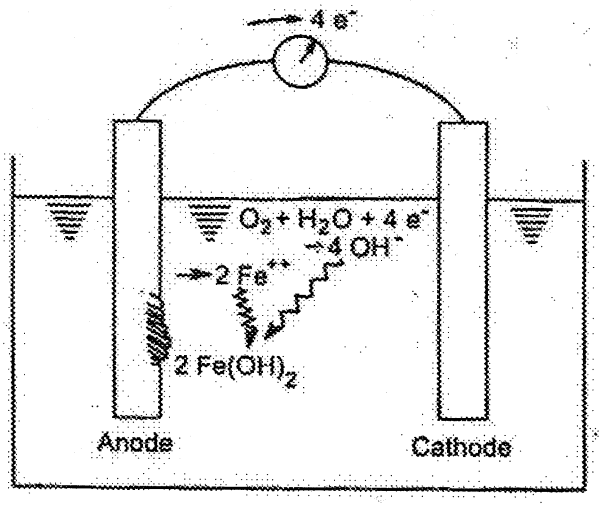

Fig 3.1-Basic form of an electrochemical cell (Richardson, 2002)

The occurrence of mixed electrode, which describes a condition in which the anode and the cathode are on the same material, may occur in reinforced concrete with the existence with the following:

i. The passive film on the reinforcement must be removed locally;

ii. The concrete must be moist enough to act as an electrolyte;

iii. The cover must be permeable to oxygen.

Figure 3.2 shows the formation of anodic and cathodic sites on a reinforcing bar. Metal oxidation occurs at the anode. Electrons are freed and these can flow through the reinforcement to the cathode. The permeability of cover concrete allows moisture to

ingress from the environment and sufficiently saturated states develops at which the moist concrete may function as an electrolyte. Microcell corrosion shown in the Figure 3.2 indicates that one part of the structure may be depassivated and become the anode while much larger area may remain passive and become the cathode. Such high cathode to anode area ratios can lead to very significant increases in corrosion current.

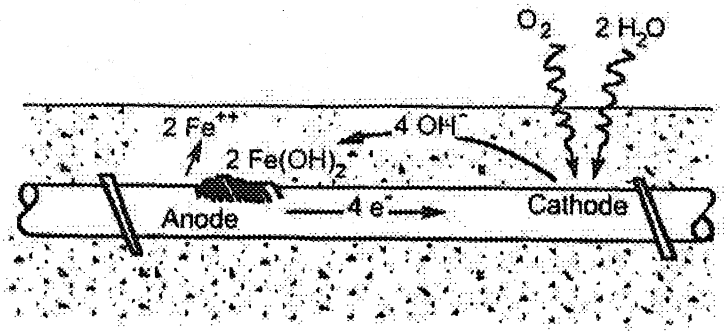

Fig 3.2-Mixed electrode in reinforced concrete (Richardson, 2002)

3.2 Effects of Corrosion on structural performance of Reinforced Concrete

Corrosion results in an early loss of both cohesion and adhesion between the concrete and reinforcing elements. Another variable that affects bond is concrete confinement. Increasing the confinement around a bar increases its bond strength. This is true whether the confinement comes from transverse steel or the stress field that exists in concrete (Kyle et al, 1999).

The structure of the interface between reinforcement and concrete is characterized by interfacial voids and interfacial phases. This structure affects the bond strength between reinforcement and concrete. Corrosion of reinforcing bars alters the interfacial structure thereby varying the bond strength between steel and concrete (Joseph, F. Bosich, 1970).

Corrosion of reinforcing steel will influence the structural performance of a reinforced concrete section in two ways: loss of steel section and deterioration of steel-concrete bond (Kyle et al, 1999). Foremost, there will be steel section loss due to rust. The rust being a brittle weak substance, does not participate in load sharing. Therefore the amount of load steel can take, reduces in proportion to steel mass loss (Yoon et al, 2000). In addition reduction cross-sectional area of reinforcing steel may cause stress concentrations in the reinforcing steel, decreasing the ductility of the structure, especially when pitting corrosion occurs (Yoon et al, 2000).

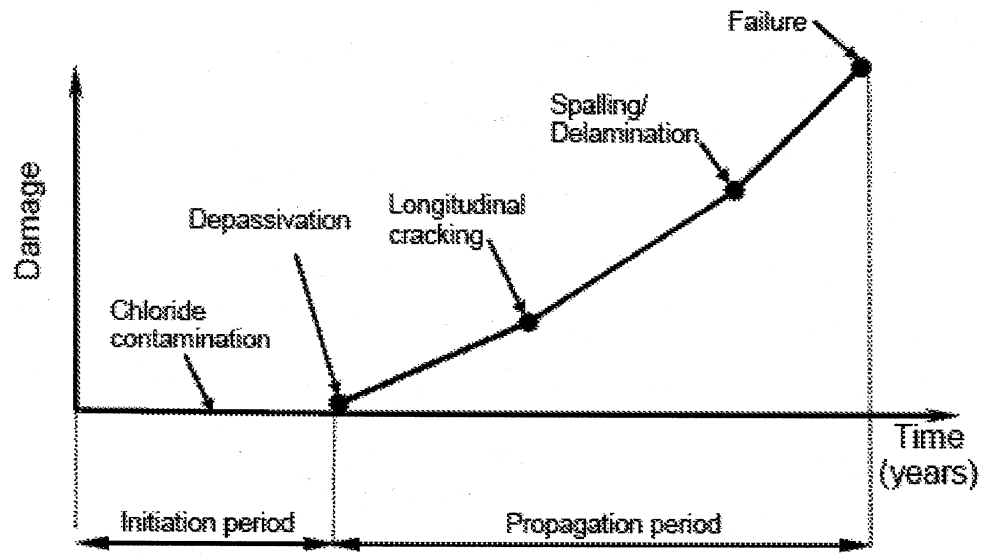

Fig 3.3- Corrosion induced damage of RC structures (Zhou et al, 2005)

The second influence of corrosion on structural performance is the deterioration of steel-concrete bond, resulting in cracking and spalling (Kyle et al, 1999). At first, corrosion of steel in reinforced structures leads to the formation of expansive products, which can have a dual mechanical effect. The formation of small amounts of these oxides can

locally reduce the concrete porosity, protect the reinforcement and eventually increase the concrete or rebar bond strength (Kyle et al, 1999). However, further increase in the corrosion level results in generating tensile stresses in the concrete surrounding the reinforcing steel, which leads to concrete cracking. Thus, formed cracks can reduce the overall strength and stiffness of the concrete structure. Moreover, these cracks can increase the ingress of aggressive ions, yielding further cracking as well as resulting in concrete deterioration. The longitudinal and transverse cracking can cause a release in the hold of the concrete to the rebar and decreases the bond capacity at the steel concrete interface. Consequently, the normal contact pressure at the rebar-concrete interface decrease. The production of large quantities of corrosion products may result in local expansions. From there, cracking, spalling and delamination of the concrete take place, resulting in failure of the structure as shown in Figure 3.3 (Zhou et al, 2005).

3.3. Factors influencing the corrosion of reinforced concrete

Steel reinforcement has a natural tendency to corrode if access to oxygen is possible in a moist environment. The durability of reinforced concrete requires conditions in which the dissolution of metal atoms is not supported and that the reinforcement be inaccessible to oxygen and moisture. Two self-defensive mechanisms are employed to achieve this. The first involves naturally occurring protective film on the reinforcement, which requires certain conditions for its survival. The second involves cover concrete of sufficient depth and impermeability. Regarding the first issue, the high pH level of fresh concrete leads to the formation of a passive skin on the surface of reinforcement. The skin prevents corrosion occurrence by preventing contact with oxygen and moisture. The passive film

may be broken down in time through carbonation or chloride ingress. Regarding cover, the rate of corrosion depends on the rate at which oxygen and moisture may penetrate the cover. This has two-fold influence: 1) oxygen and moisture are required to feed the process; 2) the concrete must be moist enough to have electrical resistance that is low enough to allow the creation of an electrochemical cell.

In the case of ferrous reinforcement the compounds formed through corrosion are hydrated iron oxides, for example, ferrous hydroxides $Fe(OH)_2$, ferric hydroxide $Fe(OH)_3$ and a secondary reaction forms rust. The initial reaction is generally the formation of ferrous hydroxide and the secondary reaction produces a form of rust dependent on the environmental conditions. Schematic descriptions are as follows (Richardson, 2002).

$$2Fe(OH)_2 + O_2 \rightarrow FeOOH \tag{3.4}$$

$$2FeOOH \rightarrow \alpha Fe_2O_3 + H_2O \tag{3.5}$$

$$4Fe(OH)_2 + O_2 + 2H_2O \rightarrow 4Fe(OH)_3 \tag{3.6}$$

$$4Fe(OH)_3 \rightarrow 2Fe_2O_3.H_2O + 4H_2O \tag{3.7}$$

The resulting oxide has a lower density than the parent metal and so a volume increase occurs when a mass of metal is replaced by the new compound. This leads to particular problems to reinforced concrete structures. Corroding reinforcement in concrete not only loses valuable cross sectional area but the concrete may also have to accommodate the increased volume of iron oxides produced. The resulting rust may occupy a volume between two and five times that of parent steel. If this cannot be accommodated

expansive pressures result. The low tensile strength of concrete may be exceeded by the pressure caused through build-up of even a microscopically thin layer of corroding reinforcement (Richardson, 2002). Cracking may result and further development to the stage of delamination and spalling is not uncommon where depth of cover is low. The various stages of this phenomenon are illustrated in Figure 3.4. The precise form of damage to the concrete depends on the bar diameter, bar spacing, and the depth of cover (Richardson, 2002). The first sign of distress could be pop outs or long thin cracks along the line of the reinforcement.

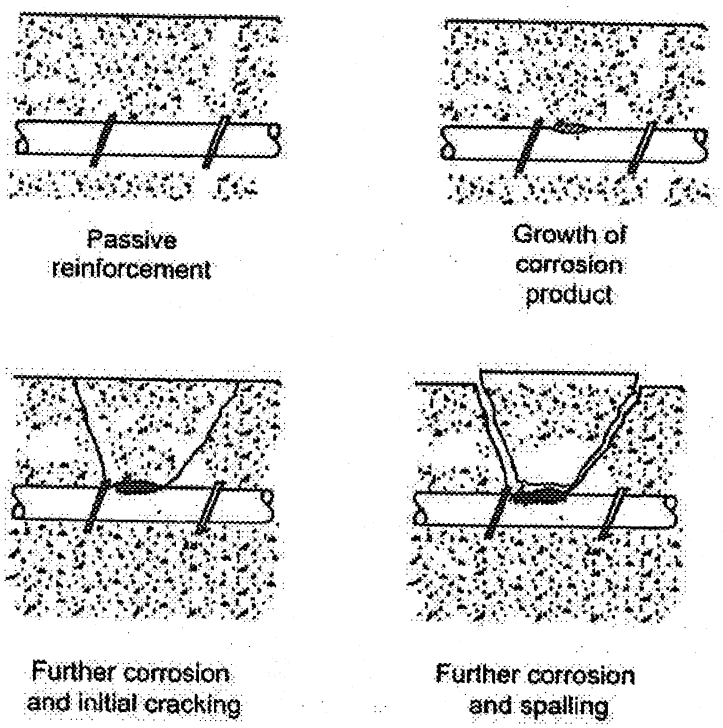

Fig 3.4-Stages in Corrosion-induced damage (Richardson, 2002)

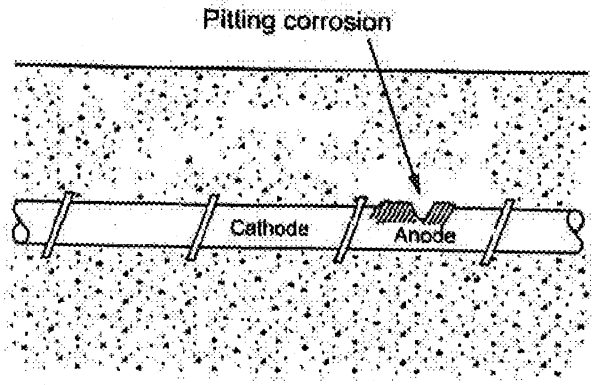

Fig 3.5-Pitting corrosion (Richardson, 2002)

A form of attack described as 'pitting corrosion' may also occur, as illustrated in Figure 3.5. A pit develops on the reinforcement surface, and the loss of effective cross-section is very significant compared to that occurring where there is general corrosion on the complete perimeter (Richardson, 2002). This form of deterioration can occur where small anodic sites are in combination with a large cathodic area. Such conditions can occur where moisture conditions vary across a structure, due to drainage conditions or leaking joints, leading to localized anodic sites. The mechanism of attack is usually related to the presence of chlorides and is dependent on the relative amount of chloride and hydroxide ions. If the chloride ions predominate, the loss of Fe^{2+} ions is accelerated and a pit develops. If the OH^- ions predominate, one gets precipitation of $FeOH^+$ which repairs the passive oxide film on the reinforcement. The loss of cross section in pitting corrosion can occur rapidly and critically reduce the load bearing capacity of the reinforced concrete member (Richardson, 2002).

3.3.1. General factors influencing the breakdown of passive layer

The following factors are the principal ones that cause the breakdown of passive layer.

1. Physical damage to the concrete surrounding the steel caused by impact or abrasion. It can allow the ingress of moisture and chemicals into the concrete down to the rebars. Carbon dioxide in the air causes carbonation of the concrete which reduces the pH of the concrete to about 9.5 (Kyle et al, 1999).
2. Macro cracks, due to shrinkage or stress, if extend down to the steel, can lead to the breakdown of the oxide film leading to corrosion of the reinforcement.
3. High permeability or high porosity surrounding the steel.
4. Inadequate thickness of the cover coat of concrete cover to resist the ingress of aggressive agents.
5. Carbonation causes the breakdown of oxide coating. Carbonation refers to the reaction between the carbon dioxide and alkalis in the pores of the cement paste. As a result of these reactions, pH in the pores of the cement paste decreases(even below pH 9) (Kyle et al, 1999) and conditions are no longer susceptible for maintaining the passive oxide coating on the steel reinforcement and the steel becomes susceptible to corrosion. The penetration of the 'carbon front' depends up on the quality of the concrete such as water-cement ratio and hydration and the degree of saturation of the pores in the cement paste. Penetration rate is low for dry concrete and also for saturated concrete and it is maximum when the concrete is in equilibrium with ambient humidities between 40% and 80% (Kyle et al, 1990)

6. The presence of chloride ions also break down the passive layer. This break down happens when the chloride ions reaches a threshold value.

Therefore there is no single minimum value of chloride ion that will break down the passive film. In the United States (Kyle et al, 1999), the general guideline is 0.2% of acid soluble chloride by mass of cement, but others suggest that it is 0.4%. The term 'acid-soluble' refers to the chloride ion content measured when the solution is prepared in acid solution. There is a controversy over whether the threshold value is based on water soluble or acid soluble chlorides.

3.4. Previous experimental investigation regarding reinforced concrete corrosion

Amleh and Mirza (1999) conducted an experimental investigation to evaluate the structural behavior of concrete elements and structures suffering from steel corrosion by studying the influence of corrosion on the progressive deterioration of bond between the concrete and the reinforcing steel with increasing levels of corrosion. The results indicated that corrosion, especially when severely localized, causes a significant reduction of the interlocking forces between the ribs and the concrete keys due to the deterioration of the reinforcing bar ribs. This results in the deterioration of the primary mechanism of the bond in deformed bars and hence, the bond strength decreases significantly. The associated decrease in the tension stiffening with an increase in the corrosion level signifies the initiation of bond breakdown, which is very much influenced by the surface conditions of the bar and the level of its adhesion and cohesion to the surrounding concrete.

Auyeung et al. (2000) conducted some experimental program to evaluate the bond strength and bond-slip behaviour of reinforcement bars corroded to various levels. They observed that small amount of corrosion increases both the bond strength and bond stiffness, but the slip at failure decreases considerably. However, when the steel mass loss exceeds 2%, bond strength and stiffness decreases considerably and the slip at failure decreases exponentially. Also it was observed that even when there is extensive corrosion with considerable cracking of concrete, bond is not completely destroyed. It was found that measurable bond strength exists even when the mass loss approaches 6% which partially explains the fact that structures with extensively corroded reinforcement sometimes sustain considerable loads.

Lazar and Gérard (2000) proposed an accelerated corrosion procedure for testing the mechanical behavior of rust formed at the steel-concrete interface. When these corrosion products were identified using X-rays diffraction, the main products recognized were akagenite (βFe(OOH)), the magnetite (Fe_3O_4) and goethite(α Fe(OOH)), which are similar to the products of natural corrosion. Using the scratching test, they have reached a conclusion about the mechanical behavior of the oxides as rust is a cohesionless assemblage of incompressible crystals.

Wang et al (2000) investigated the interactions among loading level, corrosion rate, and residual strength of reinforced concrete beams observed that as the degree of reinforcing steel corrosion increased, the failure mode of the reinforced concrete beams shifted from

a shear failure to bond splitting, which resulted in the slip and pullout of the reinforcing bar.

Maaddawy et al. (2005) reported the results of an experimental program to investigate the combined effect of corrosion and sustained loads on the structural performance of reinforced concrete beams. Test results showed that the presence of a sustained load and associated flexural cracks during corrosion exposure significantly reduced the time to corrosion cracking and slightly increased the corrosion crack width. The presence of flexural cracks during corrosion exposure initially increased the steel mass loss rate and, consequently, the reduction in the beam strength.

Chapter 4

Analytical modeling of contact pressure at the interface between concrete and reinforcing steel with uncorroded and corroded condition

An analytical model, which describes the contact pressure at the steel-concrete interface in a reinforced concrete, is developed. The effect of corrosion is then implemented in the already developed model to determine the reduction in contact pressure due to corrosion. This chapter illustrates the procedure involved in developing the expression for the contact pressure at the bar-concrete interface with and without corrosion.

4.1. Proposed analytical model for contact pressure

Tepfers (1979) studied theoretically the circumferential stress distribution over the thick-walled cylinder confining the reinforcing bar. These circumferential tensile stresses are caused by the outward stresses from the action of the deformed bar on the cylinder as shown in Figure 4.1 below. That is, whenever there is a force transfer between the steel and concrete (i.e. when bond forces exist), the stress rings shown in Fig 4.1 occur around the reinforcing bars. The radial components of the bond forces are balanced against the rings of tensile stress in the concrete. The forces exerted by the concrete on a ribbed bar in a reinforced concrete are shown in Figure 4.2.

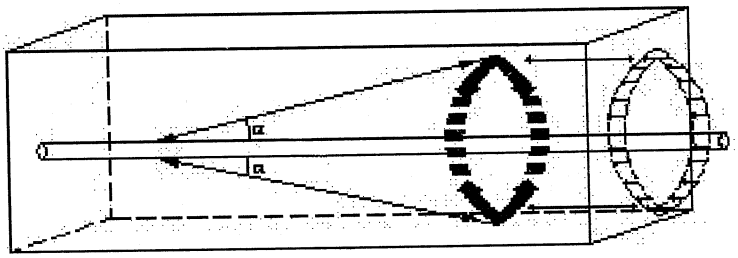

Fig 4.1-Tensile stress in concrete ring due to the force transfer between steel and concrete (Tepfers, 1979)

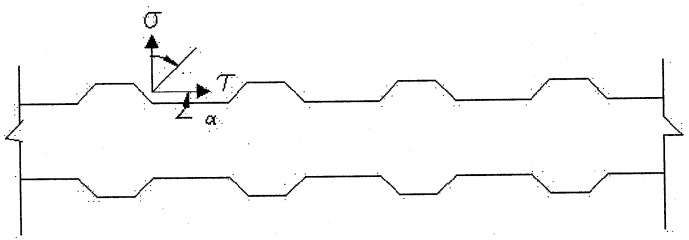

Fig 4.2-Forces exerted by the concrete on a ribbed bar in a reinforced concrete (Tepfers, 1979)

The bond stresses, along the surface of the reinforcing bar, can be divided into radial and tangential components. The bond forces between a deformed reinforcing bar and the concrete make an angle α with the bar axis.

As shown in Figure 4.2, the radial bond stress component,

$$\sigma = \tau \tan\alpha \tag{4.1}$$

4.1.1. Assumption for the study

The radial pressure σ due to bond action on the concrete can be regarded as hydraulic pressure acting on a thick-walled concrete ring as shown in Figure 4.3(a).

4.1.2. Derivation of the expression for contact pressure

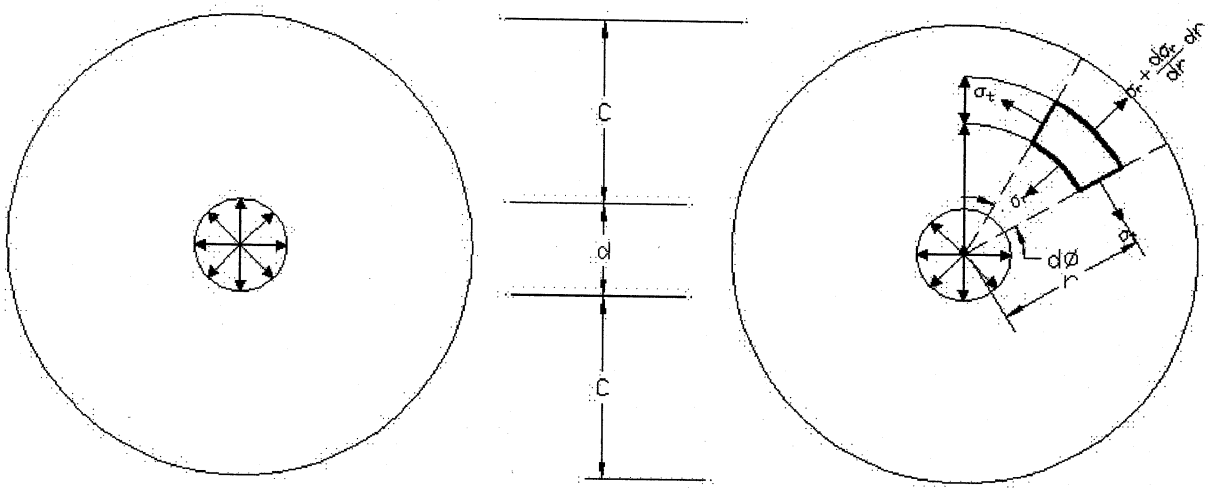

(a) (b)

Fig 4.3-Concrete ring with internal radial pressure

Using the Figure 4.3(b), the radial bond stress σ_r at a distance r from the centre of a thick walled concrete cylinder can be calculated by using the formula given by Timoshenko (1956) as,

$$\sigma_r = \frac{\left(\frac{d}{2}\right)^2 \sigma}{\left(c+\frac{d}{2}\right)^2 - \left(\frac{d}{2}\right)^2}\left[1 - \frac{\left(c+\frac{d}{2}\right)^2}{r^2}\right] \tag{4.2}$$

where c = concrete cover

d = the diameter of the bar

r = radial distance of the element from the centre of the cylinder

σ = the hydraulic pressure acting on a thick walled ring

Substituting the value of σ taken from equation (4.1) in to equation (4.2) gives:

$$\sigma_r = \frac{\left(\frac{d}{2}\right)^2 \tau \tan\alpha}{\left(c+\frac{d}{2}\right)^2 - \left(\frac{d}{2}\right)^2}\left[1 - \frac{\left(c+\frac{d}{2}\right)^2}{r^2}\right] \tag{4.3}$$

Now, the radial stress acting at the interface between the steel and the concrete is obtained by substituting $r=d/2$ in equation (4.3) would lead to:

$$\sigma_r = \frac{\left(\frac{d}{2}\right)^2 \tau \tan\alpha}{\left(c+\frac{d}{2}\right)^2 - \left(\frac{d}{2}\right)^2}\left[1 - \frac{\left(c+\frac{d}{2}\right)^2}{\left(\frac{d}{2}\right)^2}\right]$$

and

$$\sigma_r = \frac{\left(\frac{d}{2}\right)^2 \tau \tan\alpha}{\left(c+\frac{d}{2}\right)^2 - \left(\frac{d}{2}\right)^2}\left[\frac{\left(\frac{d}{2}\right)^2 - \left(c+\frac{d}{2}\right)^2}{\left(\frac{d}{2}\right)^2}\right]$$

and

$$\sigma_r = \frac{-\left(\frac{d}{2}\right)^2 \tau \tan\alpha}{\left(c+\frac{d}{2}\right)^2 - \left(\frac{d}{2}\right)^2}\left[\frac{\left(c+\frac{d}{2}\right)^2 - \left(\frac{d}{2}\right)^2}{\left(\frac{d}{2}\right)^2}\right]$$

Therefore,

$$\sigma_r = -\tau \tan\alpha \tag{4.4}$$

Equation (4.4) implies that the pressure exerted by the concrete at the interface between steel and concrete is balanced by the radial pressure exerted by the steel bar at the interface. Therefore,

$$\sigma_r = -\sigma_{concrete} \tag{4.5}$$

Figure 4.4. below shows the pressure exerted by the concrete at the bar lug.

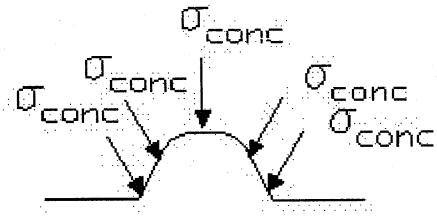

Fig 4.4-Concrete pressure acting at the bar lug

It was proved by Guiriani and Rosati (1986) that the pressure exerted by the concrete at the interface between the steel and the concrete is obtained by the equation,

$$\sigma_{concrete} = \frac{f_{ct0}}{\left(\kappa \frac{d_b}{\phi_a} \frac{w}{d_b} + 1\right)} \tag{4.6}$$

where,

f_{ct0}= concrete tensile strength when crack begins to open, i.e., when crack width, w=0

κ = experimentally determined coefficient related to fracture energy

φ_a= maximum aggregate size

d_b= diameter of the principal bar

Consider a small area dA of a rib face of a segment of the reinforcing bar as shown in Figure 4.5. while Figure 4.6 shows the orientation of the rib.

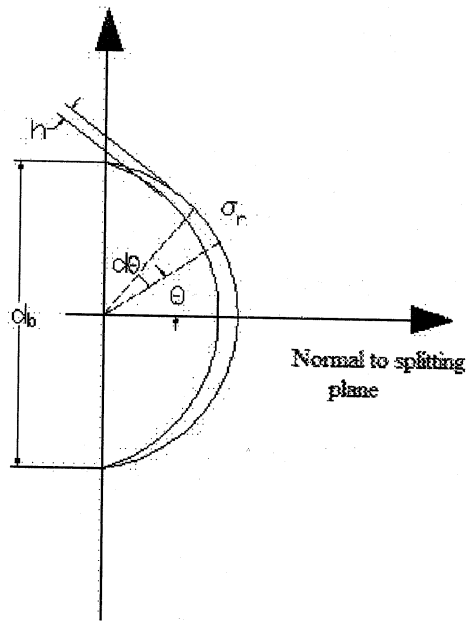

Fig 4.5-Resolution of radial bursting forces (Cairns-Abdullah model, 1996)

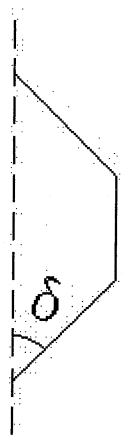

Fig 4.6-Orientation of the rib (Cairns-Abdullah model, 1996)

Area of the lug, $dA = h_r \frac{d_b}{2} d\theta$ (4.7)

where

h_r= rib height

d_b= bar diameter

θ = radial angle which the segment dA makes with the normal to the splitting plane.

The contact pressure, which is normal confining pressure exerted by the surrounding concrete on the bar surface, can be taken as the resultant of all the forces acting at a single bar lug as shown in Figure 4.4. Therefore, the contact pressure:

$$P = \int_{-\frac{\pi}{2}}^{+\frac{\pi}{2}} \sigma_r dA \cos\theta d\theta = \int_{-\frac{\pi}{2}}^{+\frac{\pi}{2}} \sigma_{concrete} dA \cos\theta d\theta \tag{4.8}$$

$$P = \int_{-\frac{\pi}{2}}^{+\frac{\pi}{2}} \frac{f_{ct0}}{\left(\kappa \frac{w}{\phi_a} + 1\right)} h_r \frac{d_b}{2} \cos\theta d\theta \tag{4.9}$$

$$P = \frac{f_{ct0}}{\left(\kappa \frac{w}{\phi_a} + 1\right)} \int_{-\frac{\pi}{2}}^{+\frac{\pi}{2}} h_r \frac{d_b}{2} \cos\theta d\theta \tag{4.10}$$

Let

$$I = \int_{-\frac{\pi}{2}}^{+\frac{\pi}{2}} h_r \frac{d_b}{2} \cos\theta d\theta \tag{4.11}$$

Then the Contact pressure

$$P = \frac{f_{ct0}}{\left(\kappa \frac{w}{\phi_a} + 1\right)} I \tag{4.12}$$

I = the lug area calculated considering the rib height in the direction at right angles to the splitting plane.

Substituting $d_b/2 = r_b$ and integrating the equation 4.11, the lug area I can be rewritten as:

$$I = h_r r_b [\sin\theta]_{-\frac{\pi}{2}}^{+\frac{\pi}{2}} \tag{4.13}$$

$$I = 2 h_r r_b \tag{4.14}$$

Substituting the value of I in Equation 4.11, the contact pressure P can be rewritten as:

$$P = 2 \frac{f_{ct0}}{(k \frac{w}{\varphi_a} + 1)} h_r r_b \tag{4.15}$$

When the crack width w = 0, the equation 4.15 for the contact pressure can be written as,

$$P = 2 f_{ct0} h_r r_b \tag{4.16}$$

4.2. Proposed analytical model for contact pressure in a corroded reinforced concrete

In general, three significant phenomena influence the deterioration of the bond strength due to the corrosion of the reinforcing steel: With increasing corrosion levels, especially in the case of severe pitting corrosion (localized corrosion), the bond behaviour is strongly influenced by the severely deteriorated reinforcing bar ribs; The effect of the formation of the corrosion products along the steel reinforcing bar surface. Furthermore, this layer of corrosion products also breaks down the friction mechanism, except for low levels of corrosion. The reduced adhesion and cohesion between the reinforcing bar and the concrete are due to the widening of the longitudinal splitting cracks.

4.2.1. Assumptions

Uniform corrosion

- In the case of uniform corrosion the depth of corrosion attack is assumed to be consistent along the reinforcing bar length.
- It is assumed that the rib height of the bar remains the same irrespective of the reduction in bar diameter.

4.2.2. Mechanical behavior of corrosion products

When a steel bar corrodes inside the reinforced concrete, depending on the environmental conditions, different corrosion products form. Generally, the main corrosion products that form are listed in the Table 4.1 below.

Table 4.1-Ratio of the volume of corrosion products

Corrosion product	Colour	Ratio, □
Fe_3O_4	Black	2.1
$Fe(OH)_2$	White	3.8
$Fe(OH)_3$	Brown	4.2
$Fe(OH)_3, 3H_2$	Yellow	6.4

4.2.3. Terms associated with reinforced bar corrosion

Let the initial radius of the bar be r_b. Once the bar corrodes, accumulation of corrosion products increases the bar radius to a value r_b+t where t is the thickness of the corrosion layer. The thickness of the corrosion products layer can be determined using the equation proposed by Corronelli (2002) (Figure 4.7):

$$t = \frac{(\upsilon - 1)xr_b}{r_b + c} \tag{4.17}$$

where

x = depth of corrosion attack

c = thickness of the concrete cover

$r_b = r$ = radius of the bar

υ = ratio of the volume of rust to the volume of steel that has corroded (varies from numerical value 2 to 6 depending on the type of corrosion products formed). Table

4.1 above shows the value of υ for different corrosion products (Palle Thoft-Christensen, 2001).

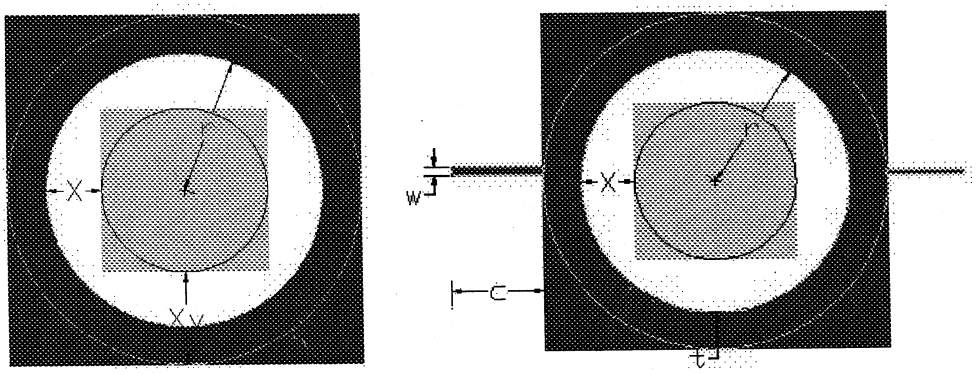

Fig 4.7-Corrosion depth (X) and bar expansion (t) (Coronelli's model, 2002)

4.2.4. Reduction in contact pressure

As a result of the corrosion of the steel bar, an additional corrosion layer with thickness 't' is introduced at the interface between the steel and the concrete and the actual effective radius of the bar is reduced due to the depth of corrosion attack equal to 'x'. Therefore, after corrosion, the net effective radius of the bar can be taken as equal to r_b-x. The actual area of contact between the concrete and the bar reduces due to the existence of this additional layer formed. This flaky corrosion layer may not take part in the load transfer between steel and the concrete because it has been proved from the experiments that the corrosion products behaves like a granular material and it corresponds to the findings that the corrosion products are cohesionless assemblage of incompressible crystals. Therefore, it can be concluded that the reduction in effective radius of the bar due to this existence of this flaky corrosion layer at the interface and the expansion of

cracks in concrete will cause a reduction in the contact pressure between the reinforcing steel and the surrounding concrete.

The reduction in contact pressure (P_R) due to the introduction of an additional corrosion layer can be determined by using the equation given below.

$$P_R = \sigma_{crack} \int_{-\frac{\pi}{2}}^{+\frac{\pi}{2}} (r_b + t) h_r \cos\theta d\theta - \sigma_{crack} \int_{-\frac{\pi}{2}}^{+\frac{\pi}{2}} (r_b - x) h_r \cos\theta d\theta \qquad (4.18)$$

In equation (4.18), the first term represents the contact pressure at the steel concrete interface due to the increment in bar radius equal to 'r_b+t' as a result of the additional corrosion layer 't'. The second term represents the net effective contact pressure which takes part in the load transfer after corrosion. Therefore the difference of these two terms can be the reduction in contact pressure due to corrosion of the reinforcing steel bar. The equation (4.18) can be rewritten as,

$$P_R = \sigma_{crack} \left[(r_b + t) h_r \int_{-\frac{\pi}{2}}^{+\frac{\pi}{2}} \cos\theta d\theta - (r_b - x) h_r \int_{-\frac{\pi}{2}}^{+\frac{\pi}{2}} \cos\theta d\theta \right] \qquad (4.19)$$

Integrating equation 4.19, reduction in contact pressure can be rewritten as,

$$P_R = \sigma_{crack} \left[(r_b + t) h_r [\sin\theta]_{-\frac{\pi}{2}}^{+\frac{\pi}{2}} - (r_b - x) h_r [\sin\theta]_{-\frac{\pi}{2}}^{+\frac{\pi}{2}} \right]$$

$$P_R = \sigma_{crack}\left[(r_b + t)h_r\left[\sin(\frac{\pi}{2}) - \sin(-\frac{\pi}{2})\right] - (r_b - x)h_r\left[\sin(\frac{\pi}{2}) - \sin(-\frac{\pi}{2})\right]\right]$$

$$P_R = \sigma_{crack}\left[(r_b + t)h_r[1-(-1)] - (r_b - x)h_r[1-(-1)]\right]$$

$$P_R = 2\sigma_{crack}\left[(r_b + t)h_r - (r_b - x)h_r\right] \tag{4.20}$$

where

h_r = height of the rib

σ_{crack} = residual tensile strength of concrete after cracking,

$$\sigma_{crack} = \frac{f_{ct0}}{\left(\kappa\frac{d_b}{\phi_a}\frac{w}{d_b} + 1\right)} \tag{4.21}$$

where,

f_{ct0} = concrete tensile strength when crack begins to open, i.e., when crack width, w=0

κ = experimentally determined coefficient related to fracture energy

Φ_a = maximum aggregate size

d_b = diameter of the principal bar

w = crack width = $2\pi t$ (coronelli, 2002)

Contact pressure after corrosion can be calculated as the difference between the contact pressure before corrosion and the reduction in contact pressure due to corrosion.

Hence, Contact pressure after corrosion, $P_1 = P - P_R$ (4.22)

4.3. Modeling bond-stress at steel-concrete interface

As shown in Figure 4.8 below, bond stress which can be defined as the shear stress which develops along the lateral surface of the bar, is a function of the normal confining pressure exerted by the surrounding concrete on the bar surface. The basic relationship between bond-stress (τ), contact pressure P and coefficient of friction (μ) at the steel-concrete interface proposed by J. Pantazopoulou and S. P. Tastani (2002) can be expressed as,

$$\tau = \mu P \tag{4.23}$$

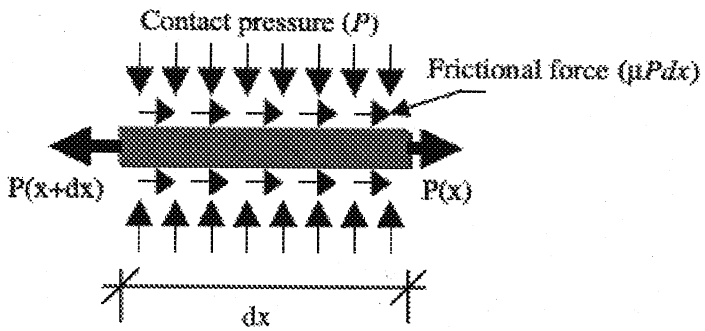

Fig 4.8-Frictional model for bond

According to the figure above, when the normal contact pressure is large, higher frictional force will be required for the pullout and higher resistance also will be there for splitting failure to occur.

4.3.1. Friction coefficient at uncorroded steel rebar–concrete interface

Lundgren and Gylltoft (2000) developed a relationship between the friction coefficient and the slip using some test results of Tepfers and Olsson (1992). It can be observed from the figure that the value of μ_s =1 and μ_k=0.4.

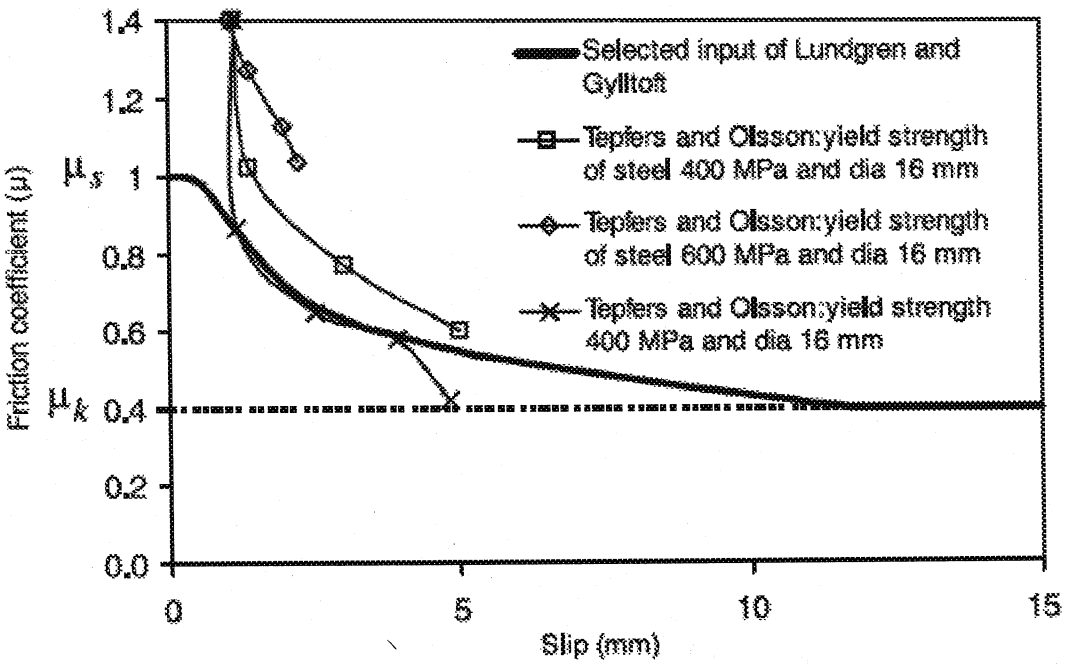

Fig 4.9-Friction coefficient as a function of the slip evaluated from tests of Tepfers and Olsson (1992), together with a selected function from Lundgren and Gylltoft (2000)

It is assumed that the friction coefficient decays exponentially from the static value to the kinetic value according to the equation 4.24 given below:

$$\mu = \mu_k + (\mu_s - \mu_k) e^{-\mathbf{d}_c \gamma_{eq}} \tag{4.24}$$

where

μ_k is the coefficient of kinetic friction (the friction coefficient at the highest slip rate)

μ_s is the coefficient of static friction (the friction coefficient that opposes the initiation of slipping from a static condition (the static friction coefficient corresponds to the value at zero slip),

d_c is a user-defined decay coefficient,

γ_{eq} is the slip

Figure 4.10 shows the variation of friction coefficient with slip for different values of the decay coefficient. It can be observed from the figure that the curve with $d_c = 0.45$ matches well the Lundgren and Gylltoft (2000) curve.

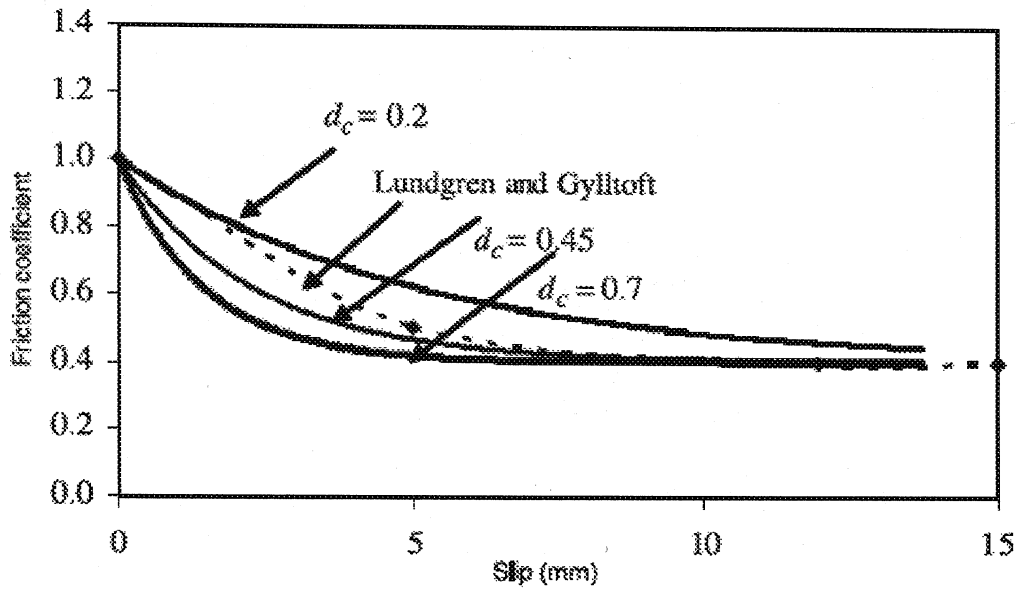

Fig 4.10-Friction model for different values of decay coefficients (Lundgren and Gylltoft, 2000)

4.3.2. Friction coefficient at corroded steel rebar–concrete interface

The flaky layer of rust performs as lubricant and reduces the friction at the steel-concrete interface. The kinetic friction coefficient is consistent and the static friction coefficient decreases with the mass loss. Parametric studies conducted by Ghosh (2004) can be used to evaluate the relationship between the static friction coefficient and mass loss and also variation of the decay coefficient with mass loss. Equations 4.25 and 4.26 show the variation of the static friction coefficient and the decay coefficient at different mass losses.

$$\mu_s = \exp - 0.035M \tag{4.25}$$

$$d_c = 0.0261M + 0.45 \tag{4.26}$$

Hence, the equation for the friction coefficient (μ) can be written as

$$\mu = \mu_k + [(\exp - 0.035M) - \mu_k]\exp - [(0.0261M + 0.45)]\gamma_{eq} \tag{4.27}$$

Now, substituting into Eq. (4.22) and (4.27) into Eq. (4.23) gives the bond stress after corrosion

$$\tau = \mu P_1 = \mu_k + [(\exp - 0.035M) - \mu_k]\exp - [(0.0261M + 0.45)\gamma_{eq}]P_1 \tag{4.28}$$

4.4. Numerical example for reduction in contact pressure due to corrosion

Consider a reinforced concrete beam having 20mm bar diameter and 75mm thick concrete cover. Let the maximum size of the aggregate used be 15mm and the experimentally determined coefficient related to fracture energy is 167. The concrete tensile strength before the crack begins is taken as 1.346MPa. When corrosion occurs, the thickness of the corrosion products formed is taken as't' as a result of the depth of corrosion attack 'x'. The volume of corrosion products formed is assumed to be 'υ' times (here, υ is takes as equal to 4) the volume of original volume of the reinforcing steel that has corroded. Calculate the reduction in contact pressure and the bond stress.

Calculation of reduction in contact pressure

Reduction in contact pressure, $$P_R = 2\sigma_c[(r_b + t)h_r - (r_b - x)h_r] \quad (4.4.1)$$

Width of crack, $$w = 2\pi t \quad (4.4.2)$$

Thickness of corrosion products, $$t = \frac{(\vartheta - 1)xr_b}{r_b + c} \quad (4.4.3)$$

Cracked tensile strength of concrete, $$\sigma_c = \frac{f_{ct0}}{\left(k\frac{w}{\varphi_a} + 1\right)} \quad (4.4.4)$$

where

r_b= bar radius in mm

t = thickness of corrosion products in mm

h_r= height of the rib in mm

x = depth of corrosion attack in mm

w = crack width in mm

υ = ratio of specific volumes of rust to the steel

c = concrete cover in mm

f_{ct0}= concrete tensile strength when crack begins to open, i.e., when crack width, w=0

κ = experimentally determined coefficient related to fracture energy

φ_a= maximum aggregate size

By substituting the value of't', Eq (5.4.2) becomes

$$w = 2\pi \frac{(\vartheta - 1) x r_b}{r_b + c} \tag{4.4.5}$$

Assume, k = 167 and φ_a = 15mm and f_{ct0} = 1.346MPa (Giuriani et al, 1991), Eq (4.4.4) becomes

$$\sigma_c = \frac{f_{ct0}}{\left(k\frac{w}{\varphi_a} + 1\right)} = \frac{1.346}{11.13w + 1} \tag{4.4.6}$$

Also, assume r_b = 10mm, h_r = 1, C = 75mm and υ = 4, Eq (5.4.3)

$$t = \frac{(4-1) \times x \times 10}{10 + 75} = \frac{6}{17} x$$

$$w = 2\pi \times \frac{6}{17} x = \frac{12}{17} \pi x$$

When x= 0.1mm,

$$t = \frac{6}{17} \times 0.1 = 0.035\,\text{mm}$$

$$w = 2 \times \pi \times 0.035 = 0.22\,\text{mm}$$

$$\sigma_c = \frac{1.346}{(11.13 \times 0.220 + 1)} = 0.3903\,\text{MPa}$$

$$P_R = 2 \times 0.3903[(10 + 0.035)1 - (10 - 0.1)1] = 0.1054\,\text{MPa}$$

Calculation of Bond stress

Bond stress, $f_b = \mu P$ (4.4.7)

Friction coefficient, $\mu = \mu_k + (\mu_s - \mu_k)e^{-d_c \gamma_{eq}}$ (4.4.8)

Contact pressure before corrosion, $P = \frac{f_{ct0}}{\left(\frac{k}{\varphi_a} w + 1\right)} \int_{\frac{\pi}{2}}^{\frac{\pi}{2}} h_r r_b \cos\theta d\theta$ (4.4.9)

$$P = \frac{1.346}{(11.13 \times 0.22 + 1)}(2 \times 1 \times 10) = 21.92\,\text{MPa}$$

When corrosion occurs, there will be slight variation with the values of static friction coefficient μ_s and the decay coefficient d_c and μ_k= 0.4. Assume slip, γ_{eq}= 0.01

$$\mu_s = \exp - 0.035M \quad (4.4.10)$$

$$d_c = 0.0261M + 0.45 \quad (4.4.11)$$

When the depth of corrosion attack, x = 0.1, mass loss M=0.5%

$$\mu_s = \exp - 0.035 \times \frac{0.5}{100} = 0.9998$$

$$d_c = 0.0261 \times \frac{0.5}{100} + 0.45 = 0.4501$$

Coefficient of friction, $\mu = \mu_k + (\mu_s - \mu_k)e^{-d_c \gamma_{eq}}$ (4.4.12)

$$\mu = 0.4 + (0.9998 - 0.4)e^{-0.4501 \times 0.01}$$

Reduction in contact pressure due to corrosion, $P_R = 0.1054$ MPa

Contact pressure after corrosion, $P_1 = P - P_R = 23.92 - 0.1054 = 21.8146$ MPa

Bond stress after corrosion, $\tau = \mu P_1 = 0.9971(23.8146) = 23.7455$MPa

Similarly, the above calculations and equations were used to calculate the reduction in contact pressure and the bond stress for different depth of corrosion attack, x, ranging between 0.1 to 0.9, and the following results were generated. Table 4.2 shows the increase in the values of reduction in contact pressure 'P_R' with the increase in depth of corrosion attack 'x'.

Table 4.2-Reduction in contact pressure with increase in depth of corrosion attack

Depth of corrosion attack, x in mm	Thickness of corrosion products, t in mm	crack width, w in mm	Cracked tensile strength of concrete, σ_c in MPa	Reduction in contact pressure, P_R in MPa
0.1	0.035	0.22	0.3903	0.1054
0.2	0.071	0.446	0.2257	0.1223
0.3	0.106	0.666	0.16	0.13
0.4	0.141	0.886	0.1239	0.1341
0.5	0.176	1.106	0.1011	0.1367
0.6	0.212	1.332	0.0851	0.1382
0.7	0.247	1.552	0.0737	0.1396
0.8	0.282	1.772	0.065	0.1407
0.9	0.318	1.998	0.0579	0.141

Figure 4.11 below shows the variation of reduction in contact pressure 'P_R' with the increase in depth of corrosion attack 'x'. The plotted graph shows a non linear increment in the reduction in contact pressure with the depth of attack. Hence, from the graph, it can be concluded that the developed expression fits very well with the actual situation, that is, contact pressure decreases with the increase in depth of corrosion attack.

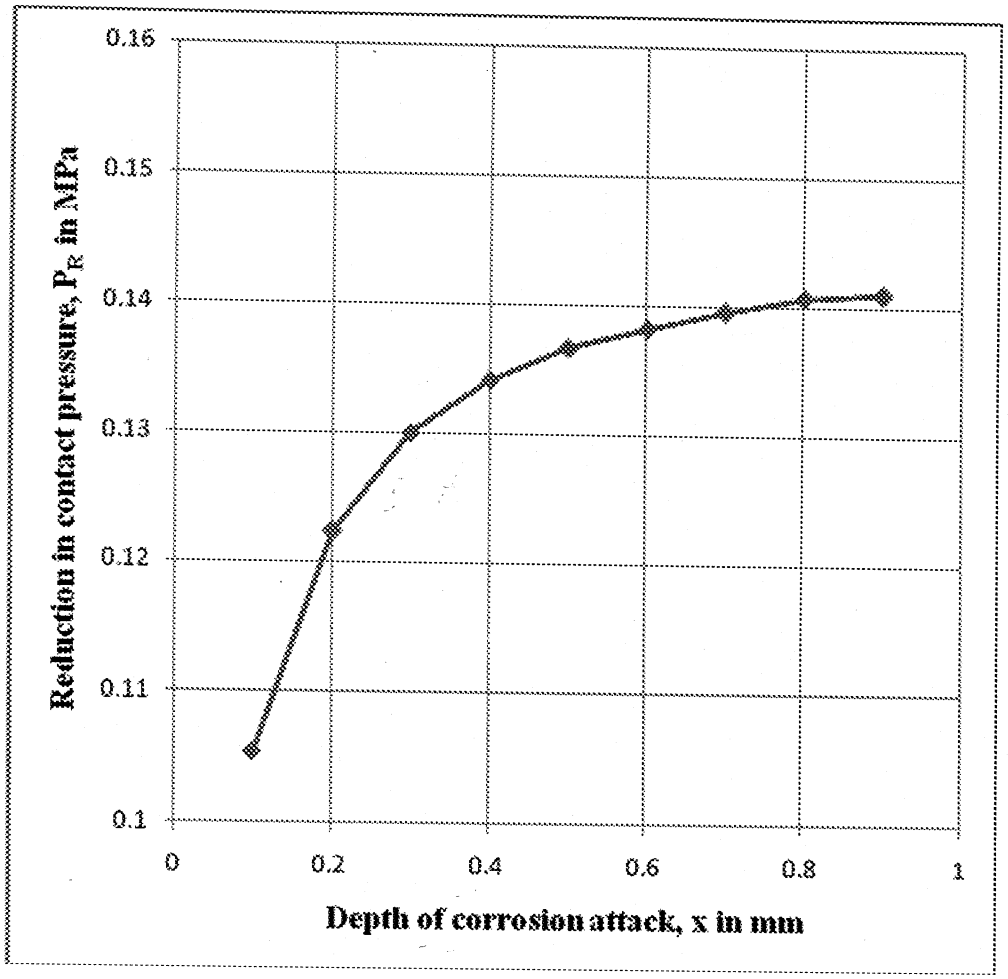

Fig 4.11-Variation of reduction in contact pressure 'V' with the increase in depth of corrosion attack 'x'

Also, Table 4.3 shows the reduction in bond stress with the reduction in contact pressure due to corrosion.

Table 4.3-Reduction in Bond stress with the reduction in contact pressure due to corrosion

Depth of corrosion attack, x in mm	Contact pressure before corrosion, P in MPa	Reduction in contact pressure P_R in MPa	Contact pressure after corrosion P_1 in MPa	Friction coefficient μ	Bond stress $\mu\vec{P}_1$ inMPa
0.1	21.92	0.1054	21.8146	0.9971	21.7455
0.2	21.92	0.1223	21.7977	0.997	21.7263
0.3	21.92	0.13	21.79	0.9968	21.7138
0.4	21.92	0.1341	21.7859	0.9966	21.705
0.5	21.92	0.1367	21.7833	0.9964	21.6976
0.6	21.92	0.1382	21.7818	0.9963	21.6938
0.7	21.92	0.1396	21.7804	0.9961	21.6876
0.8	21.92	0.1407	21.7793	0.9959	21.6818
0.9	21.92	0.141	21.779	0.9957	21.6767
1	21.92	0.1418	21.7782	0.9956	21.6735

Fig. 4.12 shows the variation of reduction in bond stress with reduction in contact pressure due to corrosion. It is observed from Fig. 4.12 that the bond stress increases with the increase in contact pressure due to corrosion. Therefore, it can be concluded that the bond stress at the steel-concrete interface is a function of contact pressure at the steel-concrete interface.

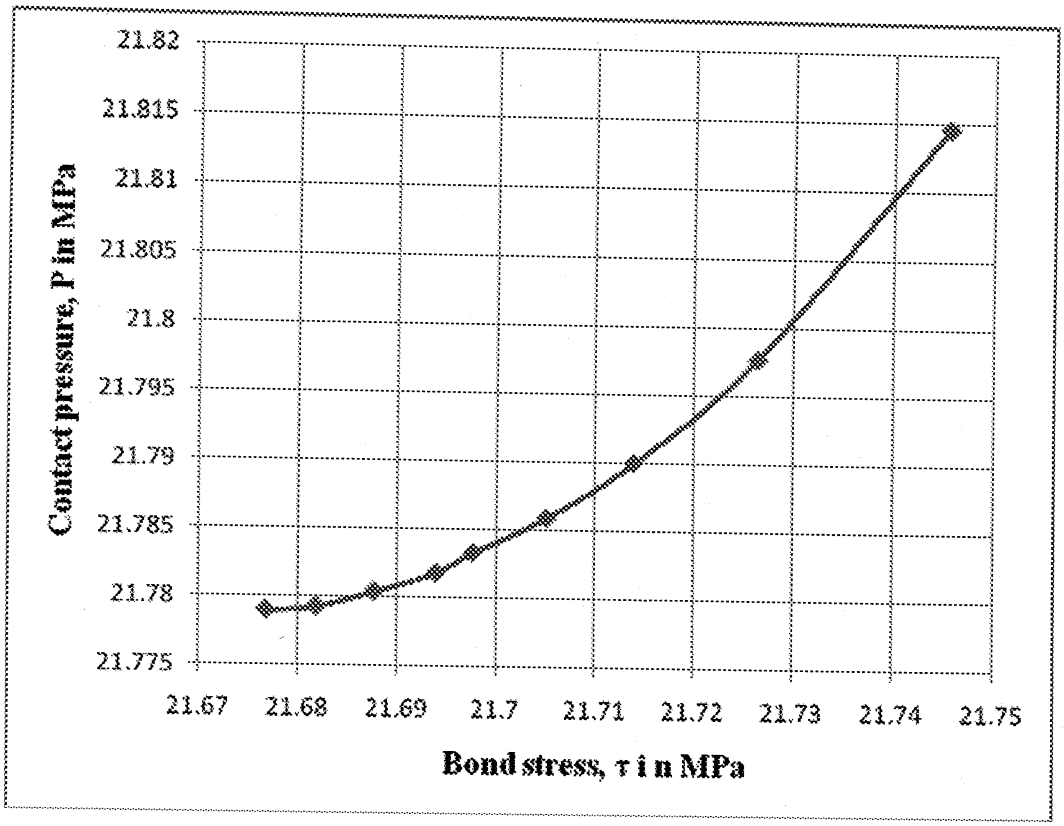

Fig 4.12-Variation of reduction in bond stress with reduction in contact pressure due to corrosion

Chapter 5

Finite Element Analysis

This chapter contains the description and applications of the FEA to analyse the behaviour of axially loaded pull-out specimens with varying concrete strength, concrete cover thickness and corrosion percentage. The program applies monotonically increasing loads and cracks are introduced in elements when one of the principal stresses equals or exceeds predetermined tensile strength. The non linear finite element software ABAQUS was used to analyse the pull-out tests on corroded reinforcement bars in concrete cylinders carried out by Amleh (2000). The computer program used in this investigation is a further development of a previous program developed by Amleh and Ghosh (2004). This chapter illustrates the procedure involved in conducting the finite element study.

5.1. Specimen details

The specimen selected for this analysis was the same as the one analysed by Ghosh (2004) which was modeled after Amleh (2000) experimental specimens. Two types of concrete mixtures, 60 MPa and 50 MPa with three different concrete cover thicknesses 25 mm, 50 mm and 75 mm were used for the pull-out specimens. 20 mm diameter reinforcing steel which was embedded in a 305 mm long concrete cylinder, with the bar protruding at one end only, was used for all specimens. The embedded length of the bar was fixed at 280 mm. Figure 5.1 shows the details of the typical pull-out specimen.

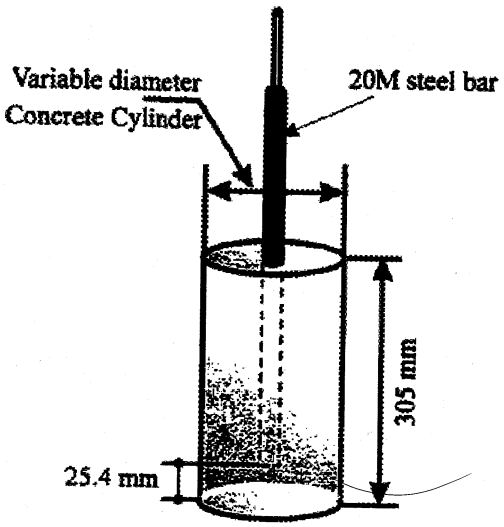

Fig 5.1-Details of the typical pull-out specimen (Amleh, 2000)

5.2. Material properties of steel

In the present investigation, the simplified elastic-plastic-strain hardening form is used. Hence, the elastic and plastic properties were used to define the nonlinear behaviour of steel. The properties of steel used in the analysis are given below.

Modulus of Elasticity, E_s = 200,000 MPa

Poisson's ratio = 0.3

Yield strength = 433 MPa

5.3. Material properties of concrete

Because of the complexities involved in the behavior of concrete, modeling of reinforced concrete in a non-linear finite element analysis is not simple one. In ABAQUS, the redistribution of internal forces due to a nonlinear material behavior is taken fully into

account and a resulting stress and deformation state satisfies all three requirements of mechanics: equilibrium of forces, compatibility of deformations and material laws. Linear or non-linear elasticity-based constitutive laws are used to characterize concrete response before yield. The elastic stress-strain relations are obtained using generalized Hooke's law and fracture stress decrements are determined using a fracture surface in strain space. Furthermore, it extends to the nonlinear behavior in the pre-failure range including both material and geometrical nonlinearities.

5.3.1. Elastic properties

Modulus of elasticity for normal density concrete with a density of about 2300 kg/m^3 and compressive strengths of 50 MPa and 60 MPa can be determined using the equation,

$$E_c = \left(3300\sqrt{f_c'} + 6900\right)\left(\frac{\gamma_c}{2300}\right)^{1.5} \qquad (5.1)$$

For 50 MPa concrete, modulus of elasticity, E_c= 30235 MPa

For 60 MPa concrete, modulus of elasticity, E_c= 32462 MPa

5.3.2 Plastic properties

5.3.2.1. Compressive behaviour

According to Thorenfeldt et al. (1987), the relationship between concrete stress and corresponding strain in concrete can be expressed by the equation,

$$\frac{f_c}{f_c^{'}} = \frac{n(\varepsilon_c/\varepsilon_c^{'})}{n-1+(\varepsilon_c/\varepsilon_c^{'})^{nk}} \tag{5.2}$$

where,

f'_c = concrete compressive strength, MPa

ε'_c = strain when f_c reaches f'_c

n = curve fitting factor = $E_c / (E_c - E'_c)$

E_c = initial tangent modulus (when $\varepsilon_c = 0$)

$E'_c = f'_c / \varepsilon'_c$

k = a factor which control the slope of the descending branch of the stress-strain curve

The values for the constants ε'_c, n, k can be obtained from the relationship proposed by Collins and Mitchel (1990).

For $\varepsilon_c / \varepsilon'_c \leq 1.0$, $k = 1.0$ (5.3)

For $\varepsilon_c / \varepsilon'_c > 1.0$, $k = 0.67 + (f'_c \geq 1.0)$ (5.4)

$n = 0.8 + f'_c / 17$ (5.5)

The strain at peak stress can be computed using the formula,

$$\varepsilon_c^{'} = \frac{f_c^{'}}{E_c}\left(\frac{n}{n-1}\right) \tag{5.6}$$

Concrete compressive stresses f_c for different strains are calculated using the equation,

$$f_c = \frac{n(\varepsilon_c/\varepsilon_c')f_c'}{n-1+(\varepsilon_c/\varepsilon_c')^{nk}} \tag{5.7}$$

Figures 5.2 and 5.3 show the variation of compressive stress with strain for 60 MPa and 50 MPa concrete respectively.

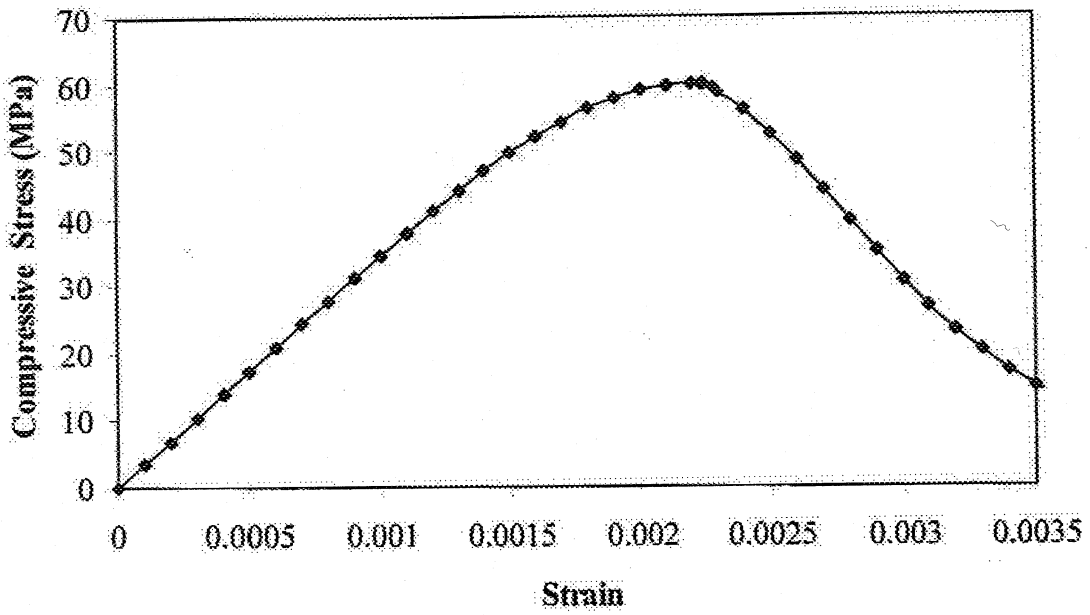

Fig. 5.2-Variation of compressive stress with strain for 60 MPa concrete (Ghosh, 2004)

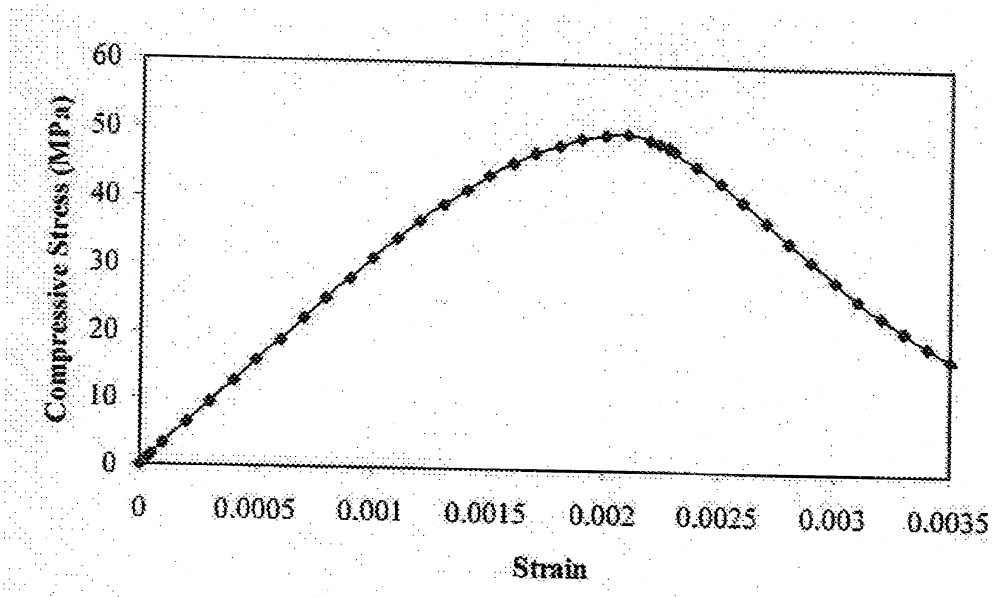

Fig. 5.3-Variation of compressive stress with strain for 50 MPa concrete (Ghosh, 2004)

From the total strain, the plastic strain is calculated using the equation,

$$\varepsilon_{pl} = \varepsilon_t - \varepsilon_{el} \tag{5.8}$$

$$\varepsilon_{el} = f_c / E_c \tag{5.9}$$

where,

ε_t = total strain

ε_{el} = elastic strain

ε_{pl} = plastic strain

f_c = compressive stress at ε_t

E_c = modulus of elasticity

Figures and show the variation of compressive stress with plastic strain for 60 Mpa and 50 MPa concrete respectively.

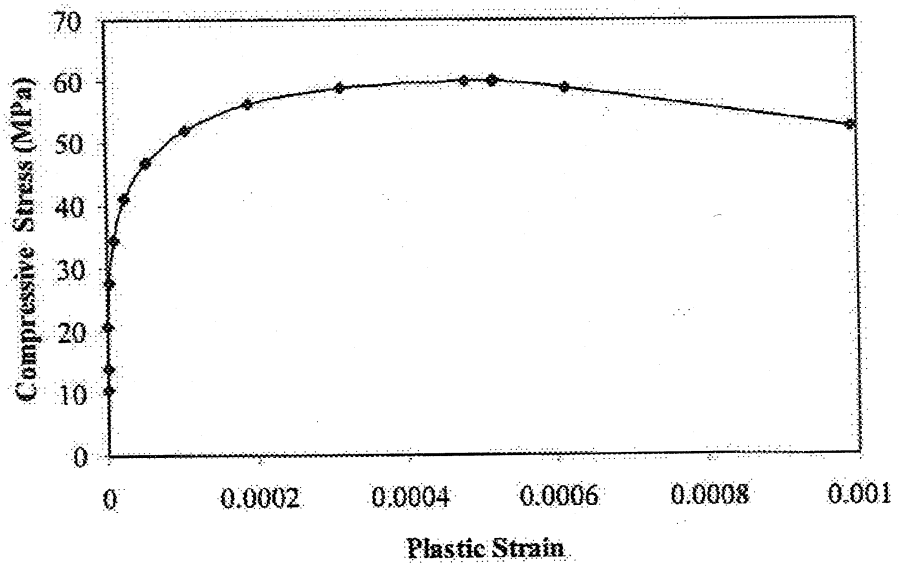

Fig. 5.4-Variation of compressive stress with plastic strain for 60 MPa concrete (Ghosh, 2004)

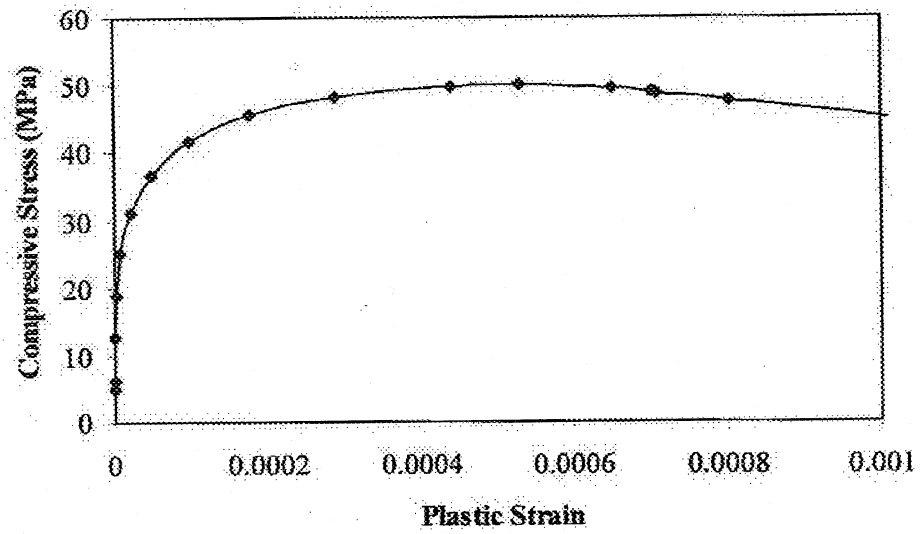

Fig. 5.5-Variation of compressive stress with plastic strain for 50 MPa concrete (Ghosh, 2004)

5.3.2.2. Smeared cracking

In order to express the behaviour of the concrete after cracking, a smeared crack model is used in the present study. In this approach, in spite of considering individual micro cracks, the localized deformation of each crack is smeared out over a characteristic length, and the response in tension is described as a continuum in terms of stress–strain relations. Smeared cracking model consists of tension stiffening and stress ratios and stain ratios to define the failure surfaces.

5.3.2.2.1. Tension Stiffening

Tension stiffening option is used to define the behaviour of concrete after cracking. This tension stiffening effect represents the capacity of the concrete between cracks to continue to carry tensile stresses and contribute to the overall stiffness. The postfailure behaviour for direct straining across cracks is modelled with the tension stiffening option which defines the strain softening behaviour for the cracked concrete. This option is used to define the residual tensile stress of the concrete normal to a crack as a function of the deformation in the direction of the normal to the crack.

The postfailure stress-strain relationship is used to express the tension stiffening. In postfailure stress-strain relationship, postfailure stress is used as a function of strain across the crack. Figure 5.6 shows the tension stiffening model where the tensile stress of concrete is a function of tensile strain. According to Figure 5.6, the concrete starts crack when it reaches the tensile strength σ_1^u and after reaching that point tensile stress at the

crack is assumed to decrease to zero linearly, which describes the strain softening behaviour of concrete.

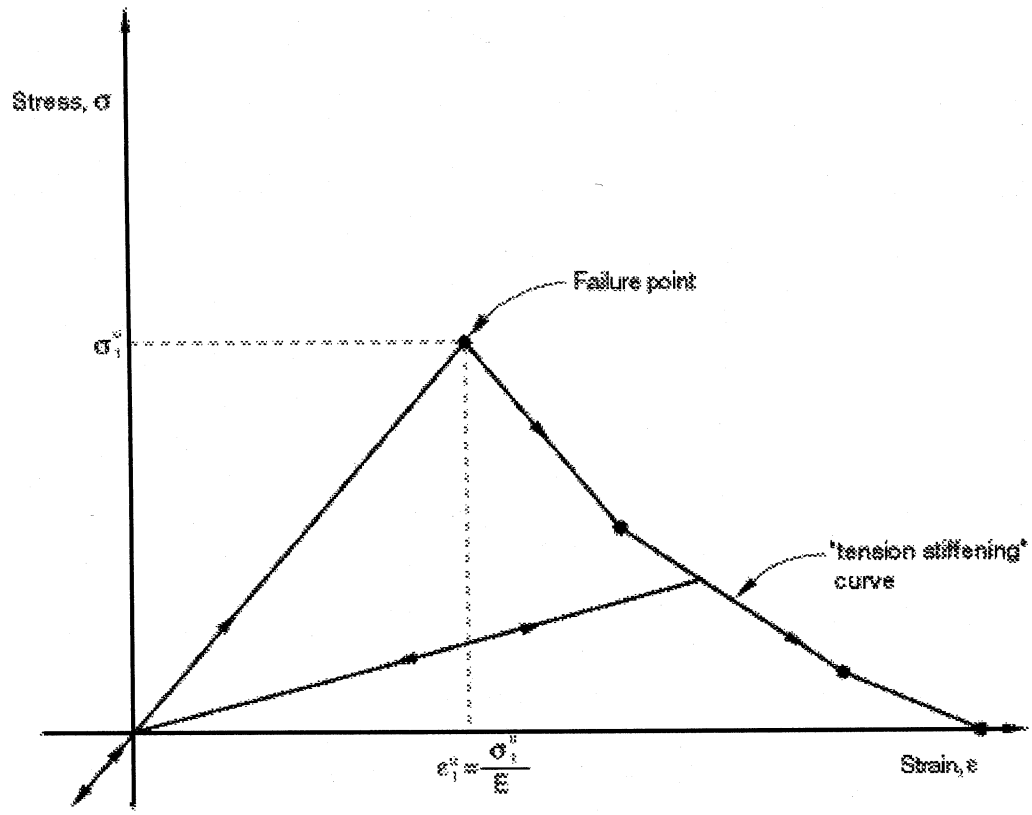

Fig. 5.6-Tension stiffening model (Abaqus/Standard Manual, Volume 2)

It is assumed that the strain softening after failure reduces the stress linearly to zero at a total strain of about 10 times the strain at the maximum stress. The strain at failure in standard concrete is 10^{-4}, which suggests that tension stiffening that reduces the stress to zero at a total strain of about 10^{-3} (Abaqus /Standard User Manual, Volume 2). In the present investigation, the difference between strain at failure and strain at zero tensile stress is calibrated to 0.001 which gave very good match with the experimental results. The input data used for tension stiffening are shown in Table 5.1.

Table 5.1. Input data for tension stiffening

Fraction of remaining stress to stress at cracking	Absolute value of the direct strain minus the direct strain at cracking
1	0
0	0.001

5.3.2.2.2. Stress Ratios and Strain ratio to define failure surface

ABAQUS specifies four failure ratios to define the shape of the failure surface for the concrete model.

1. The ratio of the ultimate biaxial compressive stress to the ultimate uniaxial compressive stress.
2. The absolute value of the ratio of the uniaxial tensile stress at failure to the ultimate uniaxial compressive stress.
3. The ratio of the magnitude of a principal component of plastic strain at ultimate stress in biaxial compression to the plastic strain at ultimate stress in uniaxial compression.
4. The ratio of the tensile principal stress at cracking, in plane stress, when the other principal stress is at the ultimate compressive value, to the tensile cracking stress under uniaxial tension.

Figure 5.7 represents the failure surfaces for the concrete.

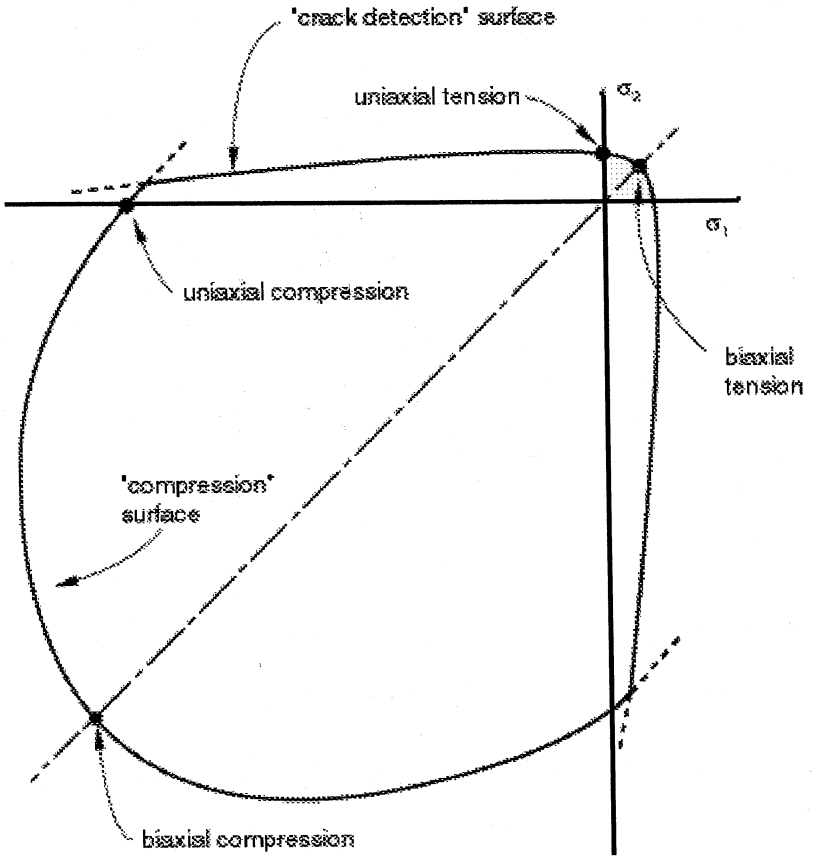

Fig. 5.7-Yield and failure surfaces in plane stress (Abaqus/Standard Manual, Volume 2)

Due to the unavailability of data, default values were used for stress ratios 1 and 4 and strain ratios 3. Stress ratio 2 was calculated using the expression given below.

For 60 MPa concrete,

Stress ratio 2 = Uniaxial tensile stress at failure / Uniaxial compressive stress

$$\text{Stress ratio} = f'_t / f'_c = 0.6\sqrt{f'_c} / f'_c \qquad (5.10)$$

$$= (0.6\sqrt{60}) / 60 = 0.07745.$$

Input data used for stress ratios and strain ratio are shown in Table 5.2.

Table 5.2 Input data for stress ratios and strain ratio

Concrete type	Stress ratio 1	Stress ratio 2	Strain ratio 3	Stress ratio 4
60 MPa concrete	1.16	0.07745	1.28	0.3333
50 Mpa concrete	1.16	0.08489	1.28	0.3333

5.4. Finite element modeling

The bond stress at the steel-concrete interface is modeled by developing the contact properties such as contact pressure and the friction at the steel-concrete interface. Mathematical expression developed for the contact pressure in chapter 4 is implemented in the finite element analysis to apply the effect of contact pressure. A surface based interaction with friction was used to define the interface between the steel bar and the concrete. The constitutive behaviour of the steel was modeled by the Von Mises yield criterion, with the associated flow rule and isotropic strain hardening. The concrete was modeled with a constitutive model based on non linear fracture mechanics. The model uses a smeared crack approach in which individual micro cracks are not taken into account. Three dimensional finite element model of the pull-out specimen is shown in Figure 5.8.

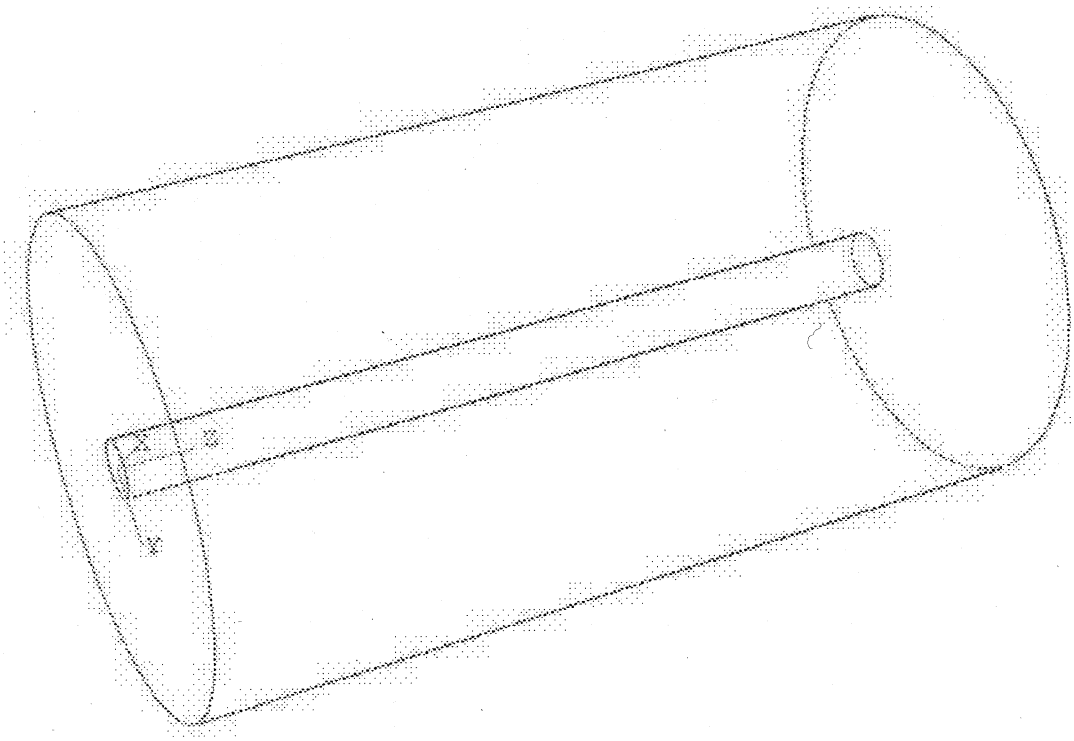

Fig 5.8-Finite element model for the pull-out specimen

5.5. Modeling the contact between steel and concrete

The contact between the inner surface of the concrete cylinder and the outer surface of the steel bar were defined using a master-slave contact algorithm described in ABAQUS. In the master-slave contact algorithm, the surface of the stiffer body should be chosen as the master surface. In the present case, when compared the stiffness factors, the concrete cylinder appeared stiffer than the steel bar and therefore, the inner surface of the concrete cylinder was taken as the master surface and the outer surface of the bar was considered as the slave surface.

5.5.1. Modeling the contact pressure and friction at the uncorroded steel-concrete interface

In this model, the softened contact, in which the contact pressure is an exponential function of the clearance between the surfaces, is used to define the contact pressure. The mathematically developed expression (Eq. 4.15) for contact pressure (Chapter 4) is used to calculate the input for contact pressure. Exponential decay friction model is used in this model for analysing the friction at the steel concrete interface. While, the input parameters such as static friction coefficient (μ_s), kinetic friction coefficient (μ_k) and decay coefficient (d_c) are taken from graph developed by Lundgren and Gylltoft (2000). The input values used for μ_s, μ_k, and d_c are 1, 0.4, and 0.45, respectively.

5.5.2. Modeling the contact pressure and friction at the corroded steel concrete interface

As stated earlier, due to the accumulation of flaky layer corrosion products at the steel concrete interface, the friction and the contact pressure at the interface between the steel and concrete decreases. The reduction in contact pressure due to corrosion is calculated using the expression (Eq. 4.20) developed in Chapter 4. The contact pressure is calculated by taking the difference between the reduction in contact pressure and the derived equation for the contact pressure of the uncorroded specimens.

The flaky layer of rust performs as lubricant and reduces the friction at the steel-concrete interface. The kinetic friction coefficient is consistent and the static friction coefficient decreases with the mass loss. Parametric studies conducted by Ghosh (2004) can be used

to evaluate the relationship between the static friction coefficient and mass loss and also variation of the decay coefficient with mass loss. Equations 5.11 and 5.12 show the variation of the static friction coefficient and the decay coefficient at different mass losses.

$$\mu_s = \exp -0.035M \tag{5.11}$$

$$d_c = 0.0261M + 0.45 \tag{5.12}$$

where

μ_s = static friction coefficient,

d_c = decay coefficient, and

M = percentage mass loss due to corrosion

5.6. Mesh generation

Eight nodded solid elements were used to develop the mesh both for the concrete cylinder and the steel rebar. Finite element mesh using eight nodded solid elements is shown in Figure 5.9.

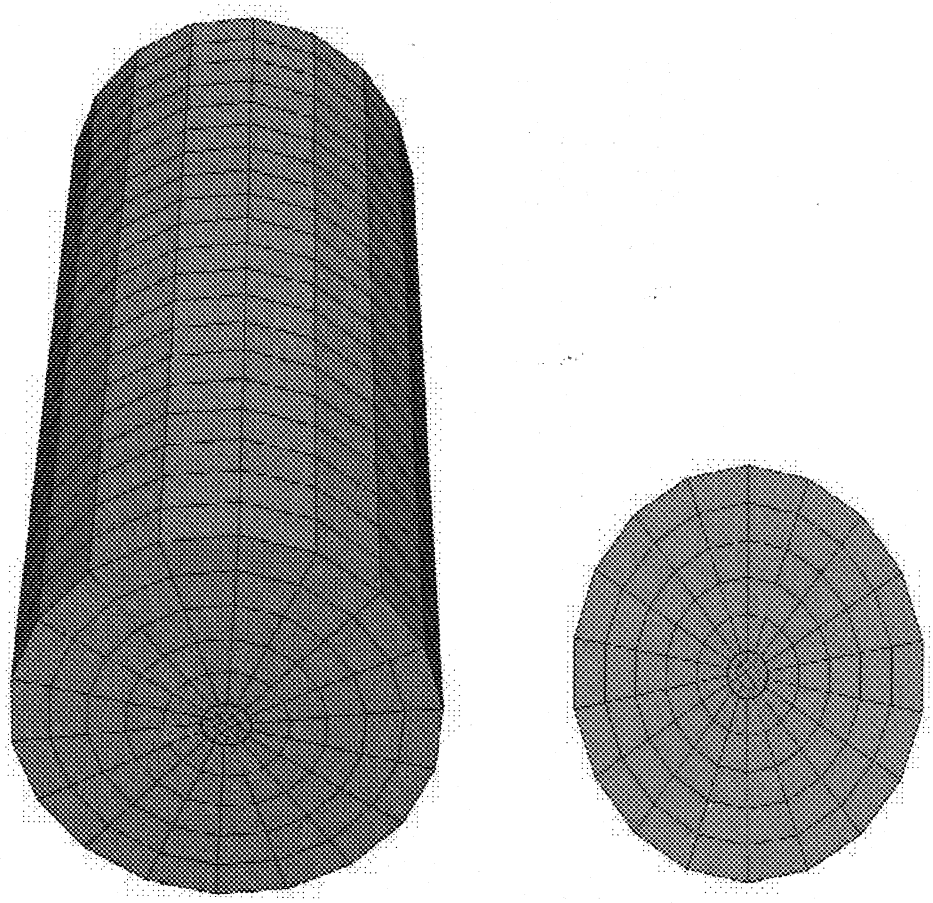

Fig 5.9 Finite element mesh with eight noded solid elements

The analysis was carried out by applying boundary conditions as both the top and the bottom surface of the concrete cylinder made fixed and a monotonic load was applied at one end of the bar and circumferential displacement of the cylinder of concrete was prevented. The applied boundary conditions and the load are shown in Figures 5.10 and 5.11 respectively.

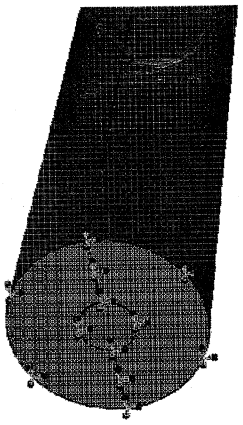

Fig 5.10-Applied boundary condition

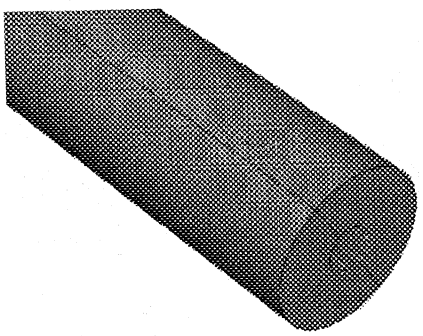

Fig 5.11-Applied load at the top of the reinforcement bar

Chapter 6

Results and Discussions of Finite Element Analysis

This chapter presents the analysis of the results obtained from the finite element analysis conducted in Chapter 5. Results obtained from the finite element analysis is compared with the results of the pull-out tests performed by Amleh (2000), by plotting the bond stress-slip curves for the reinforced concrete in uncorroded and corroded condition. Also the results obtained from the present study are compared with the results of the finite element analysis conducted by Ghosh (2004). Validation of the model is done by analyzing the pull out tests conducted by Al-Sulaimani et al (1990).

6.1. Bond stress-slip relation for the specimen with uncorroded condition

For comparative purposes the variation in bond stress with slip is plotted for the experimental values and the analytical results of the finite element analysis. Figures 6.1 to 6.6 show comparisons of experimental results of Amleh (2000) and the finite element results of the present study for different cover thicknesses and concrete strengths. A good agreement can be observed between the experimental and the finite element results. From the graphs (Figures 6.1 to 6.6), it is observed that bond strength of the 60MPa concrete is higher than that of 50MPa concrete. In the case of 50MPa concrete mixture (Figures 6.1 to 6.6), the bond stress is found to be slightly higher for experimental results than that of the FEM results, except for 25mm concrete cover thickness where the bond stress for FEM is found to be slightly higher than that of the experimental results. However, in the

case of 60MPa concrete mixture, it is observed that the bond stress for experimental results is slightly higher than the FEM for all the three concrete cover thicknesses.

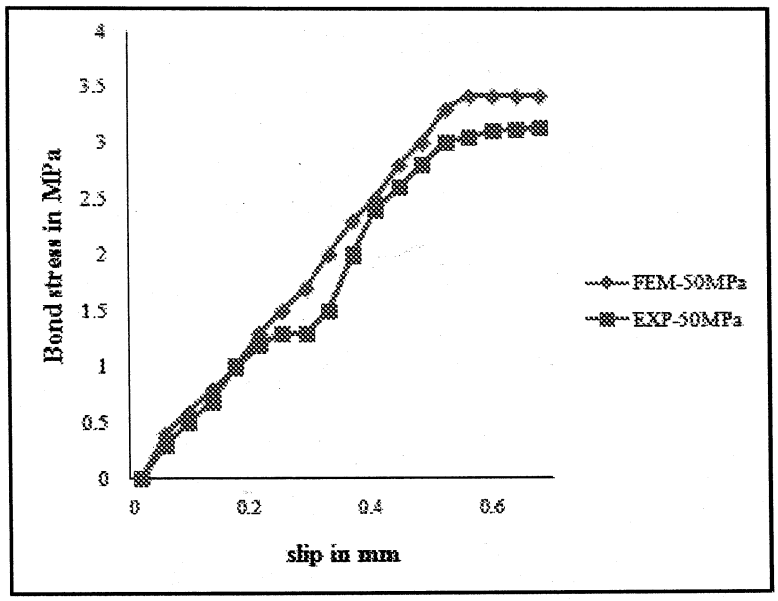

Fig 6.1-Variation of the average bond stress with slip for 25 mm concrete cover for 50 MPa concrete mixtures

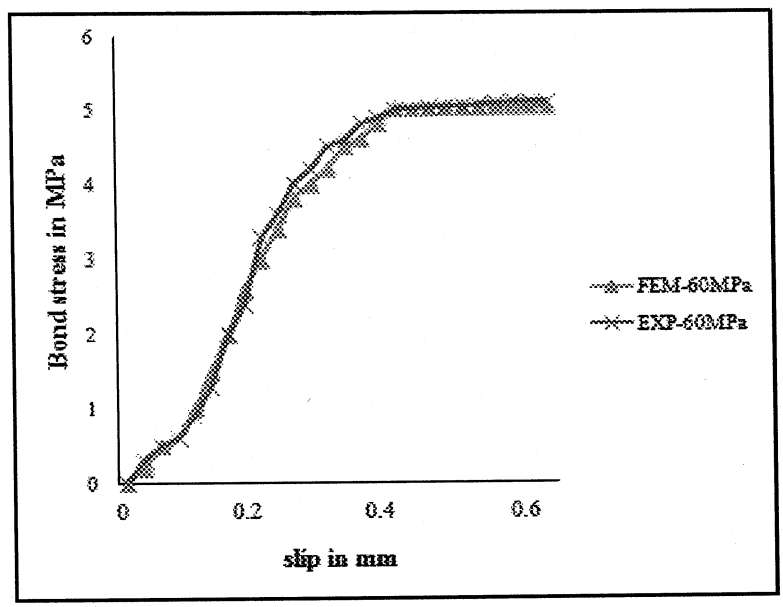

Fig 6.2-Variation of the average bond stress with slip for 25 mm concrete cover for 60 MPa concrete mixtures

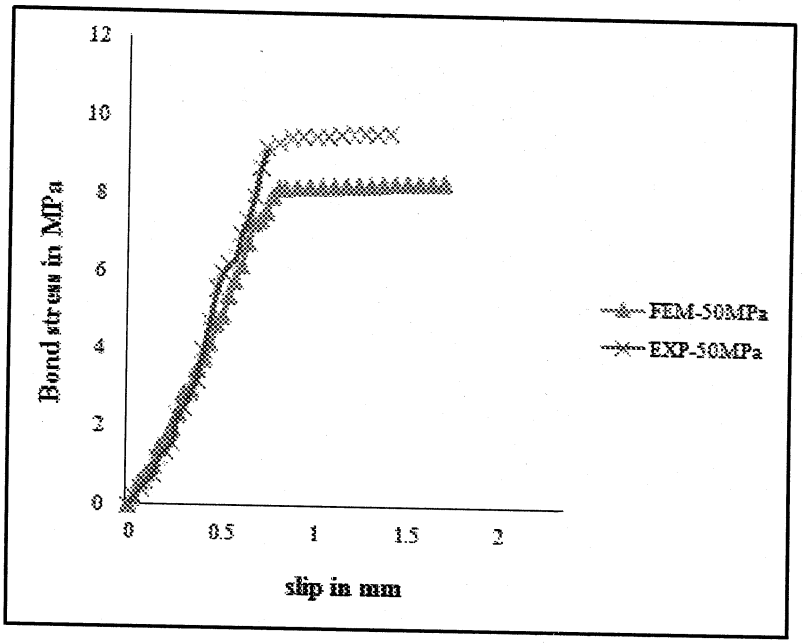

Fig 6.3-Variation of the average bond stress with slip for 50 mm concrete cover for 50 MPa concrete mixtures

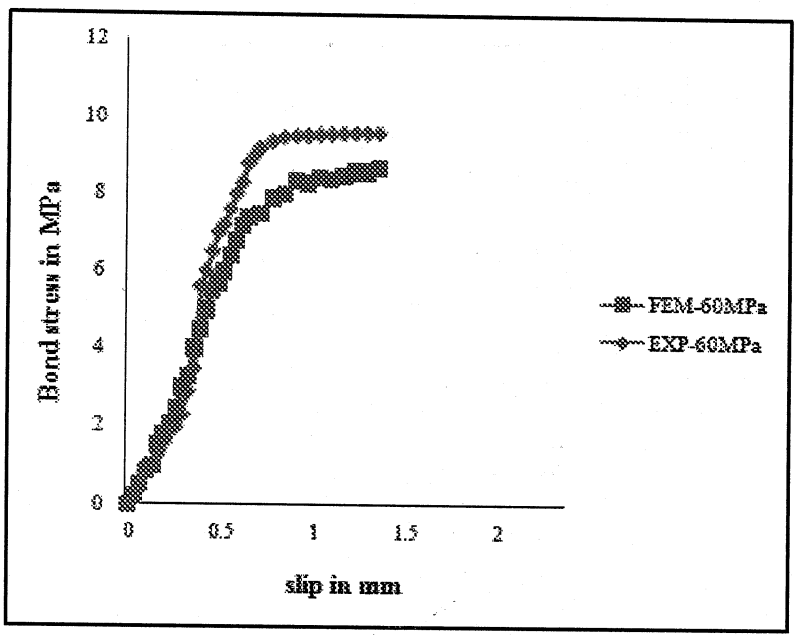

Fig 6.4-Variation of the average bond stress with slip for 50 mm concrete cover for 60 MPa concrete mixtures

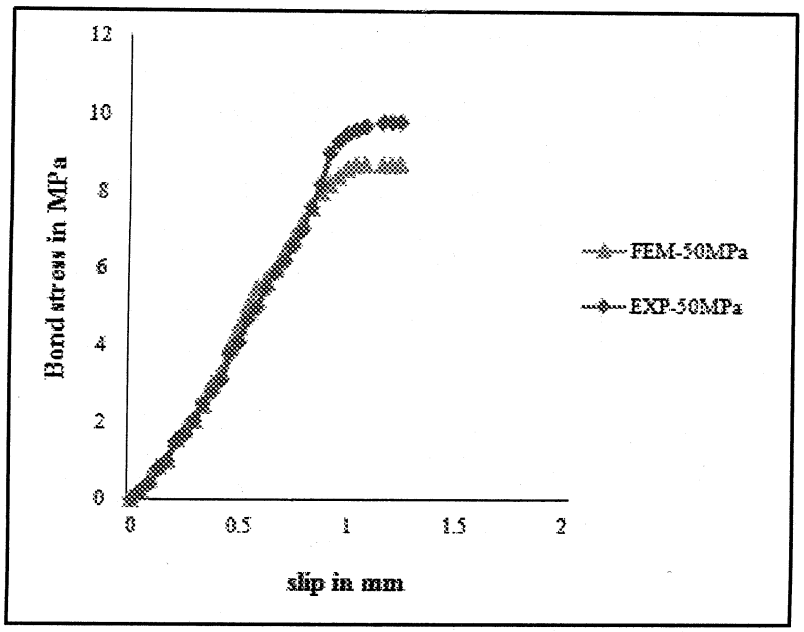

Fig 6.5-Variation of the average bond stress with slip for 75 mm concrete cover for 50 MPa concrete mixtures

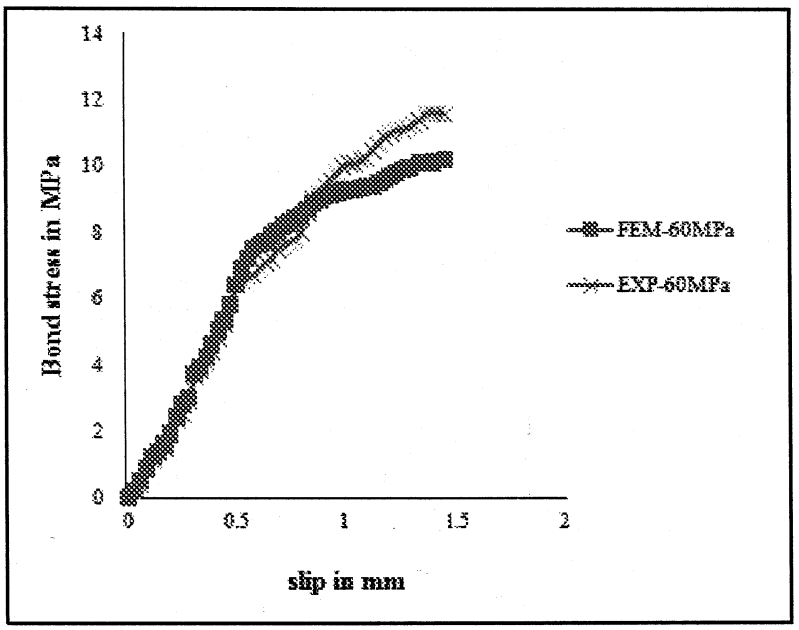

Fig 6.6-Variation of the average bond stress with slip for 75 mm concrete cover for 60 MPa concrete mixtures

6.2. Effect of concrete cover thickness on bond strength

Amleh (2000) found that the ratio of concrete cover thickness and rebar size (c/d_b) is a more decisive variable influencing the resistance of concrete to chloride ingress. With an increase in the (c/d_b) ratio from 2 to 4, the mass loss decreases from 7.1 to 1.7 percent. Several researchers have also emphasized the significance of the concrete cover thickness to the bar diameter (c/d_b) ratio on the bond between the concrete and reinforcement steel. Amleh (2000) tested 192 pullout specimens, which were made using two Normal Portland Cement concretes with water/cement ratios of 0.32 and 0.42, three fly ash concrete with different sources of fly ash (Sundance fly ash, Thunder Bay fly ash, Point Tupper fly ash), and a high alumina cement concrete. The specimens were cylindrical, 305 mm in length, and different diameters to obtain four cover thickness (25, 50, 75, and 100 mm); each specimen was reinforced with a No. 20 steel bar axially.

Figure 6.7 shows an abrupt decrease in bond strength in a specimen with a cover thickness and bar diameter (c/d_b) ratio of 1.28, while for a specimen with a (c/d_b) ratio of 5.13, the decrease in bond strength is smaller. This clearly shows that in a specimen with a higher (c/d_b) ratio, the loss of bond strength is not as significant as is the case with a lower (c/d_b) ratio. These investigations also demonstrated that the concrete cover thickness to bar diameter ratio is an important index of concrete resistance to corrosion of rebars due to the chloride ingress.

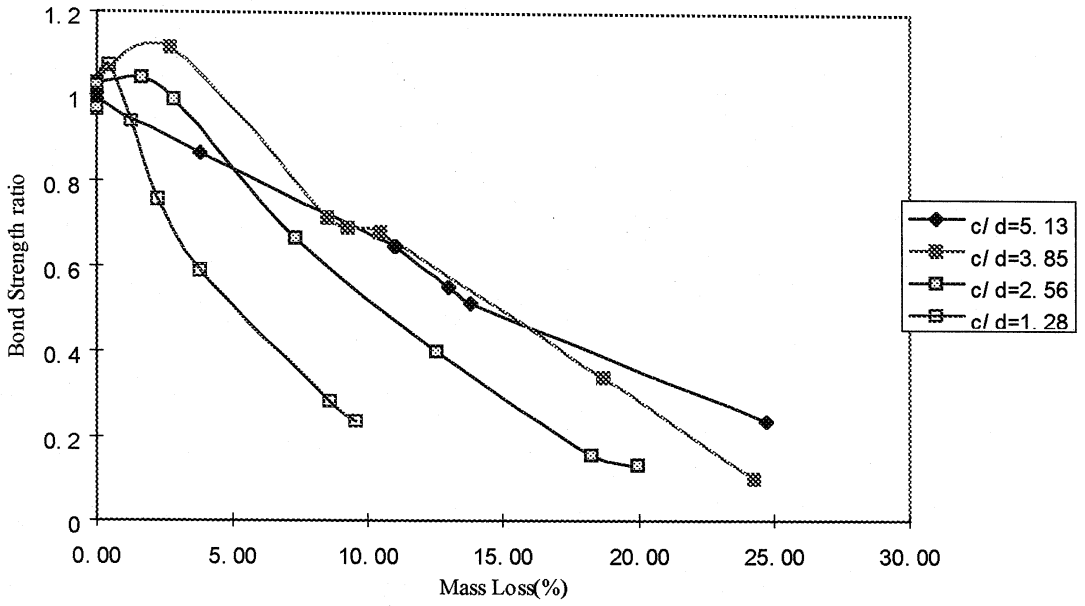

Fig. 6.7 Bond strength ratio versus level of corrosion (different cover thickness and bar diameter (c/d_b) ratio (Adapted from Amleh, 2000)

Bond strength ratio = Bond strength of corroded specimen / Bond strength of uncorroded specimen

However, more research is needed to evaluate the influence of the various parameters on the deterioration of bond at the steel-concrete interface before a reliable design procedure can be developed based on semi-probabilistic considerations (Mirza and Amleh, 2003).

Similarly, Figures 6.8 and 6.9 shows the FEA results of variation of the average bond stress with slip for three different cover thicknesses for 50 MPa and 60 MPa concrete mixtures. As was expected, these curves (Figures 6.8 and 6.9), show that the bond strength increases with the increase in the thickness of the concrete cover for both the 50 MPa and 60 MPa concrete mixtures.

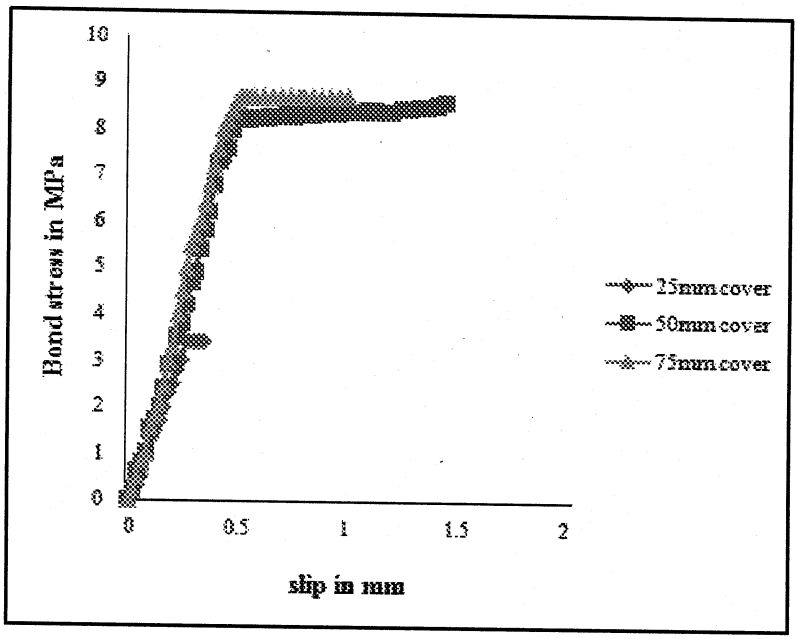

Fig 6.8- Variation of the average bond stress with slip for three different cover thicknesses for 50 MPa concrete mixtures

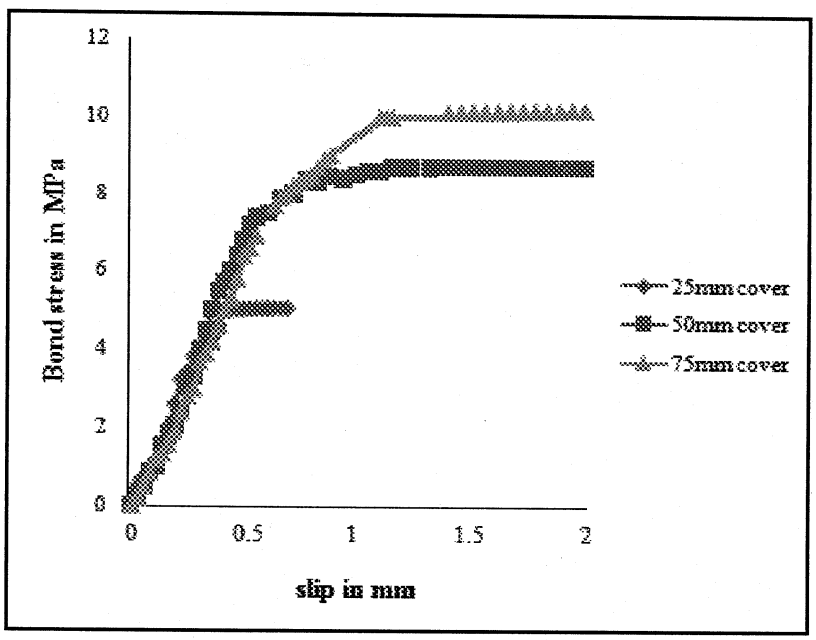

Fig 6.9- Variation of the average bond stress with slip for three different cover thicknesses for 60 MPa concrete mixtures

6.3. Comparison with Ghosh (2004) FEA results

As was mentioned earlier, the average bond strength of present study is compared with the experimental results of Amleh (2000) and the finite element study of Ghosh (2004) who also used Amleh (2000) experimental results using two different concrete strengths 60 MPa and 50 MPa and four different cover thicknesses 25 mm, 50 mm, 75 mm and 100 mm. Using the parametric studies conducted by Ghosh (2004) a relationship was developed between the contact pressure and the cover of the concrete which was applied in the finite element model. Tables 6.1 and 6.2 show the comparison of the bond strength values for both 50 MPa and 60 MPa concrete mixtures respectively. In the case of 50 MPa concrete mixtures, the ultimate bond strength values obtained from the present study are found to be slightly higher than both the experimental results and FEA results obtained from Ghosh (2004).

Table.6.1. Comparison of average bond strength for 50MPa concrete mixtures

Cover thickness (mm)	Bond strength from FEA (MPa)	Bond strength from experimental results (MPa)	Bond strength from FEA (Ghosh, 2004)	Percentage increment or decrement from experimental results	Percentage increment or decrement from FEA (Ghosh, 2004)
25	3.42	3.13	3.22	+9.26%	+6.2%
50	8.6	9.59	8.56	-10%	+0.4%
75	9.92	9.82	8.95	+1%	+1.02%

Table.6.2. Comparison of average bond strength for 60MPa concrete mixtures

Cover thickness (mm)	Bond strength from FEA (MPa)	Bond strength from experimental results (MPa)	Bond strength from FEA (Ghosh, 2004)	Percentage increment or decrement from experimntal results	Percentage increment or decrement from FEA (Ghosh, 2004)
25	5.04	5.11	4.96	-1.36%	+1.6%
50	8.72	9.59	8.59	-9.07%	+1.51%
75	10.2	11.6	9.21	-12.06%	+10.75%

In the case of 60 MPa concrete mixtures, the ultimate bond strength obtained from the experiments are found to be slightly higher than the FEA results. However, it is found to be higher than the FEA results obtained from Ghosh (2004).

6.4. Bond stress-slip relation for the specimen with corroded condition

The specimens were analyzed for different levels of corrosion such as 2.5% mass loss and 5% mass loss. Figures 6.10 to 6.25 show the variation of bond stress with slip at different levels of corrosion for three different cover thicknesses and concrete mixtures. From the graphs (figures 6.10 to 6.25), it is observed that with the increase in corrosion levels, average bond strength decreases and slip increases. Even though the bond strength decreases with the increase in mass losses, higher bond strength is observed for the specimens with higher concrete covers. A good agreement can be observed between the experimental and finite element results.

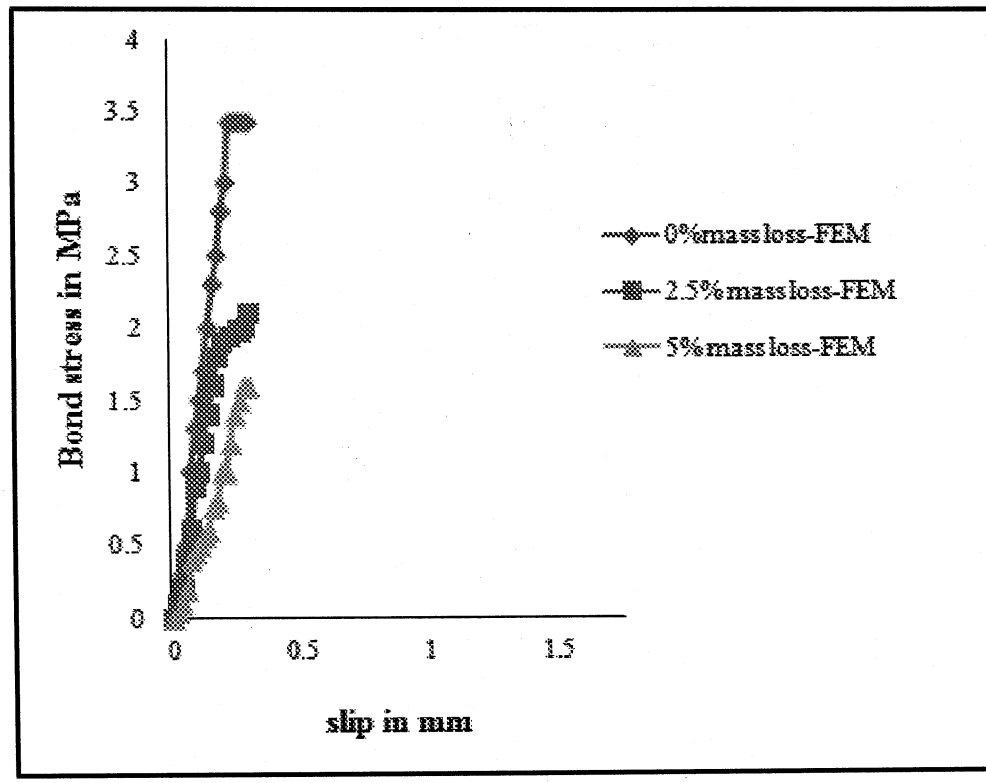

Fig 6.10-FEM results of the variation of average bond stress with slip at different corrosion levels for 25 mm concrete cover in 50 MPa concrete mixture

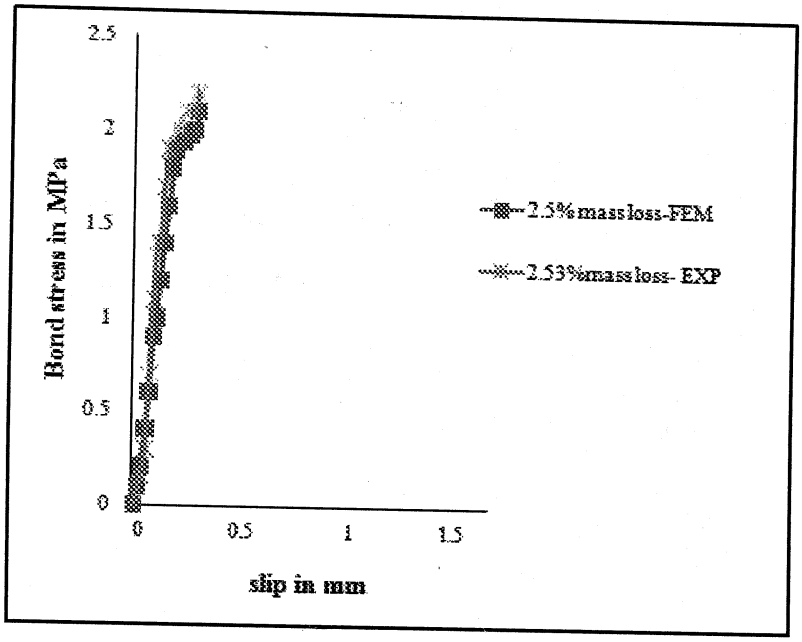

Fig 6.11-Comparison of the 'variation of average bond stress with slip' at 2.5% massloss (FEM) Vs 2.53% mass loss (EXP)for 25 mm concrete cover for 50 MPa concrete mixture

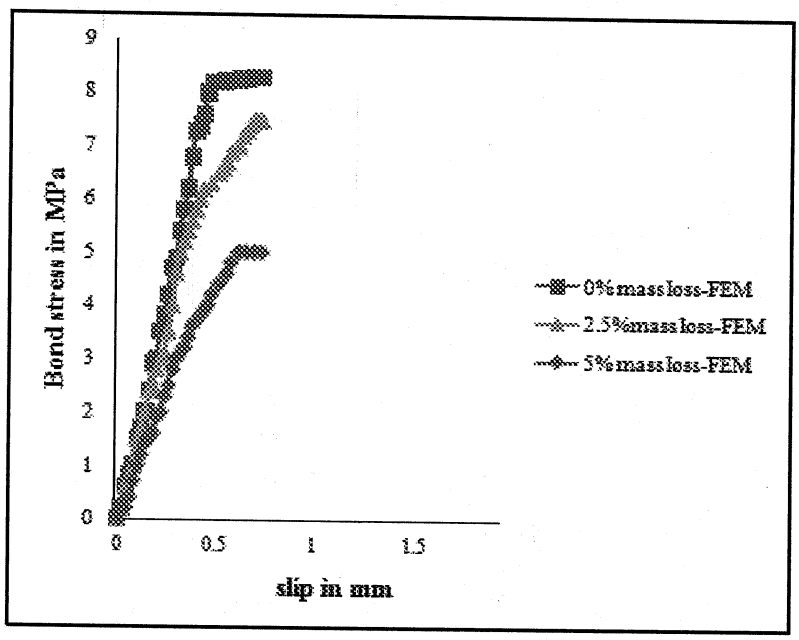

Fig 6.12-FEM results of the variation of average bond stress with slip at different corrosion levels for 50 mm concrete cover in 50 MPa concrete mixture

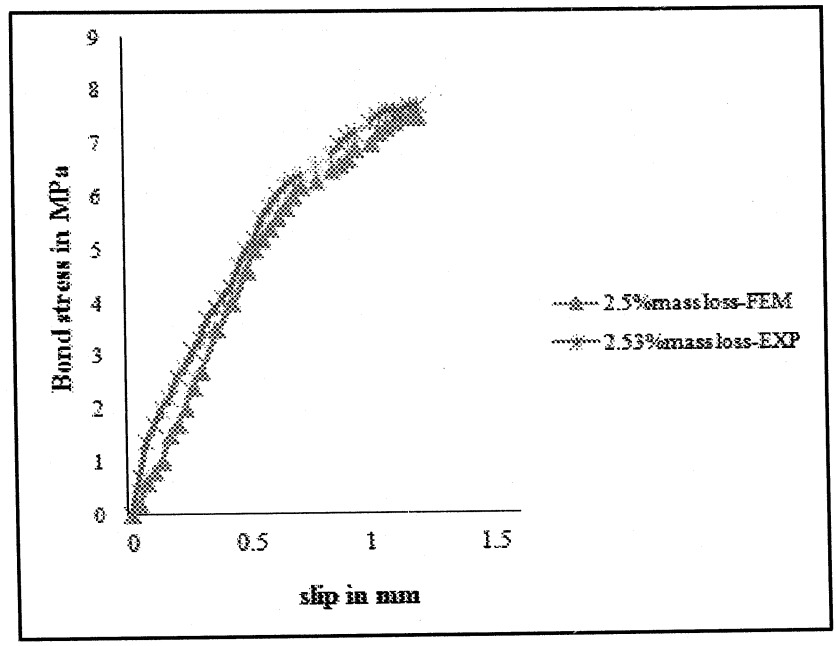

Fig 6.13-Comparison of the 'variation of average bond stress with slip' at 2.5% massloss (FEM) Vs 2.53% mass loss (EXP) for 50 mm concrete cover for 50 MPa concrete mixture

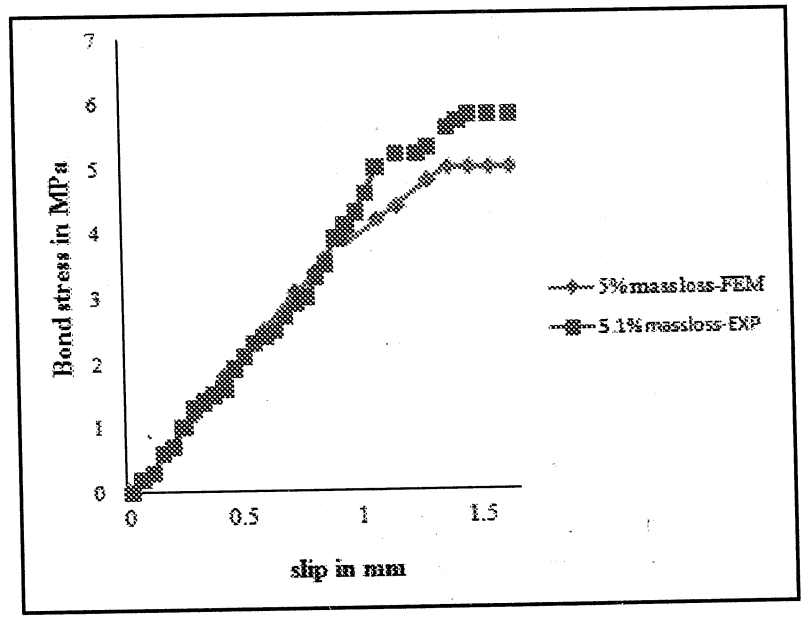

Fig 6.14-Comparison of the 'variation of average bond stress with slip' at 5% massloss (FEM) Vs 5.1% mass loss (EXP)for 50 mm concrete cover for 50 MPa concrete mixture

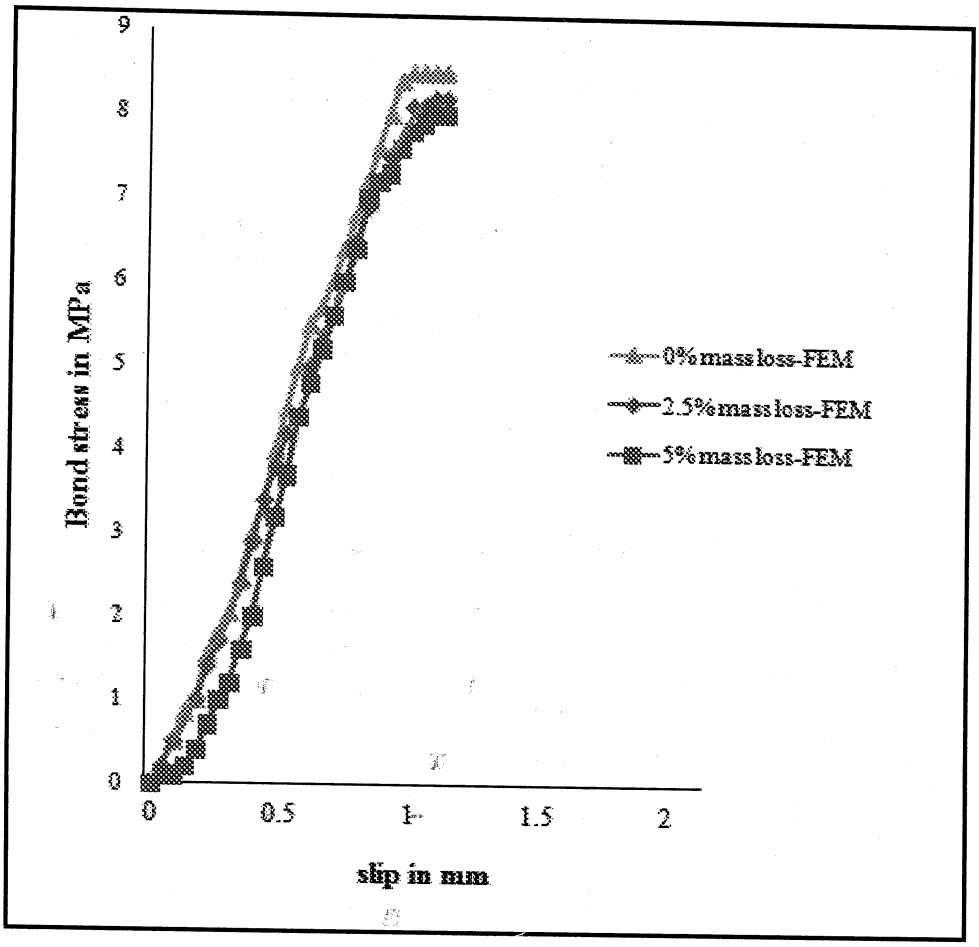

Fig 6.15-FEM results of the variation of average bond stress with slip at different corrosion levels for 75 mm concrete cover for 50 MPa concrete mixture

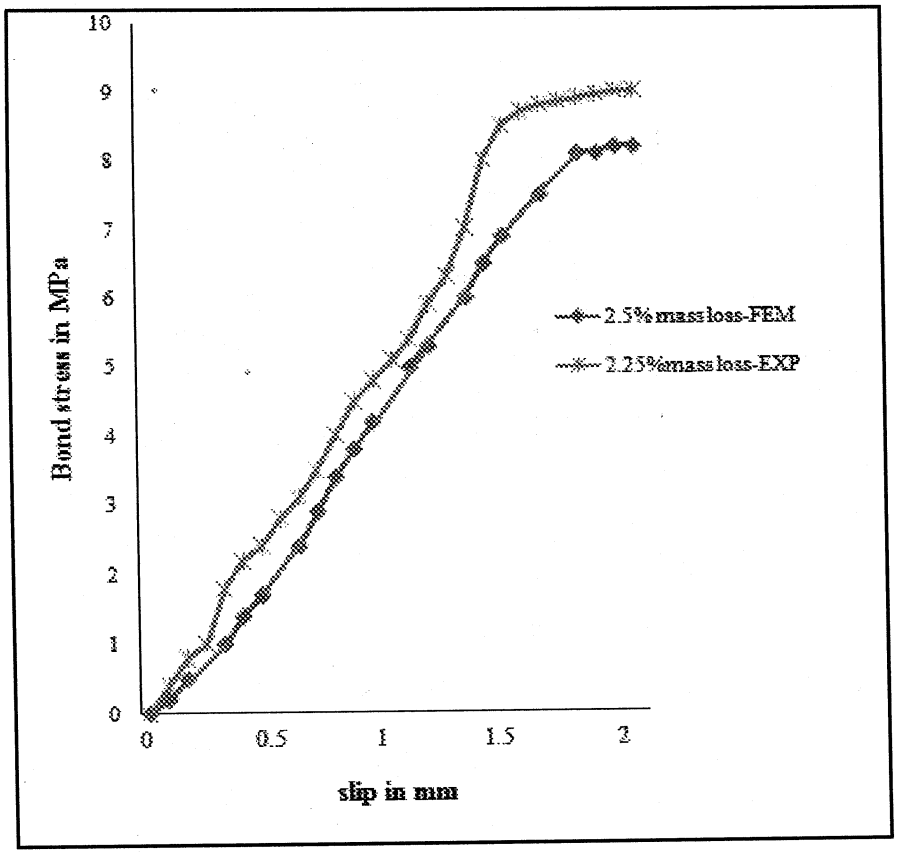

Fig 6.16-Comparison of the 'variation of average bond stress with slip' at 2.5% massloss (FEM) Vs 2.25% mass loss (EXP) for 75 mm concrete cover for 50 MPa concrete mixture

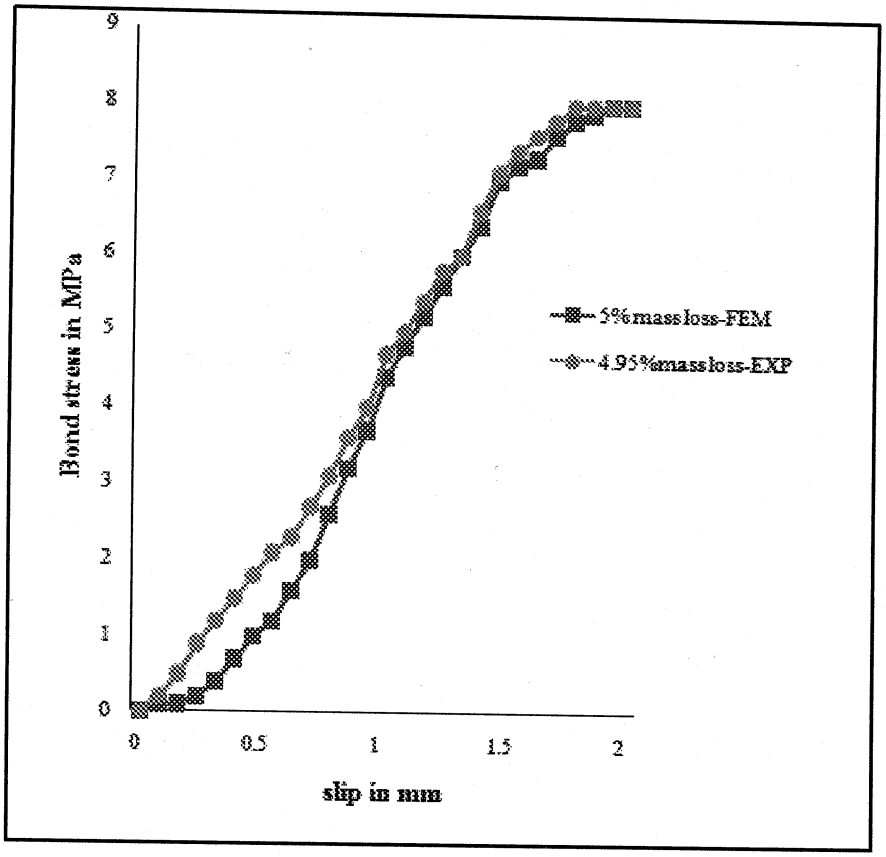

Fig 6.17-Comparison of the 'variation of average bond stress with slip' at 5% massloss (FEM) Vs 4.95% mass loss (EXP) for 75 mm concrete cover for 50 MPa concrete mixture

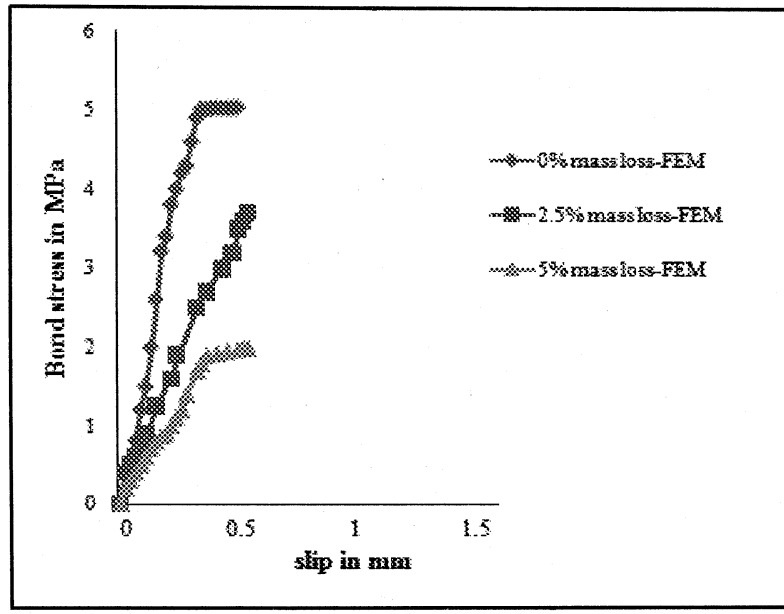

Fig 6.18-Variation of average bond stress with slip at different corrosion levels for 25 mm concrete cover for 60 MPa concrete mixture

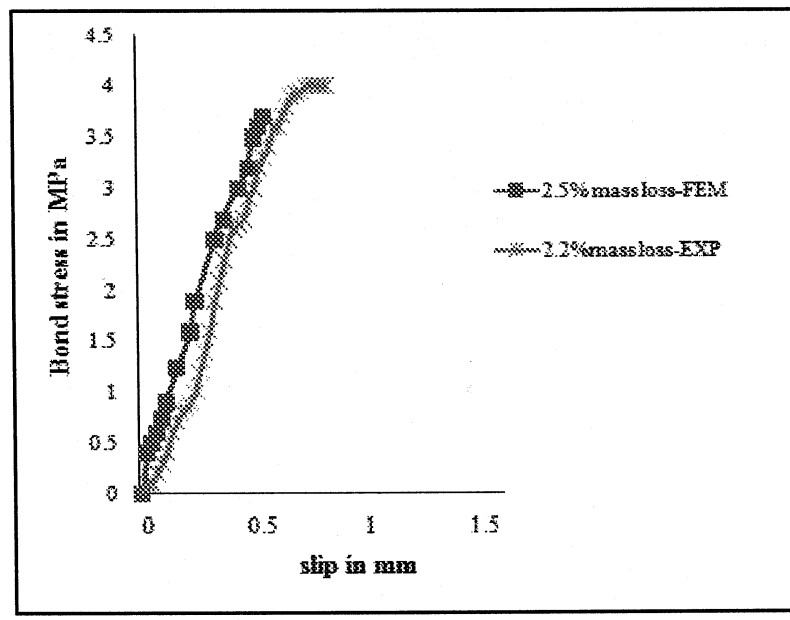

Fig 6.19-Comparison of the 'variation of average bond stress with slip' at 2.5% massloss (FEM) Vs 2.2% mass loss (EXP) for 25 mm concrete cover for 60 MPa concrete mixture

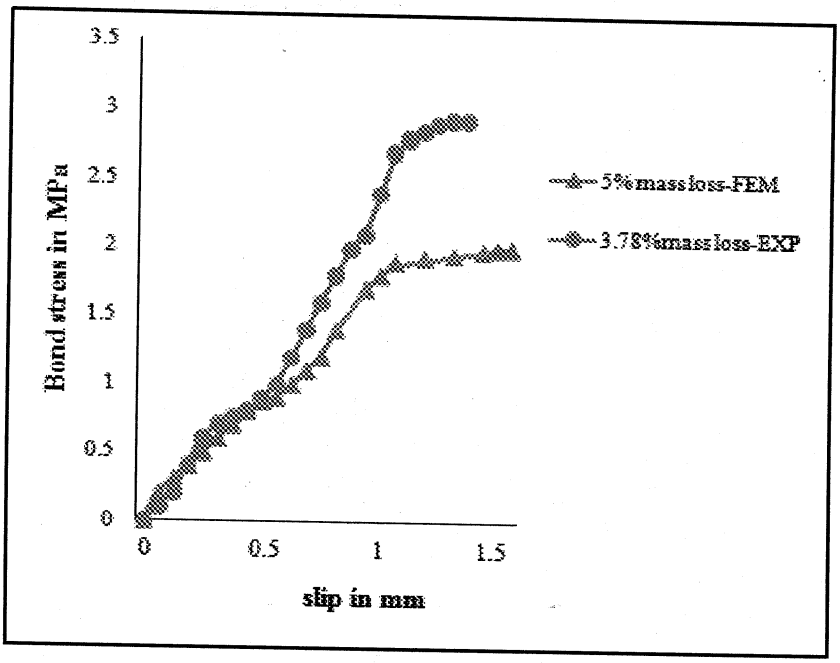

Fig 6.20-Comparison of the 'variation of average bond stress with slip' at 5% massloss (FEM) Vs 3.78% mass loss (EXP)for 25 mm concrete cover for 60 MPa concrete mixture

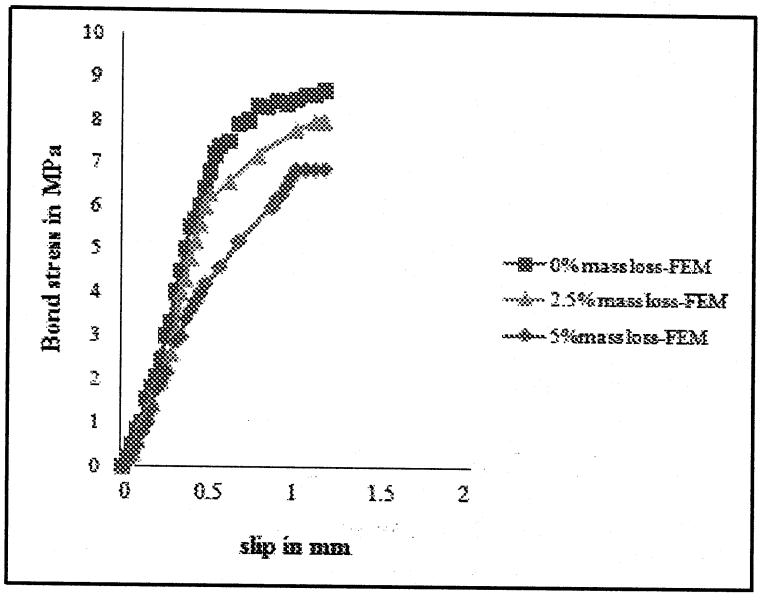

Fig 6.21-Variation of average bond stress with slip at different corrosion levels for 50 mm concrete cover for 60 MPa concrete mixture

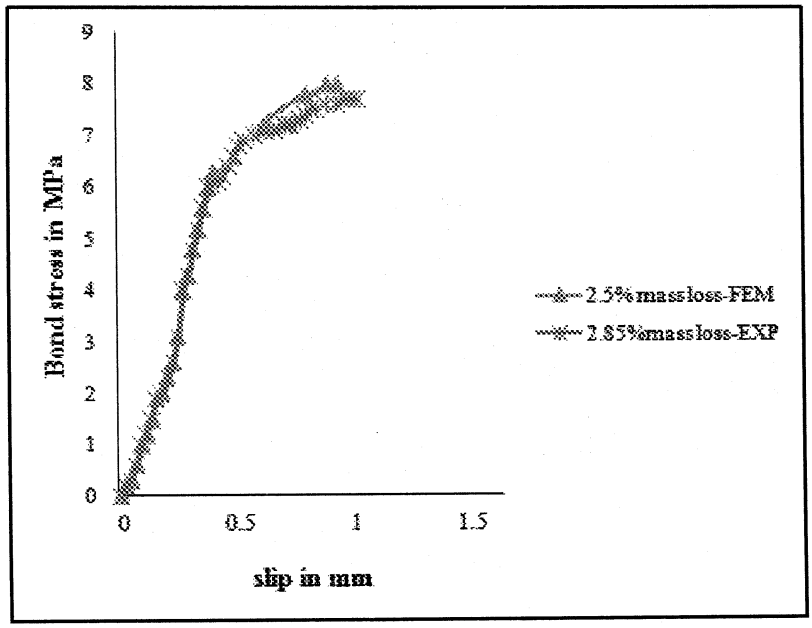

Fig 6.22-Comparison of the 'variation of average bond stress with slip' at 2.5% massloss (FEM) Vs 2.85% mass loss (EXP)for 50 mm concrete cover for 60 MPa concrete mixture

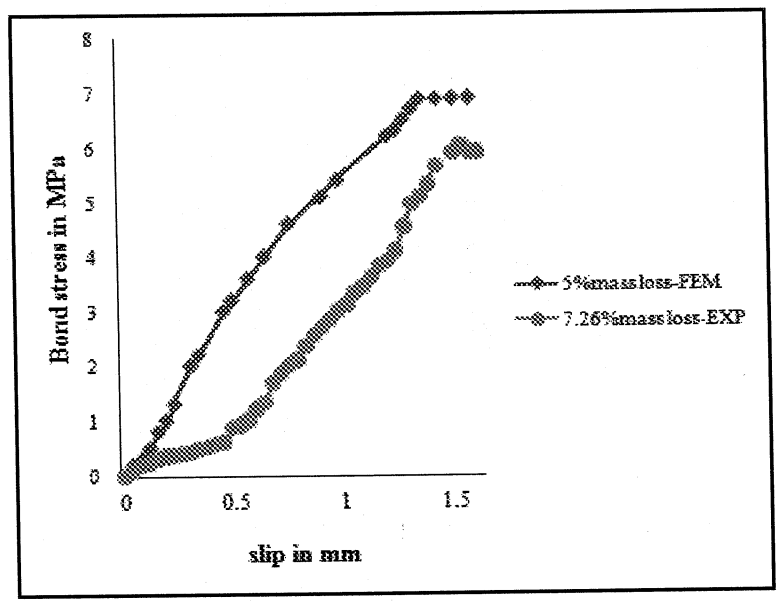

Fig 6.23-Comparison of the 'variation of average bond stress with slip' at 5% massloss (FEM) Vs 7.26% mass loss (EXP)for 50 mm concrete cover for 60 MPa concrete mixture.

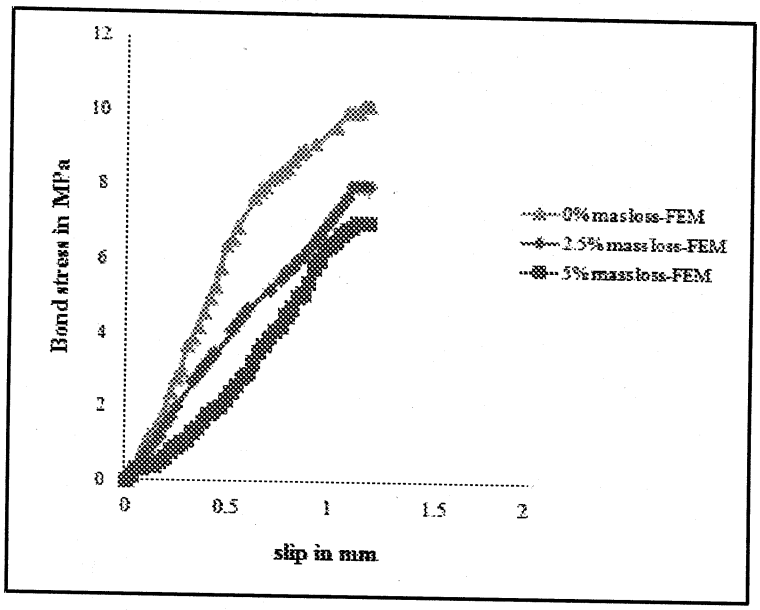

Fig 6.24-Variation of average bond stress with slip at different corrosion levels for 75 mm concrete cover for 60 MPa concrete mixture

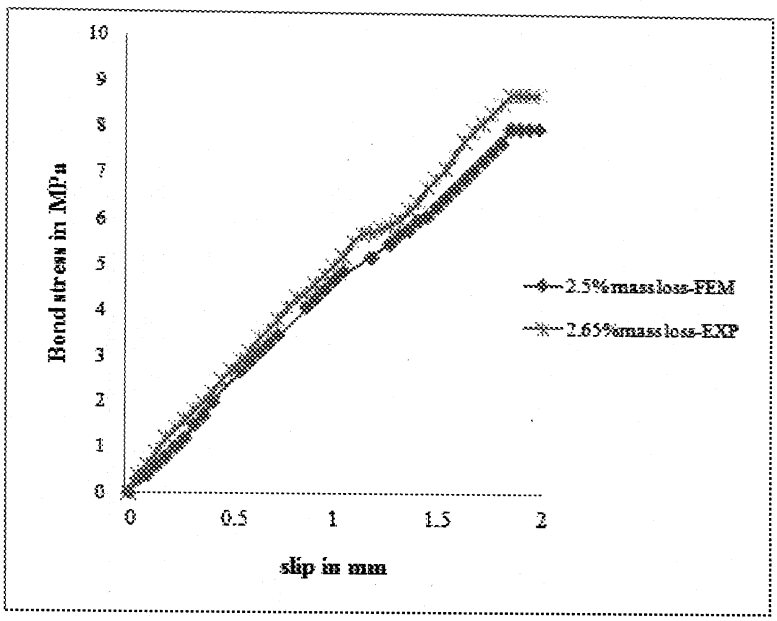

Fig 6.25-Comparison of the 'variation of average bond stress with slip' at 2.5% massloss (FEM) Vs 2.65% mass loss (EXP)for 75 mm concrete cover for 60 MPa concrete mixture

6.4.1. Comparison between FEA and experimental results of corroded specimen

Tables 6.3 and 6.4 below show the comparison of the percentage loss of bond strength of specimen at different levels of corrosion for 50 MPa and 60 MPa concrete mixtures respectively.

Table.6.3. Percentage loss of average bond strength at different levels of corrosion for 50 MPa concrete mixture

Cover thickness (mm)	FEA		FEA (Ghosh, 2004)	Experimental results (Amleh, 2000)	
	% mass loss	% loss of bond strength	%loss of bond strength	% mass loss	%loss of bond strength
25	2.5	27.1	27.26	2.53	24.5
	5	46.2	45.64	-	-
50	2.5	6.9	7.16	2.5	-2.2
	5	17.3	19.74	5.1	13.7
75	2.5	-5.2	-4.87	2.25	-13.2
	5	1.1	1.66	4.95	-1.1

Table.6.4. Percentage loss of average bond strength at different levels of corrosion for 60 MPa concrete mixture

Cover thickness (mm)	FEA		FEA (Ghosh, 2004)	Experimental results (Amleh, 2000)	
	% mass loss	% loss of bond strength	%loss of bond strength	% mass loss	%loss of bond strength
25	2.5	28.3	26.83	2.2	26.58
	5	58.1	54.03	3.78	42.43
50	2.5	4.9	4.78	2.8	1.5
	5	20.03	19.78	7.26	33.68
75	2.5	-3.1	-4.48	2.65	-3.52
	5	8	10.57	8.46	23.2

6.5. Validation of the model with the results of Al-Sulaimani et al. (1990)

The developed model to determine the bond stress in uncorroded and corroded condition is validated using the results of the pullout tests conducted by Al-Sulaimani et al (1990).

6.5.1. Pullout tests of Al-Sulaimani et al. (1990)

Pullout tests were conducted on 150 mm cubic concrete specimens with 10 mm diameter reinforcing bar embedded in the cube. The embedded length considered for the study was 4 times the bar diameter. The average 28 day compressive strength is 30 MPa, and they were subjected to accelerated corrosion to obtain differen levels of corrosion. Here, the measured corrosion penetration (evaluated from the weight loss) was used as input. Figure 6.26 shows that the bond strength decreases with corrosion for both the

experimental and finite element analysis. Results of the finite element analysis show a good agreement with the experimental results.

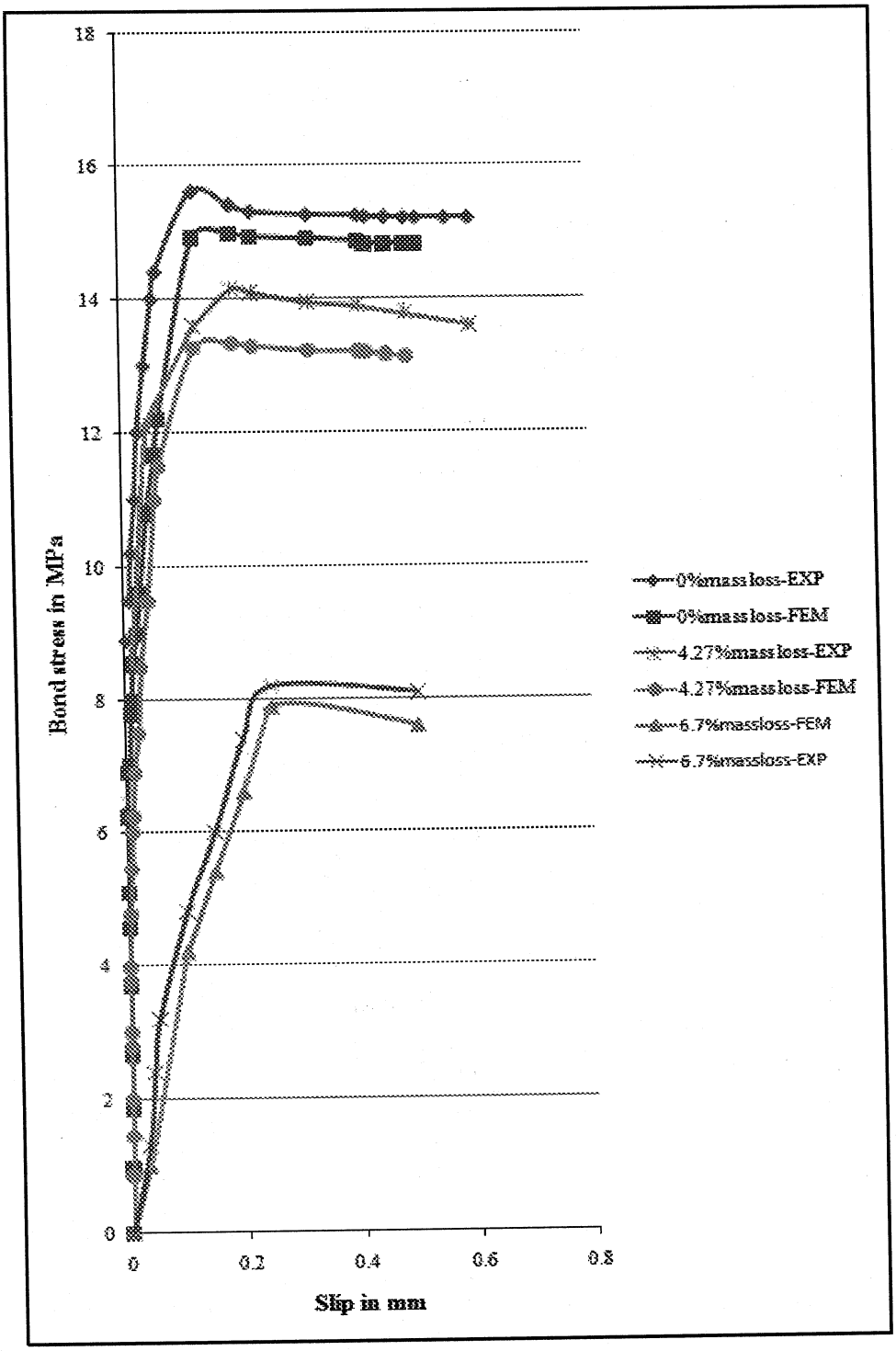

Fig 6.26-Validation of average bond stress with slip at different levels of corrosion

Chapter 7

Conclusions and Future Recommendations

7.1. Summary and Conclusions

A mathematical expression which describes the contact pressure at the steel-concrete interface in a reinforced concrete is developed. For deriving this expression, concrete is considered as a thick-walled cylinder subjected to internal pressure, which is regarded as the radial pressure due to bond action. The effect of friction is not taken in to account in order to avoid the complexity of the problem. The developed expression (equation 4.15) shows that the contact pressure at the steel concrete interface depends on the bar diameter, rib height, tensile strength of concrete, crack width, maximum aggregate size and fracture energy coefficient. From equation 4.15, it is also observed that the contact pressure decreases with the increase in crack width.

The expression for the reduction in contact pressure due to the accumulation of corrosion products is then developed using the model developed for the uncorroded reinforcing steel bar (Eq. 20). In order to elude the complex nature of the problem, it is assumed that the bar is corroded uniformly. Equation 4.20 shows that the reduction in contact pressure depends on the depth of corrosion attack, type of corrosion products formed, bar diameter and concrete cover.

Bond stress which can be defined as the shear stress which develops along the lateral surface of the bar, is a function of the contact pressure exerted by the surrounding

concrete on the bar surface. According to the equation for bond stress (equation 4.23), when the normal contact pressure is large, higher frictional force will be required for the pullout and higher resistance also will be there for splitting failure to occur.

The pull-out tests carried out by Amleh (2000) have been analysed with finite element analysis using ABAQUS. The bond stress with slip graph is plotted using the results of finite element analysis. It is observed that the bond strength increases with the increase the cover thicknesses. Also, the bond strength of the 60 MPa concrete is found to be slightly higher than that of 50 MPa concrete. The specimens were analyzed for different levels of corrosion such as 2.5% mass loss and 5% mass loss and the graph showing the variation of bond stress with slip is plotted. With the increase in corrosion levels, it is found that the average bond strength decreases and slip increases. Even though the bond strength decreases with the increase in mass losses, higher bond strength is observed for the specimens with higher bar diameter. Also, the developed model is validated using the results of the pullout tests conducted Al-Sulaimani et al (1990). It can be observed that the bond strength decreases with corrosion for both the experimental and finite element analysis. Results of the finite element analysis show a good agreement with the experimental results.

7.2. Future recommendations

1. Develop the mathematical expression for contact pressure by considering the effect of friction at the steel-concrete interface.

2. Develop the mathematical expression for contact pressure for reinforced bar with transverse reinforcement.
3. Conduct more experimental studies to understand the mechanical behaviour of the rust and the type of corrosion products formed which can be implemented both in finite element modeling and analytical modeling of reinforced concrete.

REFERENCES

ABAQUS/Standard User's Manual (2002), Vol. 2, Version 6.5, Hibitt, Karlsson and Sorensen, Inc.

ABAQUS/Standard User's Manual (2002), Vol. 3, Version 6.5, Hibitt, Karlsson and Sorensen, Inc.

ACI Committee 408 (1966), "Bond Stress- The State of the Art", *Journal of the American concrete Institute*, Vol. 63, No. 11, pp.1161-1188

ACI Committee 408 (2005), "Bond Under Cyclic Loads", *Journal of the American concrete Institute*

Auyeung, Y., Balaguru, P., Chung, L., (2000), "Bond Behavior of Corroded Reinforcement Bars", *ACI Materials Journal* , Vol. 97, No. 2, pp. 214-221

Alavi-Fard, M., and Marzouk, H., (2002), *Canadian Journal of Civil Engineering,* "Bond behavior of high strength concrete under reversed pull-out cyclic loading", Vol. 29, pp.191-200

Alavi-Fard, M., and Marzouk., (2004), "Bond of high strength concrete under monotonic pull out loading", *Thomas Telford Journals*, Vol. 56, Issue. 9, pp.545-557

Al-Sulaimani, G. J., Kaleemullah, M., Basunbul, I. A., and Rsheeduzzafar, (1990), "Influence of corrosion cracking on bond behavior and strength of reinforced concrete members," ACI St. 96, No. 3, pp. ructural Journal, Vol. 87, No.2, pp. 220-231

Amleh, L., and Mirza, S., (1999), "Corrosion influence on bond between steel and concrete", ACI Structural Journal, Vol415–423

Amleh, L., (2000), "Bond deterioration of reinforcing steel in concrete due to corrosion", Ph D Thesis, McGill University, Canada, pp. 1-377

Amleh, L., Ghosh, A., (2006), "Modeling the effect of corrosion on bond strength at the steel concrete interface with finite-element analysis", *Canadian Journal of Civil Engineering*, Vol.33, pp. 672-683

Berra, M.; Castellani, A.; and Coronelli, D., (1997), "Bond in Reinforced Concrete and Corrosion of Bars," *Seventh International Structural Faults and Repair*, Edinburgh, UK, pp. 349-356

Cairns, J., and Abdullah, R. B., (1996), "Bond strength of black and epoxy-coated reinforcement- a theoretical approach, *ACI Materials Journal,* Vol. 93, No. 4, pp.362-370

Castel, A., Francois, R., and Arliguie, G., (2000), "Mechanical Behavior of Corroded Reinforced Concrete Beams-Part 2: Bond and Notch Effects," *Materials and Structures*, Vol. 33, No. 233, pp. 545-551

Choi, C. O., and Lee, S. W., (2002), "Interfacial bond analysis of deformed bars to concrete", *ACI Structural Journal,* Vol. 99, No. 6, pp. 750-756

Coronelli, D., and Gambarova, P.G., (2000), "A mechanical model for bond strength of corroded reinforcement in concrete", *In* Proceedings of EM2000, 14th ASCE Engineering Mechanics Conference, Austin, Tex. CD-ROM. American Society of Civil Engineers, Reston

Coronelli, D., (2002), "Corrosion Cracking and Bond Strength Modeling for Corroded Bars in Reinforced Concrete", *ACI Structural Journal*, Vol. 99, No. 3, pp. 267-276

Elmorsi, M., Kianoush, M. R., and Tso, W. K., (2000), "Modeling bond–slip deformations in reinforced concrete beam–column joints", *Canadian Journal of Civil Engineering*, Vol. 27, pp.490-505

Ghosh, A., (2004), "Modeling the effect of corrosion on bond strength at the steel concrete interface with finite-element analysis", MASc Thesis, Ryerson University, Canada, pp. 1-117

Girard, C., and Bastien, J., (2002), "Finite-Element Bond-Slip Model for Concrete Columns under Cyclic Loads", *Journal of structural Engineering,* Vol. 128, No. 12.

Harajli, M. H., (2007), "Numerical Bond Analysis Using Experimentally Derived Local Bond Laws: A Powerful Method for Evaluating the Bond Strength of Steel Bars", *Journal of Structural Engineering*, Vol. 133, No.5

Joseph, F. Bosich, (1970), *Corrosion Prevention for Practicing Engineers*, pp 94-104, Barnes & Noble Inc. New York.

Kwak, H., and Filippou, F. C., (1990), "Finite element analysis of reinforced concrete structures under monotonic loads", Department of Civil Engineering, University of California, Berkeley

Kyle, S., Hooton, R. D., Pantazopoulou, S. J., (1999), "Corrosion effects on bond strength in reinforced concrete", *ACI Structural Journal*, V. 96, No. 6, pp. 915-922

Lundgren, K., and Gyltoft, K., (2000), "A model for the bond between concrete and reinforcement", *Magazine of concrete Research,* Vol. 52, No. 1, pp.53-63

Lundgren, K., and Magnusson, J., (2001), "Three Dimensional Modeling of Anchorage Zones In Reinforced Concrete", *Journal of Engineering mechanics*, ASCE, Vol. 127, No.7

Lundgren, K., (2005), "Bond between ribbed bar and concrete. Part 1: Modified model", *Magazine of Concrete Research*, Vol. 57, No. 7, pp.371-382

Lu, X., and Dong, Y., (2006), "Numerical simulation on local bond-slip between steel and concrete with experimental verification", *Joint International Conference on Computing and Decision Making in Civil and Building Engineering,* Montréal, Canada

Maaddawy, T. E., Soudki, K., and Topper, T., (2005), "Long-term performance of corrosion-damaged reinforced concrete beams", *ACI Structural Journal*, Vol. 102, No. 5, pp. 649-656

Mitchell, D. W., and Marzouk, H., (2007), "Bond Characteristics of High-Strength Lightweight Concrete", *ACI Structural Journal*, V. 104, No. 1, pp. 22-29

Molina F., Alonso C., and Andrade C., (1993), "Cover cracking as a function of bar corrosion: Part 2 – Numerical model", *Materials and Structures*, 26, pp.532-548.

Nawy, E. G., (1996), *Reinforced Concrete: A Fundamental Approach* 3rd Ed. Prentice-HallCanada, Inc. Toronto c, pg. 415

Noghabai, K., (1996), "Environmental effects on bond in R/C structures", 7th Int. Conf. *Durability of Building Materials and Components*, Stockholm,Sweden,May,pp.605-614.

Pantazopoulou, J., and Tastani, S. P., (2002), "Experimental evaluation of the direct tension pullout tests", *Bond in Concrete – from research to standards* , Budapest

Pantazopoulou, J., Papoulia, K. D., (2001), "Modeling cover-cracking due to reinforcement corrosion in RC structures", *Journal of Engineering Mechanics*, Vol. 127, No. 4, pp.342-351

Peter-Lazer, I., and Gerard, B., (2000), "Mechanical Behaviour Of Corrosion Products Formed At The Steel –Concrete Interface.Testing And Modelling", *In Proceedings EM 2000, Fourteenth Engineering Mechanics Conference,* ASCE, Austin, Texas, USA.

Raymond, E.U., and R. L. Henry, R. L., (1965), "Influence of normal pressure on bond strength", Journal of American Concrete Institute, Vol. 62, No.5, pp.577-586

Richardson, M. G., (2002), *Fundamentals of durable reinforced concrete*, pp. 51-75, Modern concrete Technology Series, Taylor & Francis, Edition 1

Tassios, T. P., and Yannapoulos, P. J., (1981), "E ´ tudes analytiques sur l'adhe´rence acier-be´ton et la fissuration du be´ton arme´ sous charges cycliques", *Annales de l'Institut technique du ba^timent et des travaux publics,* pp. 46–62

Tepfers, R. A., (1979), "Cracking of concrete cover along anchored deformed reinforcing bars", *Magazine of Concrete Research,* Vol. 31, No. 106, pp. 3-12

Timoshenko, S., (1956), *Strength of materials. Part 11: Advanced theory and Problems*, Princeton, N. J., D. van Nostrand Company Inc., pp. 205-210.

Vandewalle, L., and Mortelmans, F., (1988), "The bond stress between a reinforcement bar and concrete: is it theoretically predictable", *Materials and Structures,* Vol. 21, pp.179-181

Yoon, S., Wang, K., Weiss, W. J., and Shah, P. S., (2000), "Interaction between loading corrosion and serviceability of reinforced concrete", *ACI Materials Journal,* Vol. 97, No. 6, pp.637-644

Zhou, K., Martin-Pérez, B., Lounis, Z, (2005), "Finite Element Analysis of Corrosion Induced Cracking, Spalling and Delamination of RC Bridge Decks", 1st Canadian Conference on Effective Design of Strucutres, Hamilton, On, pp. 187-196

APPENDIX

A1. Input file for 50 mm cover specimen of 60 MPa concrete is given below as sample:

```
*Heading

** Job name:analysis1 Model name: Model-1
*Preprint, echo=NO, model=NO, history=NO, contact=NO
**
** PARTS
**
*Part, name=Part-1
*End Part
**
*Part, name=bar
*End Part
**
**
** ASSEMBLY
**
*Assembly, name=Assembly
**
*Instance, name=bar-1, part=bar
*Node
     1, -2.81732559,  9.5949297,        0.
     2, -5.40640831,  8.41253567,       0.
     3, -7.55749559,  6.54860735,       0.
     4, -9.09632015,  4.15415001,       0.
     5, -9.89821434,  1.42314839,       0.
     6, -9.89821434, -1.42314839,       0.
```

```
 7, -9.09632015, -4.15415001,         0.
 8, -7.55749559, -6.54860735,         0.

*Elset, elset=__PickedSurf21_S5, internal, instance=bar-1, generate
 36, 5280,   57
*Elset, elset=__PickedSurf21_S2, internal, instance=bar-1, generate
 1, 57,  1
*Surface, type=ELEMENT, name=_PickedSurf21, internal
__PickedSurf21_S4, S4
__PickedSurf21_S6, S6
__PickedSurf21_S2, S2
__PickedSurf21_S3, S3
__PickedSurf21_S5, S5
*Elset, elset=__PickedSurf23_S2, internal, instance=bar-1, generate
 1, 57,  1
*Surface, type=ELEMENT, name=_PickedSurf23, internal
__PickedSurf23_S2, S2
*End Assembly
**
** MATERIALS
**
*Material, name=concrete
*Concrete
  10.46,         0.
  13.94, 2.64318e-08
 20.8954,  5.3779e-07
 27.7914, 2.69795e-06
 34.5436, 8.98619e-06
 41.0041, 2.36424e-05
 46.9552, 5.29125e-05
  52.117, 0.000104829
```

56.1791, 0.000188292
58.8586, 0.000311418
59.9711, 0.000479503
60., 0.000516674
59.9983, 0.000516823
58.7604, 0.000614238
52.5505, 0.00099239
*Failure Ratios
1.16, 0.07745, 1.28, 0.3333
*Tension Stiffening
1., 0.
0., 0.001
*Elastic
32462., 0.15
*Material, name=steel
*Elastic
200000., 0.3
*Plastic
433.,0.
**
** INTERACTION PROPERTIES
**
*Surface Interaction, name=IntProp-1
1.,
*Friction, elastic slip=0.001, exponential decay
1., 0.4, 0.45
*Surface Behavior, pressure-overclosure=EXPONENTIAL
2., 9.5
**
** BOUNDARY CONDITIONS
**

```
** Name: BC-1 Type: Symmetry/Antisymmetry/Encastre
*Boundary
_PickedSet22, ENCASTRE
** INTERACTIONS
**
** Interaction: Int-1
*Contact Pair, interaction=IntProp-1, small sliding, adjust=25.
_PickedSurf21, _PickedSurf20
** ----------------------------------------------------------------
**
** STEP: Step-1
**
*Step, name=Step-1, nlgeom=YES, inc=20
*Static, riks
0.02, 1., 1e-05, 1., ,
**
** LOADS
**
** Name: Load-1   Type: Pressure
*Dsload
_PickedSurf23, P, -200.
**
** OUTPUT REQUESTS
**
*Restart, write, frequency=1
**
** FIELD OUTPUT: F-Output-1
**
*Output, field
*Contact Output
CDISP, CSTRESS
```

```
**
** HISTORY OUTPUT: H-Output-1
**
*Output, history
*Contact Output

CDISP, CSTRESS
*El print, freq=1
loads,
*Node print, freq=999999
*End Step
```